

# TOPOLOGICAL QUBITS IN QUANTUM SPIN CHAINS

By  
**ABHINAV SAKET**  
PHYS10200604011

THE INSTITUTE OF MATHEMATICAL SCIENCES, CHENNAI.

A thesis submitted to the  
Board of Studies in Physical Sciences

In partial fulfillment of the requirements

For the Degree of

**DOCTOR OF PHILOSOPHY**

*of*

**HOMI BHABHA NATIONAL INSTITUTE**



April 1, 2013

# Homi Bhabha National Institute

## Recommendations of the Viva Voce Board

As members of the Viva Voce Board, we certify that we have read the dissertation prepared by **ABHINAV SAKET** entitled “Topological Qubits in Quantum Spin Chains” and recommend that it may be accepted as fulfilling the dissertation requirement for the Degree of Doctor of Philosophy.

----- **Date :**  
Chairman : R. Shankar

----- **Date :**  
Convener : - - -

----- **Date :**  
Member : - - -

----- **Date :**  
Member : - - -

Final approval and acceptance of this dissertation is contingent upon the candidate’s submission of the final copies of the dissertation to HBNI.

I hereby certify that I have read this dissertation prepared under my direction and recommend that it may be accepted as fulfilling the dissertation requirement.

----- **Date :**  
Guide : R. Shankar

## STATEMENT BY AUTHOR

This dissertation has been submitted in partial fulfillment of requirements for an advanced degree at Homi Bhabha National Institute (HBNI) and is deposited in the Library to be made available to borrowers under rules of the HBNI.

Brief quotations from this dissertation are allowable without special permission, provided that accurate acknowledgement of source is made. Requests for permission for extended quotation from or reproduction of this manuscript in whole or in part may be granted by the Competent Authority of HBNI when in his or her judgment the proposed use of the material is in the interests of scholarship. In all other instances, however, permission must be obtained from the author.

ABHINAV SAKET

## DECLARATION

I hereby declare that the investigation presented in the thesis has been carried out by me. The work is original and the work has not been submitted earlier as a whole or in part for a degree/diploma at this or any other Institution or University.

ABHINAV SAKET

Dedicated to my parents,  
Mrs Indu Sinha  
and  
Mr Om Prakash Sinha.

## ACKNOWLEDGEMENTS

First of all, my heartfelt gratitude to my Ph. D. supervisor Prof. R Shankar for his patience, advice, constant encouragement. His fatherly guidance brought the right spirit in me to carry out the research work. It was a pleasure to interact with him.

My sincere gratitude to Prof. G Baskaran who had introduced me to my research problem. It was always a pleasure to listen the intricacies of his "beautiful physics".

Here, I express my special thanks to Dr. S R Hasan for many discussions and especially about numerics. His friendly attitude certainly made things easier. Many times it was hard to appreciate his emphasis with every details but later it would bring a sense of completeness.

I thank all my friends and fellow colleagues Saptarshi, Kamil, Shiraj, Anilkumar, Srikanth, Archana and Rajesh karn who hepled me at various times.

I am grateful to the library and the computer staffs for their help. I wish to acknowledge all the non-academic staffs for their work. I must thank the institute and its academic and administrative members for ensuring an excellent academic atmosphere and facilities for research work.

Last, but not the least, I want to thank my sister Noopur who kept constantly encouraging me during this work. I want to thank my brother-in-law Gunjan and wife Sweta who always have been there with me. I want to express my love for my nephew Dhaval.

# Synopsis

In this thesis, we investigate one dimensional generalisations of the Kitaev model and study robustness of topological qubits in one dimensional quantum spin chains. The Kitaev model, a two dimensional model on honeycomb lattice, was proposed by A. Yu. Kitaev for possible implementation of topological quantum computation [1]. This model has anisotropic type nearest neighbour spin-spin interaction which depends on the direction of the bonds. The Hamiltonian can be written as follows,

$$H = -J_x \sum_{x-link} \sigma_i^x \sigma_j^x - J_y \sum_{y-link} \sigma_i^y \sigma_j^y - J_z \sum_{z-link} \sigma_i^z \sigma_j^z.$$

Here x, y and z links are three different bonds in the hexagonal lattice which are related by  $120^\circ$  rotation and i, j denote nearest neighbour sites. This model has conserved quantities associated with each hexagonal plaquette and all closed loops. The spin model has been fermionised by Jordan-Wigner transformation. This fermionisation process maps the original spin 1/2 Hamiltonian into a tight binding Hamiltonian of Majorana fermion where hopping amplitude contains the local static  $Z_2$  gauge fields. It has been shown that ground state sector belongs to the case where all  $Z_2$  gauge fields take value +1. The translational invariance of  $Z_2$  gauge fields in the hopping amplitude has allowed to calculate the ground state energy and a set of low lying excited states exactly. For this particular gauge configuration the spectrum has two distinct phases. For certain values of parameter the spectrum is gapless otherwise it is gapped. While the gapped phase contains abelian anyonic excitations, the gapless phase contains non-abelian excitations. In presence of magnetic field the gapless phase acquires a gap. The fact that Kitaev model has non-abelian excitations which can be used for Quantum Computation attracted our attention and we started studying one-dimensional generalisations of this model.

Kitaev's honeycomb model can be generalised to a variety of other lattices [2,3,4,5,6]. All generalised Kitaev models are integrable in the sense that all of them reduce to systems of non-interacting Majorana fermions. They can be constructed on any lattice with coordination number three, if all the bonds can be coloured using three colours. In this thesis, we consider two generalised models the Tetrahedron model and the XYZ-Ising model.

The thesis is divided into five chapters. We present a summary of main results in each chapter below:

## Introduction

In chapter 1, we give a brief introduction to quantum computation and all kinds of errors which can happen in a Quantum Computer. We discuss a few schemes of Quantum error correcting codes which achieve fault tolerance. Then, we present a brief introduction to Topological Quantum computation. We explain how fault tolerance can be achieved in this scheme and discuss the Kitaev model where these goals have been achieved. Finally, various schemes of physical realisation are discussed.

## Tetrahedron Model

In chapter 2, we construct and study one dimensional generalisation of Kitaev model we call the "Tetrahedral model" for which we derive several exact results. The Hamiltonian of the model can be written as,

$$H = \sum_i \left( J_x (\sigma_{i,2}^x \sigma_{i,3}^x + \sigma_{i,4}^x \sigma_{i+1,1}^x) + J_y (\sigma_{i,1}^y \sigma_{i,2}^y + \sigma_{i,3}^y \sigma_{i,4}^y) + J_z (\sigma_{i,2}^z \sigma_{i,4}^z + \sigma_{i,1}^z \sigma_{i,3}^z) \right).$$

In each unit cell two set of operators exist which commute with Hamiltonian,

$$W_i^L = \sigma_{i,1}^x \sigma_{i,2}^z \sigma_{i,3}^y \quad W_i^R = \sigma_{i,4}^x \sigma_{i,3}^z \sigma_{i,2}^y.$$

We express the Hamiltonian in terms of Majorana fermions using the Jordan-Wigner transformation. We choose the Jordan-Wigner path to go along the  $x$  and the  $y$  bonds from left to right. At every site we have two bonds that are tangential to the path. We denote the incoming bond by  $t_1$  and the outgoing bond by  $t_2$ . The third bond on each site is normal to the path and denoted by  $n$  with the sign defined by  $\hat{n} = \hat{t}_1 \times \hat{t}_2$ . We define Jordan-Wigner transformation in terms of this



new basis in following way,

$$\begin{aligned}\xi_{i,\alpha} &= \sigma_{i,\alpha}^{t_1} \prod_{j,\beta < i,\alpha} (\sigma_{j,\beta}^n), \\ \eta_{i,\alpha} &= \sigma_{i,\alpha}^{t_2} \prod_{j,\beta < i,\alpha} (\sigma_{j,\beta}^n),\end{aligned}$$

where  $\xi_{i,\alpha}$  and  $\eta_{i,\alpha}$  are called Majorana operators and follow fermionic anti-commutation relation with one additional property that they are hermitian operators.

In terms of Majorana fermions we get a non-interacting Hamiltonian in the background of  $Z_2$  gauge field as shown below,

$$\begin{aligned}H &= \sum_i^N J_x (i\xi_{i-1,4}\xi_{i,1} + i\xi_{i,2}\xi_{i,3}) \\ &\quad + J_y (i\xi_{i,1}\xi_{i,2} + i\xi_{i,3}\xi_{i,4}) \\ &\quad + J_z \left( -iu_i^L \xi_{i,1}\xi_{i,3} + iu_i^R \xi_{i,2}\xi_{i,4} \right),\end{aligned}$$

where the gauge fields,  $u_i^{L(R)}$ , are defined as

$$\hat{u}_i^L \equiv i\eta_{i,3}\eta_{i,1} \quad \hat{u}_i^R \equiv i\eta_{i,2}\eta_{i,4}.$$

The gauge field operators are the commuting operators in Jordan-Wigner basis, therefore they also commute with the Hamiltonian. As square of each gauge field operator is unity matrix we can replace them by their eigenvalues  $u_i^{L(R)} = \pm 1$ . Therefore, we could obtain the following results [7]:

1. Numerically, we found that the translationally invariant fluxes through the unit cells, namely  $u_i^L = -1$  and  $u_i^R = -1$  is the ground state sector of the model.
2. Since the fermionic gap is twice the value of the lowest single particle energy eigenvalue and lowest single particle energy belongs to translationally invariant flux configuration, we could give an analytic expression for fermionic gap.
3. Since we got a tight binding Hamiltonian it became viable for us to write analytical solution for zero energy modes of Majorana fermions. The existence of unpaired degenerate zero modes has been shown.
4. It has been shown that by tuning flux configuration we can manipulate the zero mode wavefunction. The regions in parameter space for homogenous chains

has been shown where the zero modes occur.

5. We further show that there is a large parameter space for inhomogenous chains where the unpaired modes occur.

6. Another result we prove in the model is that every state of the system has a  $2^{N/4}$  fold degeneracy, where  $N$  is the number of sites.

## XYZ-Ising Model: Exact Solutions

In chapter 3, we study another one dimensional generalisation “XYZ-Ising model” for possible physical realisation by Josephson junction quantum circuits [8]. The Tetrahedron model has three-spin commuting operator whereas in this model the commuting operators are two-spin operators.

Hamiltonian of this model is defined by

$$H = \sum_i (J_x \sigma_{i,1}^x \sigma_{i,2}^x + J_y \sigma_{i,1}^y \sigma_{i,2}^y + J_z \sigma_{i,1}^z \sigma_{i,2}^z + \sigma_{i,2}^z \sigma_{i+1,1}^z).$$

Commuting operators are,

$$W_i = \sigma_{i,1}^z \sigma_{i,2}^z.$$

Here, since the commuting operator are two spin operators, the physical realisation of the model becomes possible using Josephson junction quantum circuits [8]. The z bond in the Hamiltonian is nothing but two spin commuting operators. Therefore, we study the special case  $J_z = 0$  of Hamiltonian which we call the XY-Ising model. All the eigenstates and eigenvalues of the XYZ-Ising and the XY-Ising model is same.

In XY-Ising model we define Jordan-Wigner path through the y and the z bond. Applying the JW transformation, we get again a non-interacting Hamiltonian,

$$H = \sum_{i=1}^N (J_y - J_x \hat{u}_i) i\xi_{i,1} \xi_{i,2} + \sum_{i=1} i\xi_{i,2} \xi_{i+1,1},$$

where the gauge fields,  $\hat{u}_i$  are defined as,

$$\hat{u}_i \equiv i\eta_{i,1}\eta_{i,2}.$$

As in case of Tetrahedron model,  $\hat{u}_i$  can be replaced by its eigenvalues  $u_i = \pm 1$ .

The results we have got so far [9]:

1. Being a tight binding Hamiltonian we could solve the XY-Ising model exactly and prove that for  $J_x = J_y$  the ground state lies in translationally invariant flux sector  $u_i = -1$ .
2. We showed that ground state sector of XY-Ising model is gapped for certain range of parameters of the Hamiltonian.
3. Nature of low energy excitations in XY-Ising model has been studied analytically.

## XYZ-Ising Model: Phase Diagram

In chapter 4, the XYZ-Ising model,

$$H = \sum_i^N (J_x \sigma_{i,1}^x \sigma_{i,2}^x + J_y \sigma_{i,1}^y \sigma_{i,2}^y + J_z \sigma_{i,1}^z \sigma_{i,2}^z + \sigma_{i,2}^z \sigma_{i+1,1}^z),$$

can also be solved using the Kitaev's trick even if it's not a Kitaev type three link model.

In 1961, Lieb, Schultz and Mattis studied a special case of similar quantum mechanical model where the interactions are alternately Ising and isotropic Heisenberg interactions, and solved exactly in the sense that the ground state, all the elementary excitations and the free energy has been found [10].

Here are the results:

1. We study ground state of the XYZ-Ising model for all  $J_x, J_y$  and  $J_z$  numerically which agree in extreme limits with analytical results.
2. The zero temperature phase diagram of the system has been plotted by calculating ground state numerically. We find that model undergoes a first order phase transition as a function of coupling constant  $J_z < 0$ . For  $J_z > 0$ , the model has a topological phase transition.

# Topological Qubits in XY-Ising Model

In chapter 5, We define a qubit and study the interaction of the system with the environment.

Here are the results we achieved [9]:

1. As in case of the Tetrahedron model, analytical solution for zero mode Majorana fermions in the XY-Ising model has been obtained.

2. Unpairing of degenerate zero modes has been shown. It has been shown that by tuning flux configuration we can manipulate the zero mode wavefunction.

3. We propose a Qubit made up of two degenerate modes of the model.

4. We have studied, using first order degenerate perturbation theory, the protection of this Qubit from decoherence by environmental perturbation,

$$V = \sum_{i,\alpha} (B_x^{i,\alpha} \sigma_{i,\alpha}^x + B_y^{i,\alpha} \sigma_{i,\alpha}^y + B_z^{i,\alpha} \sigma_{i,\alpha}^z),$$

and showed that z part of the potential induces the transition between the qubit-subspace which can be made small by tuning parameters  $J$  and  $J_z$ . We also showed that for x and y part of potential the protection from decoherence is perfect.

5. We show explicitly, following the scheme proposed by You et al [8], how the XY-Ising model and the XYZ-Ising model can be realised by Josephson junction quantum circuits.

## References

- [1] A. Y. Kitaev. Fault-tolerant quantum computation by anyons. *Ann. Phys. (N.Y.)* **303**, 2003; Anyons in an exactly solved model and beyond. **321**, 2 (2006).
- [2] H. Yao and S. A. Kivelson. Exact Chiral Spin Liquid with Non-Abelian Anyons. *Phys. Rev. Lett.* **99**, 247203 (2007).
- [3] S. Yang, D. L. Zhou and C. P. Sun. Mosaic spin models with topological order. *Phys. Rev. B* **76**, 180404(R)(2007).
- [4] S. Mandal and N. Surendran. Exactly solvable Kitaev model in three dimensions. *Phys. Rev. B* **79**, 024426 (2009).
- [5] Z. Nussinov and G. Ortiz. Bond algebras and exact solvability of Hamiltonians:

- Spin  $S=1/2$  multilayer systems. Phys. Rev. B **79**, 214440 (2009).
- [6] G. Baskaran, S. Santhosh and R. Shankar. Exact quantum spin liquids with Fermi surfaces in spin-1/2 models. arXiv:0908.1614 (unpublished).
- [7] Abhinav Saket, S. R. Hassan and R. Shankar. Manipulating unpaired Majorana fermions in a quantum spin chain. Phys. Rev. B **82**, 174409 (2010).
- [8] J. Q. You, X. F. Shi, X. Hu and F. Nori. Quantum emulation of a spin system with topologically protected ground states using superconducting quantum circuits. Phys. Rev. B **81**, 014505 (2010).
- [9] Abhinav Saket, S.R. Hassan and R. Shankar. Topological Qubits in a quantum spin chain (under preparation).
- [10] E. Lieb, T. Schultz and D. Mattis. Two Soluble Models of an Antiferromagnetic Chain. Annals of Physics: **16**, 407-466 (1961).

## Publications

1. Abhinav Saket, S. R. Hassan and R. Shankar. Manipulating unpaired Majorana fermions in a quantum spin chain. Phys. Rev. B **82**, 174409 (2010).
2. Abhinav Saket, S.R. Hassan and R. Shankar. Topological aspects of an exactly solvable spin chain (to be published in PRB).

# Contents

<b>1</b>	<b>Introduction</b>	<b>1</b>
1.1	Overview . . . . .	1
1.2	Quantum Computation . . . . .	2
1.2.1	Turing Machine . . . . .	3
1.2.2	Quantum Turing Machine . . . . .	5
1.2.3	Quantum Circuits . . . . .	6
1.2.4	Reversible Computer . . . . .	11
1.2.5	Quantum Algorithm- Deutsch Algorithm . . . . .	11
1.3	Fault tolerant Quantum Computation . . . . .	13
1.3.1	Quantum Decoherence . . . . .	13
1.3.2	Other Errors . . . . .	14
1.4	Quantum Error Correcting Codes . . . . .	16
1.5	Physical Realisations . . . . .	19
1.5.1	Ion Trap Method . . . . .	20
1.5.2	Nuclear Magnetic Resonance . . . . .	20
1.5.3	Optical Cavity QED . . . . .	21
1.6	Topological Quantum Computation . . . . .	22
1.6.1	Anyon and Non-abelian Anyon . . . . .	23
1.6.2	Kitaev Model . . . . .	24
1.7	Qubits from Zero mode Majorana Fermions . . . . .	25
1.7.1	Hamiltonian . . . . .	25
1.7.2	Jordan-Wigner Transformation . . . . .	26
1.7.3	Majorana Fermions . . . . .	27
1.7.4	Zero Mode Majorana Fermions and Unpairing . . . . .	28
1.8	Unitary Gate Operation on the Qubit . . . . .	31
1.9	Josephson Junction Quantum Circuits . . . . .	33
1.10	Organisation of the thesis . . . . .	40
<b>2</b>	<b>Tetrahedral Model</b>	<b>42</b>
2.1	The Hamiltonian . . . . .	42
2.2	Fermionisation . . . . .	43
2.3	Diagonalisation . . . . .	45

2.3.1	Boundary Conditions . . . . .	47
2.4	The Degeneracy of the States . . . . .	48
2.5	The Ground States and gaps . . . . .	51
2.6	Zero modes . . . . .	52
2.6.1	Periodic Boundary Condition . . . . .	55
2.6.2	Open Boundary Condition . . . . .	58
2.6.3	Inhomogenous chains . . . . .	59
2.6.4	The Qubit . . . . .	60
2.6.5	Tuning the flux configuration . . . . .	61
<b>3</b>	<b>XYZ-Ising Model: Exact Solutions</b>	<b>63</b>
3.1	The Hamiltonian . . . . .	63
3.2	Fermionisation . . . . .	65
3.3	Diagonalisation . . . . .	67
3.4	Exact Solution for all Sectors . . . . .	69
3.4.1	The 0-defect sector . . . . .	69
3.4.2	The 1-defect sector . . . . .	71
3.4.3	The $n_D$ -defect sector . . . . .	77
3.5	Ground State and Gap . . . . .	77
3.5.1	Nature of low energy excitations . . . . .	81
3.5.2	Zero modes . . . . .	81
<b>4</b>	<b>XYZ-Ising Model: Phase Diagram</b>	<b>91</b>
4.1	The Hamiltonian . . . . .	91
4.2	Ground State in Extreme Limit of Coupling Constants . . . . .	92
4.3	The Ground States in all defect sectors . . . . .	94
4.4	Zero Temperature Phase Diagram . . . . .	97
<b>5</b>	<b>Topological Qubits in XY-Ising Model</b>	<b>109</b>
5.1	The Qubit . . . . .	109
5.1.1	Tuning the flux configuration . . . . .	111
5.2	Protection from Decoherence . . . . .	112
5.3	Physical Realisation . . . . .	118

<b>6 Conclusion</b>	<b>121</b>
6.1 Summary . . . . .	121
6.2 Outlook . . . . .	122
<b>Bibliography</b>	<b>123</b>



# List of Figures

1.1	Main elements of a Turing machine . . . . .	4
1.2	Controlled NOT gate . . . . .	9
1.3	Toffoli gate . . . . .	10
1.4	The Kitaev Model. The $x, y$ and $z$ bonds are as indicated. . . . .	24
1.5	The 4 site XY-Ising Model. The $x, y$ and $z$ bonds are as indicated. . . . .	26
1.6	The superconducting qubit box. . . . .	33
1.7	Josephson junction quantum circuit to realise x bond . . . . .	38
1.8	Josephson junction quantum circuit to realise y bond . . . . .	39
1.9	Josephson junction quantum circuit to realise z bond . . . . .	40
2.1	The tetrahedral chain. There are four sites per unit cell. The $x, y$ and $z$ bonds are as indicated. . . . .	42
2.2	The contours of equal gap in the defect free flux sector plotted in the $J_y - J_z$ plane at $J_x = 1$ for a 100 a site system. It can be seen that the contours are circular with the unit circle being gapless. . . . .	53
2.3	The gap in the defect free flux sector plotted against $J \equiv \sqrt{J_y^2 + J_z^2}$ for a 100 site system. The points fall on straight lines with slopes $\pm 2$ . . . . .	54
2.4	The region in the $J_y - J_z$ plane at $J_x = 1$ that supports zero energy modes in sectors with defects. . . . .	57
2.5	The wavefunctions of the two Majorana zero modes for $N = 25$ , $M = 7$ with open boundary conditions. . . . .	59
2.6	Unpairing with 1, 5, 10, 15, 20 and 25 defects in figure (a), (b), (c), (d), (e) and (f) respectively. The defects have been put from the left end of the chain of 25 unit cells. . . . .	62
3.1	The XYZ-Ising chain. There are two sites per unit cell. The $x, y$ and $z$ bonds are as indicated. . . . .	63
3.2	The XY-Ising chain. There are two sites per unit cell. The $x, y$ and $z$ bonds are as indicated. . . . .	64
3.3	$J - e^{ika} = \epsilon_k e^{i\alpha_k}$ in Argand plane. For $J > 1$ , $\alpha(0) = 0$ and $\alpha(\pi) = 0$ . . . . .	74
3.4	$J - e^{ika} = \epsilon_k e^{i\alpha_k}$ in Argand plane. For $J < 1$ , $\alpha(0) = 0$ and $\alpha(\pi) = \pi$ . . . . .	75

3.5	The red line shows the plot between $k$ and $n$ without the correction $\alpha_k$ . The green and blue line shows the plot between $k$ and $n$ for $J < 1$ and for $J > 1$ respectively. . . . .	76
3.6	First excitation in XY-Ising Model . . . . .	82
4.1	The XYZ-Ising chain. There are two sites per unit cell. The $x, y$ and $z$ bonds are as indicated. . . . .	91
4.2	The phase diagram of XYZ-Ising Model in $J - J_z$ plane. The boundary of the figure indicates the extreme limits of $J$ and $J_z$ . The blue, red and green line of the figure shows the range for large $J$ and $J_z$ in which the spin triplet (ST) state, spin singlet (SS) state and spin 1 antiferromagnetic (SPIN 1 AFM) state is the ground state respectively. . . . .	93
4.3	. . . . .	101
4.4	The ground state energy is plotted for various partitions of $N=10$ shown in the light green patch (for example (9, 1), (8, 2) etc). The color variation of the graph shows the magnitude of ground state energy. . . . .	102
4.5	The ground state energy is plotted for various partitions of $N=10$ shown in the light green patch. The color variation of the graph shows the magnitude of ground state energy. . . . .	103
4.6	The ground state energy is plotted for various partitions of $N=10$ shown in the light green patch. The color variation of the graph shows the magnitude of ground state energy. . . . .	104
4.7	The ground state energy is plotted for various partitions of $N=10$ shown in the light green patch. The color variation of the graph shows the magnitude of ground state energy. . . . .	105
4.8	The ground state energy is plotted for various partitions of $N=10$ shown in the light green patch. The color variation of the graph shows the magnitude of ground state energy. . . . .	106
4.9	The ground state energy is plotted in full defect sector in $J - J_z$ plane. The color variation of the graph in figure (a) shows the magnitude of the ground state energy and in figure (b) sign of the ground state energy. . . . .	107

4.10	The ground state energy versus $J$ is plotted for $J_z = -2$ in figure (a) and for $J_z = -4$ in figure (b). The kink in the ground state energy shows the first order transition. . . . .	107
4.11	The red line in the phase diagram shows the first order transition and green line shows the topological phase transition at $J = \pm 1$ described by the order parameter winding number. . . . .	108
4.12	The first and second order derivative of the ground state energy is plotted in $J - J_z$ plane for $J_z > 0$ in figure (a) and figure (b). . . .	108
5.1	The absolute value of eigenvalues versus modes have been plotted. .	110
5.2	The unpaired zero mode is moving on the chain with 1, 10, 20, 30, 40 and 50 defects shown in fig.(a), (b), (c), (d), (e) and (f). The defects have been put from the left end of the chain. . . . .	119
5.3	There are two sites per unit cell in the model. The $x, y$ and $z$ bonds are as indicated. . . . .	120
5.4	The circuit equivalent of XY-Ising Model. The $x, y$ and $z$ bonds are designed by coupling the superconducting qubit box through mutual inductance $M$ , wire and capacitor $C_m$ respectively. We have shown a unit cell of the XY-Ising model of the corresponding circuit diagram where $x, y$ and $z$ bonds are shown by blue, green and red colour lines. . . . .	120

# 1

## Introduction

### 1.1 Overview

Quantum computers can solve some problems faster than any classical computer, but they are far more prone for making errors than classical computers. Some method of controlling and correcting those errors has to be found to prevent a quantum computer from failure. There are many reasons that a quantum computer may fail. The biggest enemy of the quantum computer is decoherence. Even if we manage to control decoherence by isolating our computer from the environment, we can not expect to execute quantum logic gates with perfect accuracy. The quantum gates that the quantum computer executes, are unitary transformations that operate on a qubit. These unitary matrices form a continuum and, therefore, execution of the transformation will not be flawless. Small errors in the gates can accumulate over the course of a computation, eventually causing failure. One way to achieve fault tolerance is through Topological Quantum Computation. Topology concerns the global properties of an object that remain unchanged when we deform the object locally. The central idea of Topological Quantum computation is to store and manipulate quantum information in a 'global' form so that it is protected from local disturbances [1]. In this scheme, we apply the logic gate operation on a qubit by performing braiding operation on two dimensional quasiparticles called Anyons. Local perturbations do not change the topological properties of the braids and therefore cannot introduce errors in the quantum computation. Kitaev [2] showed this on a two dimensional spin-1/2 model that using the topological properties of braids, "fault tolerance" can be achieved. The Kitaev's model is a

two dimensional model. Our aim in this thesis is to study how far one can go if one takes a one-dimensional model. Recently, Jason Alicea *et al* [3] has showed a way to perform braiding operation on non abelian anyons in one dimensional model. In this thesis, we study two one-dimensional generalisations of the Kitaev model namely, “Tetrahedron model” and “XY-Ising model”.

After Kitaev proposed his model, there have been many attempts to realise the his model experimentally. J. Q. You et al [4] realised the model using Josephson junction Quantum Circuits. But complete realisation of braiding operation is not possible in the model. In this thesis, we make an attempt in this direction too.

## 1.2 Quantum Computation

A quantum computer is a device for computation that makes use of superposition principle to perform operations on data [5]. A classical computer has a memory made up of bits, where each bit is either one or zero where as a quantum computer’s memory is made up of Qubits. A Qubit is a quantum superposition of two states zero and one [10]. We write it as

$$|\psi\rangle = a|0\rangle + b|1\rangle \quad (1.1)$$

where  $|0\rangle$  and  $|1\rangle$  are orthogonal states and  $|a|^2 + |b|^2 = 1$ . Further, coefficients  $a$  and  $b$  are complex numbers. These complex numbers specify the quantum state of the qubit.

In general, a quantum computer with  $N$  qubits can be in an arbitrary superposition of  $2^N$  different states (This can be compared to a normal computer that can only be in one of these  $2^N$  states at any time).

The logic gate is applied on the qubit through Unitary time evolution of the system,

$$U|\psi\rangle = e^{-iHt/\hbar}|\psi\rangle \quad (1.2)$$

The allowed operations on the qubits are unitary matrices, which are nothing but complex rotations. Consequently, Benioff [6] and Feynman [7] realised computations are reversible as rotations can be undone by rotating backward.

A quantum computer operates by manipulating qubits with a fixed sequence of quantum logic gates. The sequence of gates to be applied is called a quantum algorithm.

Final question: How do we read the result obtained by quantum computation as it is the quantum superposition of states?

In the case of a probabilistic classical computer, we sample, for example, from the probability distribution of the three-bit register to obtain one definite three-bit string, say 000. Quantum mechanically, we measure the three-qubit state, which is equivalent to collapsing the quantum state down to a classical distribution (with the coefficients in the classical state being the squared magnitudes of the coefficients for the quantum state) which is followed by sampling from that distribution. Many algorithms will only give the correct answer with a certain probability. The probability of getting the correct answer can be increased by initializing, running and measuring the quantum computer many times.

Many theoretical models have been proposed for quantum computer. We will describe two models, one based on Turing machine and another based on quantum circuits.

### 1.2.1 Turing Machine

The traditional computer science works on the idea of Turing machine discovered by Alan Turing in 1936. According to Turing [8, 9],

“Every function which would naturally be regarded as computable can be computed by the universal Turing machine.”

This assertion is known as Church-Turing thesis. Many people have spent a great deal of time gathering evidence to the contrary for Church-Turing thesis. In sixty years no evidence has been found. The broad acceptance of this thesis laid the foundation for the development of Computer Science. The way quantum mechanics impacts working of the Turing machine, we will describe in later section. Right now, let us start the discussion from conventional Turing machine.

A Turing machine contains four elements:(a) a finite state control, which acts like a stripped down microprocessor, co-ordinating the other operations of the machine; (b) tape, which acts like a computer memory; (c) a program, like an ordinary computer; and (d) a read and write head, which points to the position on

the tape which is currently readable or writable [10]. The basic element of Turing machine are shown in the following figure 1.1.

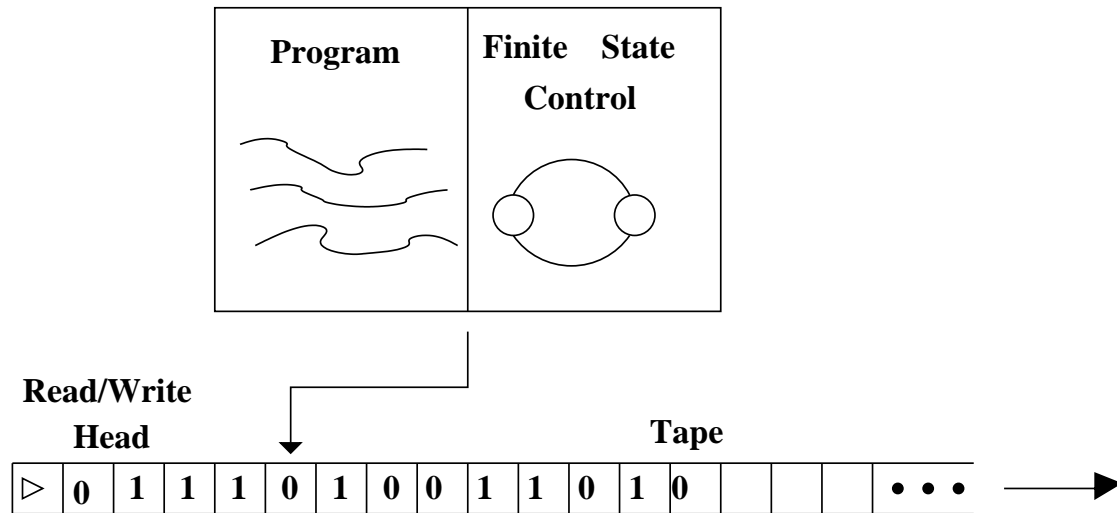


Figure 1.1: Main elements of a Turing machine

Let us discuss these in more detail.

**The Finite state control:** This is also known as finite state machine. In the finite state control, there are a finite set of internal states,  $q_1, \dots, q_m$  including two special states, labelled  $q_s$  and  $q_h$ . We call these states the starting state and halting state. At the beginning of the computation, the Turing machine is in starting state  $q_s$ . The execution of the computation causes the Turing machine's internal states to change. After the end of computation, the Turing machine ends up in the state  $q_h$ .

**Tape:** Turing machine tape is a one dimensional object which consists of an infinite sequence of squares. Each square contain one symbol taken from some alphabet,  $\Gamma$ , which contains a finite number of distinct symbols.  $\Gamma$  contains four symbols, which we denote by 0,1,b(blank symbol), and  $\rightarrow$ , to mark the left hand edge of the tape. Initially, the tape contains a  $\rightarrow$  at the left end, a finite number of 0's and 1's and rest of the tape squares are blanks. The readwrite tape head identifies a single square on the Turing machine tape as the square that is currently being read by the machine.

**Program:** A program for Turing machine is a finite ordered list of program lines of the form  $\langle q, x, q', x', s \rangle$ . The first object in the program line,  $q$ , is a state

from the set of internal states of the machine. The second object,  $x$ , is taken from the alphabet,  $\Gamma$ . On each machine cycle, Turing machine searches through the list of program lines in order for a line  $q, x, s, \dots$  such that the current internal state of the machine is  $q$ , and the symbol being read on the tape is  $x$ . If it does not find such a program line, the internal state of the machine is changed to  $q_h$ , and the machine halts operation. If such a line is found, then that program line is executed. Execution of a program line involves the following steps: the internal state of the machine is changed to  $q'$ ; the symbol  $x$  on tape is overwritten by the symbol  $x'$ , and tape-head moves left, right or stand still, depending on whether  $s$  is  $-1, +1$  or  $0$  respectively. This is Turing machine model of computation. It turns out that this model can be used to compute a wide variety of functions. More than that it turns out that a Turing machine can be used to simulate all the operations performed on modern computer. Indeed, according to the thesis put forward independently by Church and by Turing, the class of functions computable by a Turing machine corresponds exactly to the class of functions which we would naturally regard as being computable by an algorithm.

### 1.2.2 Quantum Turing Machine

How quantum mechanics can alter the working of Turing machine? Such Turing machines were first proposed by David Deutsch [11]. He suggested a stronger version of Church-Turing thesis, as follows,

“Every finitely realisable physical system can be perfectly simulated by a universal model computing machine operating by finite means.”

This version is so strong that it is not satisfied by Turing’s machine in classical physics because in classical dynamics, the possible states of a classical system necessarily form a continuum. But there are only countable ways of preparing a finite input for Turing’s universal computer. Consequently, Turing universal computing machine cannot perfectly simulate any classical dynamical system. Deutsch showed in his classic paper [11] that every real (dissipative) finite physical system can be perfectly simulated by an Universal Quantum Turing machine. Thus, quantum theory is naturally compatible with the strong form of the Church-Turing Principle. Computing machines based on strong form of Church-Turing Principle can, in principle, be built and would have many remarkable properties not reproducible



by any Turing machine. One of them is "quantum parallelism", a method by which certain probabilistic tasks can be performed faster by a universal quantum computer than by any classical counterpart of it.

### 1.2.3 Quantum Circuits

The another theoretical model proposed for quantum computation is based on Quantum circuits. The Quantum logic gates play the same role in quantum computation as the classical logic gates play in classical computation.

It is simplest to "quantize" NOT gate. We consider quantum NOT gate as a two level system. If the basis states are  $|0\rangle = \begin{bmatrix} 1 \\ 0 \end{bmatrix}$  and  $|1\rangle = \begin{bmatrix} 0 \\ 1 \end{bmatrix}$  then execution of quantum NOT gate on the basis states accomplish following changes:

$$\begin{array}{l} |0\rangle \longrightarrow |1\rangle \\ \begin{bmatrix} 1 \\ 0 \end{bmatrix} \longrightarrow \begin{bmatrix} 0 \\ 1 \end{bmatrix} \end{array}$$

and

$$\begin{array}{l} |1\rangle \longrightarrow |0\rangle \\ \begin{bmatrix} 0 \\ 1 \end{bmatrix} \longrightarrow \begin{bmatrix} 1 \\ 0 \end{bmatrix}. \end{array} \quad (1.3)$$

The execution of quantum NOT gate on the basis states is achieved by a unitary matrix  $U$ ,

$$U = \begin{bmatrix} 0 & 1 \\ 1 & 0 \end{bmatrix} \quad (1.4)$$

which can be written in terms of Pauli spin matrices simply as,

$$U = \sigma^x. \quad (1.5)$$

Then we can express the execution of quantum NOT gate in the following manner,

$$U(\alpha|0\rangle + \beta|1\rangle) = \alpha|1\rangle + \beta|0\rangle. \quad (1.6)$$

In 1985 Deutsch [15] made an important observation that mappings on these basis states uniquely specify the dynamics of an arbitrary initial quantum state, simply on account of the linearity of the Schrodinger equation. In this way of thinking, the time evolution of any quantum gate can be expressed as

$$U = \exp\frac{i}{\hbar} \int H(t)dt. \quad (1.7)$$

or simply for small time  $\Delta t$ ,

$$U = \exp\frac{iH\Delta t}{\hbar}. \quad (1.8)$$

From quantum NOT gate unitary operator it is possible to ‘get back’ the Hamiltonian which time evolution would implement the quantum NOT gate,

To compute H, we first find the matrix P which would diagonalise U,

$$P = \frac{1}{\sqrt{2}} \begin{bmatrix} 1 & 1 \\ 1 & -1 \end{bmatrix}. \quad (1.9)$$

Now eqn. (1.8) can be written as,

$$P^\dagger U P = P^\dagger \exp\frac{iH\Delta t}{\hbar} P. \quad (1.10)$$

or,

$$D = \exp\frac{i\Delta t P^\dagger H P}{\hbar}, \quad (1.11)$$

where D is the diagonalised matrix given by

$$D = \begin{bmatrix} 1 & 0 \\ 0 & -1 \end{bmatrix}. \quad (1.12)$$

We take log on both sides in eqn. (1.8) to get

$$\log D = \frac{i\Delta t P^\dagger H P}{\hbar} \quad (1.13)$$

where

$$\log D = \begin{bmatrix} 0 & 0 \\ 0 & \pi \end{bmatrix}. \quad (1.14)$$

Therefore,

$$H = \frac{\hbar}{i\Delta t} P \log D P^\dagger = \begin{bmatrix} -\frac{\pi\hbar}{2\Delta t} & -\frac{\pi\hbar}{2\Delta t} \\ \frac{\pi\hbar}{2\Delta t} & -\frac{\pi\hbar}{2\Delta t} \end{bmatrix}. \quad (1.15)$$

In terms of Pauli matrices it can be expressed as

$$H = -\frac{\pi\hbar}{2\Delta t} I + \frac{\pi\hbar}{2\Delta t} \sigma^x. \quad (1.16)$$

We have found out here a time independent Hamiltonian but in many other applications it is actually a time-dependent Hamiltonian which is used to execute the quantum gate operation.

One of the gates, which is important in the quantum circuit is quantum Ex-OR gate or the controlled-NOT gate as shown in the figure (1.2). This gate works as follows: the 'a' bit is unchanged while the 'b' bit is transformed to the 'a Ex-OR b' (denoted by  $a \oplus b$ ). The inclusion of the 'a' bit makes the gate reversible. The input is a unique function of the output as shown in the truth table (1.1).

Table 1.1: Truth Table for X-OR gate

Input		Output	
a	b	a'	b'
0	0	0	0
0	1	0	1
1	0	1	1
1	1	1	0

The action of the controlled NOT gate is described as a Hamiltonian process

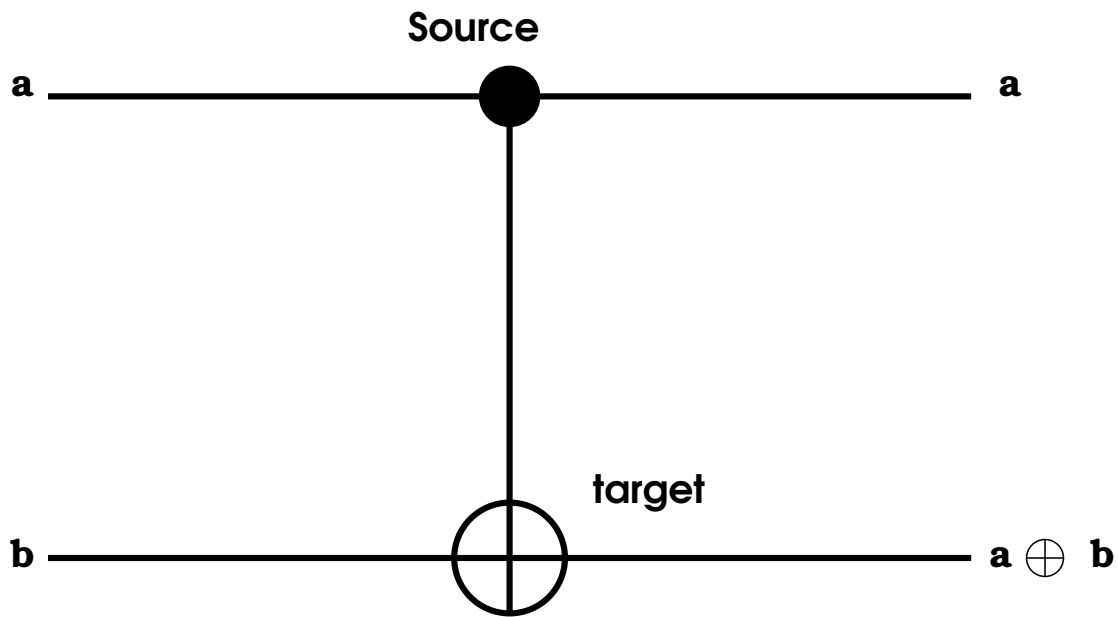


Figure 1.2: Controlled NOT gate

which maps the two-qubit basis states according to the XOR truth table, viz.,

$$\begin{aligned}
 |00\rangle &\rightarrow |00\rangle, \\
 |01\rangle &\rightarrow |01\rangle, \\
 |10\rangle &\rightarrow |11\rangle, \\
 |11\rangle &\rightarrow |10\rangle.
 \end{aligned} \tag{1.17}$$

This can be expressed as unitary time evolution matrix which relates the initial wavefunctions coefficients to the final wavefunctions coefficients. For the quantum Ex-OR the unitary matrix,

$$U = \begin{bmatrix} 1 & 0 & 0 & 0 \\ 0 & 1 & 0 & 0 \\ 0 & 0 & 0 & 1 \\ 0 & 0 & 1 & 0 \end{bmatrix}. \tag{1.18}$$

In terms of Pauli matrices,  $U$  can be written as

$$U = \frac{1 + \sigma^z}{2} \otimes I + \frac{1 - \sigma^z}{2} \otimes \sigma^x. \tag{1.19}$$

The fact that  $U^2 = I$  makes it simple to get back the Hamiltonian using formula  $e^{i\pi U/2} = iU$ . The Hamiltonian is therefore, in terms of Pauli matrices, can be written as

$$H = \frac{\pi\hbar}{2it} \left( \frac{1 + \sigma^z}{2} \otimes I + \frac{1 - \sigma^z}{2} \otimes \sigma^x \right) + \text{constant}. \quad (1.20)$$

Toffoli discovered another quantum gate which is universal gate for quantum computation [14]. This gate is called the Toffoli gate and symbolized in the fig.(1.3). A universal logic gate is one from which one can design a circuit which will evaluate any arbitrary Boolean function. In classical computation, NAND gate is the universal gate.

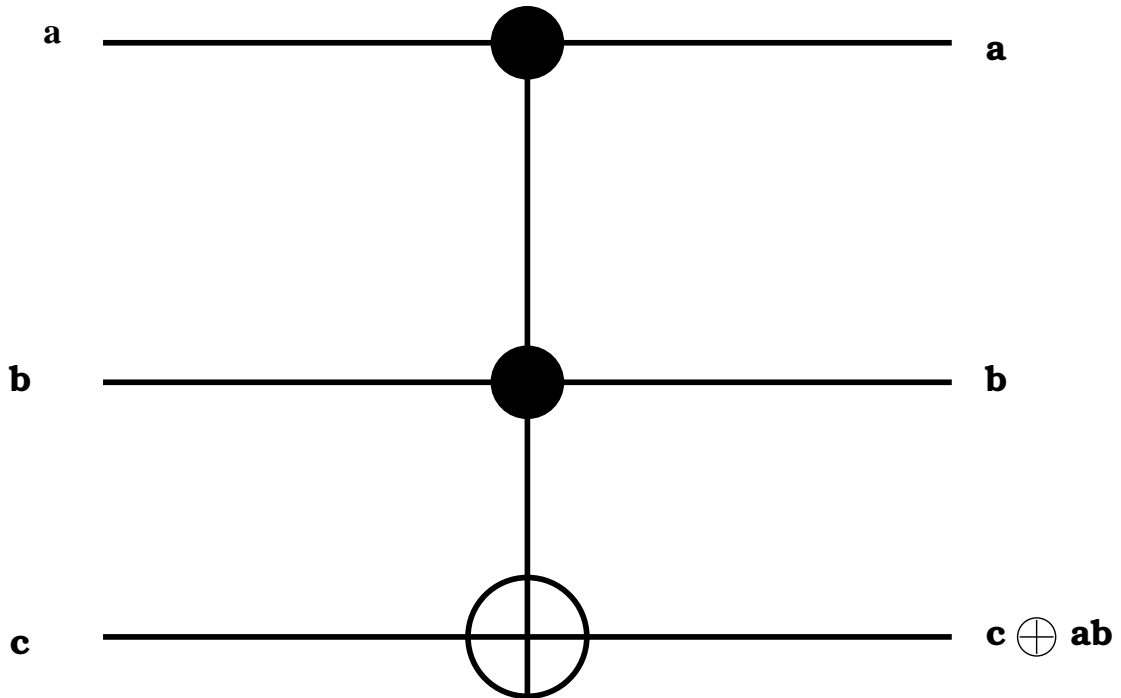


Figure 1.3: Toffoli gate

In Toffoli gate, both input bits 'a' and 'b' are unchanged, while bit 'c' is replaced by ' $c \oplus a \wedge b$ ' as shown in the truth table (1.2). Unitary matrix for Toffoli gate in terms of Pauli spin operators is given by

$$U = \frac{1 + \sigma^z}{2} \otimes I \otimes I + \frac{1 + \sigma^z}{2} \otimes \frac{1 - \sigma^z}{2} \otimes I + \frac{1 + \sigma^z}{2} \otimes \frac{1 - \sigma^z}{2} \otimes \sigma^x. \quad (1.21)$$

Table 1.2: Truth Table for Toffoli gate

Input			Output		
a	b	c	a'	b'	c'
0	0	0	0	0	0
0	0	1	0	0	1
0	1	0	0	1	0
0	1	1	0	1	1
1	0	0	1	0	0
1	0	1	1	0	1
1	1	0	1	1	1
1	1	1	1	1	0

As we show in case of quantum Ex-OR gate, Hamiltonian for this case is also same as  $U$  because  $U^2 = 1$ .

#### 1.2.4 Reversible Computer

Motivated by the work of Landauer [12] about the restrictions which thermodynamics imposes on computation, Charles Bennett [13], found that, in one important respect, thermodynamics does not constrain computation: computation can be done reversibly. In thermodynamics, a process is said to be reversible if there is no increase in entropy. In the classical irreversible computation the energy dissipated is  $KT \ln 2$  per bit operation. Energy dissipated in Reversible computation is zero because it results in no increase of entropy. In the late 70's Tom Toffoli, inspired by the Bennett reversible computer, investigated how reversible computing could be done in the traditional language of Boolean logic gates. He showed that a set of modified gates could be used in place of the traditional Boolean logic gates like AND, OR and NOT. It turned out that quantum computation is a reversible computation because gate operation is done by unitary time evolution operator.

#### 1.2.5 Quantum Algorithm- Deutsch Algorithm

A classical algorithm is a step-by-step procedure for solving a problem, where each step or instruction can be performed on a classical computer. Similarly, a quantum algorithm is a step-by-step procedure, where each of the steps can be performed

on a quantum computer. In other words, a Quantum algorithm gives us a way to solve the problem on Quantum computer.

Various algorithms have been proposed to solve specific problems. In 1994, Peter Shor [16] proposed an algorithm to find out all prime factors of any integer  $N$ . Shor's algorithm takes polynomial time ( $\log N$ ) to factor an integer  $N$ . Luv Grover [17] in 1996 proposed an algorithm for searching an unsorted database with  $N$  entries in  $O(N^{1/2})$  time and using storage space  $O(\log N)$ .

David Deutsch and Richard Jozsa, in 1992 [18], devised an algorithm which can be described by a following game. Anamika, in Agra choose a number  $x$  from 0 to  $2^N - 1$  to mail it in a letter to Bharat, in Bhopal. Bharat evaluates some function and replies with the result. Bharat has been instructed to use a function which is either constant or balanced (returns 1 for half of all possible  $x$  and 0 for the other half). Anamika's task is to find out whether Bharat has chosen a constant function or balanced function.

Classically, Anamika can send only one value of  $x$  in each letter. At worst, she will have to send  $2^{N/2} + 1$  times to tell that Bharat's function is balanced. What would have been the situation if they could exchange qubits instead of bits. According to Deutsch and Jozsa algorithm, Anamika can achieve her goal in just one correspondence with Bharat.

Let us describe here for the sake of brevity and completeness one simpler version of Deutsch-Jozsa algorithm called Deutsch algorithm. In Deutsch algorithm, we are given a boolean function whose input is 1 bit,  $f : \{0, 1\} \rightarrow \{0, 1\}$  and asked if it is constant. We have to check the condition  $f(0) = f(1)$ . It is equivalent to check  $f(0) \oplus f(1)$  (where  $\oplus$  is addition modulo 2). If this is zero, then  $f$  is constant, otherwise  $f$  is not constant. We begin with the two-qubit state  $|0\rangle|1\rangle$  and apply a Hadamard transform to each qubit.

Hadamard Transform is defined as

$$H = \frac{1}{\sqrt{2}} \begin{bmatrix} 1 & 1 \\ 1 & -1 \end{bmatrix}.$$

This gives

$$\frac{1}{2}(|0\rangle + |1\rangle)(|0\rangle - |1\rangle). \quad (1.22)$$

Let us consider a quantum implementation of the function  $f$  which maps  $|x\rangle|y\rangle$  to  $|x\rangle|f(x) \oplus y\rangle$ . Applying this function to our current state we get,

$$\begin{aligned} \frac{1}{2}(|0\rangle(|f(0) \oplus 0\rangle - |f(0) \oplus 1\rangle) + |1\rangle(|f(1) \oplus 0\rangle - |f(1) \oplus 1\rangle)) &= \frac{1}{2}((-1)^{f(0)} \\ &\quad |0\rangle(|0\rangle - |1\rangle) + (-1)^{f(1)}|1\rangle(|0\rangle - |1\rangle)) \\ &= (-1)^{f(0)}\frac{1}{2}(|0\rangle + (-1)^{f(0)\oplus f(1)}|1\rangle)(|0\rangle - |1\rangle). \end{aligned} \quad (1.23)$$

We ignore the last bit and the global phase factor and therefore have the state

$$\frac{1}{\sqrt{2}}(|0\rangle + (-1)^{f(0)\oplus f(1)}|1\rangle). \quad (1.24)$$

Applying again a Hadamard transform to this state, we get

$$\begin{aligned} \frac{1}{2}(|0\rangle + |1\rangle + (-1)^{f(0)\oplus f(1)}|0\rangle - (-1)^{f(0)\oplus f(1)}|1\rangle) &= \frac{1}{2}((1 + (-1)^{f(0)\oplus f(1)})|0\rangle \\ &\quad + (1 - (-1)^{f(0)\oplus f(1)})|1\rangle). \end{aligned} \quad (1.25)$$

Obviously  $f(0) \oplus f(1) = 0$  if and only if we get  $|0\rangle$ . Therefore the function is constant if and only if we get zero.

## 1.3 Fault tolerant Quantum Computation

Fault-tolerance is the property that enables a computer to operate properly in the event of the failure of one or more faults within some of its components.

### 1.3.1 Quantum Decoherence

The essential property of a qubit in all physical realisations of quantum computers exploits is the existence of nonlocal correlations among the different parts of a physical system and with environment. The interactions between a quantum device and its environment establish nonlocal correlations between the two. If someone looks at only part of the system at a time, he can decode only very little of the information encoded in the system. Due to such nonlocal correlations, encoded information decay quite rapidly in practice. This phenomenon is known as quantum decoherence. The problem is, our quantum system is, inevitably in



contact with a larger system, its environment. It is impossible to perfectly isolate a big quantum system from its environment. Eventually, the quantum information that we initially encoded in the device becomes encoded in correlations between the device and the environment. Then, we can no longer access the information by observing only the device. In other words, the information is irrevocably lost. In order to operate a quantum computer reliably, we must find a way to prevent or correct these errors, which means isolating the system from its environment.

### 1.3.2 Other Errors

Decoherence is not the only problem. Even if we could achieve perfect isolation from the environment, we can not expect a quantum gate operation to implement on a qubit or quantum computer with perfect accuracy [20]. The quantum gates that the machine executes are unitary transformations that operate on a qubit. These unitary matrices form a continuum. We may have a protocol for applying  $U_0$  to qubits, but our execution of the protocol will not be flawless, so the actual transformation  $U$ ,

$$U = U_0(1 + O(\epsilon)) \tag{1.26}$$

will differ from  $U_0$  by some amount of order  $\epsilon$ . After about  $1/\epsilon$  gates are applied, these errors will accumulate and induce a serious failure.

Classical devices have similar problems, but small errors are much less of a problem for devices that perform boolean logic. They achieve such a high accuracy with dissipation. We can think of a classical gate acting on a bit, as a ball residing at one of the two minima of a double-well potential. The gate may push the ball over the intervening barrier to the other side of the potential. Of course, the gate won't be implemented perfectly; it may push the ball a little too hard. Over time, these imperfections might accumulate and cause an error. To improve the performance, we cool the bit after each gate. This is a dissipative process that releases heat to the environment and compresses the phase space of the ball, bringing it close to the local minimum of the potential. So the small errors that we may make result in heating the environment rather than compromising the performance of the device. We cannot cool a quantum computer this way. Interaction

with the environment would destroy encoded quantum information.

A sophisticated machinery called Quantum error correcting codes has been developed to handle these and other errors. This method works on the lines of classical error correcting codes. We have to, basically, ‘quantize’ the **Classical Error Correcting Code**. Let us describe some simple classical code namely repetition code. We replace the bit we wish to protect by 3 copies of the bit,

$$\begin{aligned} 0 &\rightarrow (000) \\ 1 &\rightarrow (111). \end{aligned} \tag{1.27}$$

Now an error may occur that causes one of the three bits to flip; if it’s the first bit, say,

$$\begin{aligned} (000) &\rightarrow (100) \\ (111) &\rightarrow (011). \end{aligned} \tag{1.28}$$

Now in spite of the error, we can still decode the bit correctly, by majority voting.

Of course, if the probability of error in each bit were  $p$ , it would be possible for two of the three bits to flip, or even for all three to flip. A double flip can happen in three different ways, so the probability of a double flip is  $3p^2(1-p)$ , while the probability of a triple flip is  $p^3$ . Altogether, then, the probability that majority voting fails is  $3p^2(1-p) + p^3 = 3p^2 - 2p^3$ . But for  $3p^2 - 2p^3$  to be less than  $p$ ,  $p$  has to be greater than  $\frac{1}{2}$ . Thus, a classical computer with noisy components can work reliably, by employing sufficient redundancy.

Similarly, we can enhance the reliability of quantum computer by employing redundancy in qubit in following manner,

$$a|0\rangle + b|1\rangle \rightarrow a|\bar{0}\rangle + b|\bar{1}\rangle = a|000\rangle + b|111\rangle. \tag{1.29}$$

But we can immediately see that there are difficulties at the quantum level while employing redundancy.

**1. Phase errors.** With quantum information, more things can go wrong. In

addition to bit-flip errors

$$\begin{aligned} |0\rangle &\rightarrow |1\rangle \\ \text{and } |1\rangle &\rightarrow |0\rangle, \end{aligned} \tag{1.30}$$

there can also be phase errors

$$\begin{aligned} |0\rangle &\rightarrow |0\rangle \\ \text{and } |1\rangle &\rightarrow -|1\rangle. \end{aligned} \tag{1.31}$$

A phase error is serious, because it makes the state  $\frac{1}{\sqrt{2}}(|0\rangle + |1\rangle)$  flip to the orthogonal state  $\frac{1}{\sqrt{2}}(|0\rangle - |1\rangle)$ . The classical method is designed to correct large (bit flip) errors. But phase error kind of situation does not occur in classical coding.

**2. Small errors.** As already noted, quantum information is continuous. If a qubit is supposed to be in the state

$$a|0\rangle + b|1\rangle, \tag{1.32}$$

an error might change  $a$  and  $b$  by an amount of order  $\epsilon$ , and these small errors can accumulate over time.

**3. Measurement causes disturbance.** In the majority voting scheme, we are expected to measure the bits in the code to detect and correct the errors. But we can't measure qubits without disturbing the quantum information that they encode because measurement would destroy the quantum state.

**4. No cloning.** With classical coding, we protect information by making extra copies of it. But quantum information cannot be copied with perfect fidelity.

These error corrections in qubit and protection of qubit from decoherence is called **Fault tolerant quantum computation**. For a fault tolerant Quantum computation Quantum error correcting codes are used which is our next topic.

## 1.4 Quantum Error Correcting Codes

The one way to understand how quantum error correction works is to examine Shor's original code [20, 21]. It is a straightforward 'quantization' of the classical

3-bit repetition code.

We encode a single qubit with 3 qubits,

$$\begin{aligned} |0\rangle &\rightarrow |\bar{0}\rangle = |000\rangle \\ \text{and } |1\rangle &\rightarrow |\bar{1}\rangle = |111\rangle, \end{aligned} \tag{1.33}$$

or, in other words, we encode a superposition

$$a|0\rangle + b|1\rangle \rightarrow a|\bar{0}\rangle + b|\bar{1}\rangle = a|000\rangle + b|111\rangle. \tag{1.34}$$

Suppose we want to correct a bit flip error without destroying this superposition. If we measure the encoded qubit and get the result  $|\bar{0}\rangle$ , then we end up preparing the state  $|\bar{0}\rangle$  of all three qubits, and we have lost the quantum information encoded in the coefficients  $a$  and  $b$ .

In shor's code we measure a 3-qubit state  $|x, y, z\rangle$  by the two-qubit observables  $Y \oplus Z$  and  $X \oplus Z$  (where  $\oplus$  denotes addition modulo 2). Let us define the action of  $X$ ,  $Y$  and  $Z$  on 3-qubit state  $|x, y, z\rangle$ ,

$$\begin{aligned} X|x, y, z\rangle &= x|x, y, z\rangle, \\ Y|x, y, z\rangle &= y|x, y, z\rangle \\ \text{and } Z|x, y, z\rangle &= z|x, y, z\rangle. \end{aligned} \tag{1.35}$$

If the first bit flips i.e.

$$a|000\rangle + b|111\rangle \rightarrow a|100\rangle + b|011\rangle, \tag{1.36}$$

then the measurement of  $(Y \oplus Z, X \oplus Z)$  gets the result  $(0,1)$ , which is the binary equivalent of 1 indicating to flip the first bit and repair the error.

If the second bit flips i.e.

$$a|000\rangle + b|111\rangle \rightarrow a|010\rangle + b|101\rangle, \tag{1.37}$$

then the measurement of  $(Y \oplus Z, X \oplus Z)$  gets the result  $(1,0)$ , which is the binary equivalent of 2 indicating to flip the second bit and repair the error.

Similarly, if the third bit flips, one can check that measurement of  $(Y \oplus Z, X \oplus Z)$

gets the result (1,1), which is the binary equivalent of 3 indicating to flip the third bit and repair the error.

All these 3-qubit states are eigenstates of two qubit observables ( $Y \oplus Z, X \oplus Z$ ), therefore, after the measurement they remain in the same state which means that measurement by these two qubit observables has not destroyed the eigenstate. Thus, we have diagnosed the error without destroying the 3-qubit state.

Instead of bit flip errors, there can be small errors: let us consider an error in first bit,

$$\begin{aligned} |000\rangle &\rightarrow |000\rangle + \epsilon|100\rangle, \\ |111\rangle &\rightarrow |111\rangle - \epsilon|011\rangle. \end{aligned} \tag{1.38}$$

In this case too we can show that above procedure works well. Again, we act two qubit observable ( $Y \oplus Z, X \oplus Z$ ) on the three qubit state getting the result (0, 0) corresponding to the original state  $a|000\rangle + b|111\rangle$  and (0, 1) corresponding to the bit flip state  $|100\rangle + b|011\rangle$ . So, when we get the result (0, 0) we project the damaged state to the original state but when we get (0, 1), the damaged state is projected to  $|100\rangle + b|011\rangle$  but the result (0, 1) indicates the error at the first bit. Thus, protection against the small errors can also be achieved.

Now we want to protect against phase errors. In phase error our encoded state  $a|0\rangle + b|1\rangle$  gets transformed to  $a|0\rangle - b|1\rangle$  and the encoded quantum information gets damaged. As we protected the qubit against bit-flip errors by encoding bits redundantly, we protect against phase-flip by encoding phases redundantly as follows:

$$\begin{aligned} |0\rangle &\rightarrow (|000\rangle + |111\rangle) (|000\rangle + |111\rangle) (|000\rangle + |111\rangle) \\ \text{and } |1\rangle &\rightarrow (|000\rangle - |111\rangle) (|000\rangle - |111\rangle) (|000\rangle - |111\rangle). \end{aligned} \tag{1.39}$$

Now suppose that a phase flip occurs, say, in the first cluster,

$$\begin{aligned} |000\rangle + |111\rangle &\rightarrow |000\rangle - |111\rangle, \\ \text{and } |000\rangle - |111\rangle &\rightarrow |000\rangle + |111\rangle. \end{aligned} \tag{1.40}$$

Then, the nine qubit state becomes

$$\begin{aligned} |0\rangle &\rightarrow (|000\rangle - |111\rangle)(|000\rangle + |111\rangle)(|000\rangle + |111\rangle) \\ \text{and } |1\rangle &\rightarrow (|000\rangle + |111\rangle)(|000\rangle - |111\rangle)(|000\rangle - |111\rangle). \end{aligned} \quad (1.41)$$

This means that the relative phase of the damaged cluster differs from the phases of the other two clusters.

We would need six qubit observables to diagnose the error,

$$Z_1 Z_2 Z_3 Z_4 Z_5 Z_6, Z_4 Z_5 Z_6 Z_7 Z_8 Z_9.$$

A phase error in any one of the qubit in a particular cluster will change the value of  $ZZZ$  in that cluster relative to other two clusters resulting in the identification of the cluster in which the error has occurred.

Here, for the sake of brevity and completeness, we want to mention that other error corrections like large bit flip error, small bit flip error etc. have been achieved in nine qubit code as mentioned in three qubit code.

Thus, Shor's code restores the quantum state irrespective of the nature of the error and we can say that the code protects against decoherence and achieves fault tolerance.

## 1.5 Physical Realisations

For physical realisation of a quantum computer, we need technology which enables us to manipulate qubits. The machine will need to meet some stringent criteria:

**1. Storage:** We need to store qubits for a long time, long enough to complete an computation.

**2. Isolation:** The qubits must be well isolated from the environment to minimize decoherence errors.

**3. Readout:** We need to measure the qubits efficiently and reliably.

**4. Gates:** We need to manipulate the quantum states of individual qubits, and to induce controlled interactions among qubits so that we can perform quantum gates.

**5. Precision:** The quantum gates should be implemented with high precision if the device is to perform reliably.

There are a number of physical realisations proposed for quantum computer, for example in Ion traps, Nuclear Magnetic Resonance and Optical Cavity Quantum Electro-Dynamics (QED).

### 1.5.1 Ion Trap Method

One possible realisation, suggested by Ignacio Cirac and Peter Zoller [22], is Ion trap method. In this method, a string of ions is confined by a combination of oscillating and static electric fields in a linear ‘Paul trap’ in high vacuum ( $10^{-8}Pa$ ). A single laser beam is split by beam splitters into many beam pairs, one pair illuminating each ion. Each ion has two long-lived states,  $|g\rangle$  and  $|e\rangle$ . Each laser beam pair can drive coherent Raman transitions between the internal states of the relevant ion. This allows any single qubit quantum gate to be applied to any ion. The two-qubit gates requires an interaction between ions which is provided by their Coulomb repulsion.

The main experimental problem in the ion trap method is to cool the string of ions to the ground state of the trap (a microKelvin temperature), and the main reason of decoherence is the heating of this motion due to the coupling between the charged ion string and noise voltages in the electrodes.

### 1.5.2 Nuclear Magnetic Resonance

DeVincenzo [23] first suggested the use of nuclear spins in quantum computation. Gershenfeld and Chuang [24], and independently, Cory, Fahmy, and Havel [25] pointed out that Nuclear Magnetic Resonance (NMR) provides a useful implementation of quantum computation. In this scheme qubits are carried by nuclear spins in a particular molecule. Each spin can either be aligned ( $|\uparrow\rangle = |0\rangle$ ) or antialigned ( $|\downarrow\rangle = |1\rangle$ ) with an applied constant magnetic field. The spins take a long time to relax or decohere, therefore the qubits can be stored for a reasonable time.

In NMR, we apply a rotating magnetic field with frequency  $\omega$  (where  $\omega$  is the energy splitting between the spin-up and spin-down states), and induce Rabi oscillations of the spin. By timing the pulse suitably, we can perform a desired unitary transformation on a single spin. All the spins in the molecule are exposed to the rotating magnetic field but only those on resonance respond.

Furthermore, the spins have dipole-dipole interactions, and this coupling can be exploited to perform a gate operation. The splitting between  $|\uparrow\rangle$  and  $|\downarrow\rangle$  for one spin depends on the state of neighboring spins. So, whether a driving pulse is on resonance to tip the spin over is conditioned on the state of another spin.

In NMR systems, the typical temperature might be of order of a million times larger than the energy splitting between  $|0\rangle$  and  $|1\rangle$ . This means that the quantum state of our computer (the spins in a single molecule) is very noisy because it is subjected to strong thermal fluctuations. This noise will destroy the quantum information. Another problem with NMR systems is that we actually perform our measurement not on a single molecule, but on a macroscopic sample containing of order  $10^{23}$  computers, and the signal we read out of this device is actually averaged over this ensemble. Quantum algorithms are probabilistic, because of the randomness of quantum measurement. Hence, averaging over the ensemble may destroy the results. Gershenfeld and Chuang and Cory, Fahmy and Havel explained how to overcome these difficulties. They described how ‘effective pure states’ can be prepared, manipulated, and monitored by performing suitable operations on the thermal ensemble. The idea is to arrange for the fluctuating properties of the molecule to average out when the signal is detected, so that only the underlying coherent properties are measured.

But there are serious limitations with NMR method. The ratio of the coherent signal to the background declines exponentially with the number of spins per molecule. In practice, it is be very challenging to perform an NMR quantum computation with more than 10 qubits.

### 1.5.3 Optical Cavity QED

An alternative hardware design based on optical cavity is suggested by Pellizzari, Gardiner, Cirac, and Zoller) [26]. In this method, several neutral atoms are kept in optical cavities of very high Quality. Quantum information can again be stored in the internal states of the atoms and atoms interact because they are all coupled to the normal modes of the electromagnetic field in the cavity. In a very high-quality optical cavity, a strong coupling can be achieved between a single atom or ion and a single mode of the electromagnetic field. This coupling can be used to apply quantum gates between the field mode and the ion.



## 1.6 Topological Quantum Computation

Topological concepts can be applied in quantum error correction to achieve fault-tolerant computation [27]. Topology concerns the global properties of an object that remain unchanged when we deform the object locally. The central idea of quantum error correction is to store and manipulate quantum information in a ‘global’ form that is protected from local disturbances. A fault-tolerant gate should be designed to act on this global qubit in such a way that the action it performs on the encoded data remains unchanged even if we deform the gate slightly, that is, even if the implementation of the gate is not perfect.

In our search for physical realisation of fault-tolerant quantum computation, we look for systems in which physical interactions have a topological character. There is one such example before us - the Aharonov-Bohm effect. If an electron is moved around a perfect magnetic solenoid (perfect in the sense that outside magnetic field is zero), its wave function acquires a phase  $e^{ie\phi}$ , where  $e$  is charge of electron charge and  $\phi$  is the magnetic flux enclosed by the solenoid. The Aharonov-Bohm phase is a topological property of the path traversed by the electron because it depends only on how many times the electron moves around the solenoid and is unchanged when the path is smoothly deformed. Therefore, if a qubit can be encoded in a form that can be measured and manipulated through Aharonov-Bohm interactions or topological interactions that are immune to local disturbances then realisation of fault tolerant quantum computer is possible.

Another way we can describe a topological quantum computer is through two-dimensional quasiparticle called anyon, whose world lines cross over one another to form braids in a three-dimensional spacetime (one temporal plus two spatial dimensions). These braids form the Quantum logic gates which has to be applied on qubit or anyons. When anyons are braided, the transformation of the quantum state of the system depends only on the topological class of the anyons’ trajectories (which are classified according to the braid group). Hence, local perturbations do not change the topological properties of the braids and therefore cannot introduce errors in the quantum computation. In 2005, Sankar Das Sarma, Michael Freedman, and Chetan Nayak [29] proposed a quantum Hall device which would realise a topological qubit.

### 1.6.1 Anyon and Non-abelian Anyon

In space of three or more dimensions, indistinguishable particles are either Fermions or Bosons, according to their statistical behaviour. Fermions obey the so-called Fermi-Dirac statistics while Bosons obey the Bose-Einstein statistics. Let us consider the behavior of two particle states under the exchange of particles.

$$|x_1x_2\rangle = \pm |x_2x_1\rangle \quad (1.42)$$

The left hand side denotes the state in which particle 1 is at position  $x_1$  and particle 2 at position  $x_2$  and right hand side denotes the position in which particle 1 is at position  $x_2$  and particle 2 at position  $x_1$ . Here the '+' corresponds to both particles being bosons and the '-' to both particles being fermions.

In two-dimensional systems, however, quasiparticles can be observed which obey statistics ranging continuously between Fermi-Dirac and Bose-Einstein statistics [28]. This looks as follows:

$$|x_1x_2\rangle = e^{i\theta} |x_2x_1\rangle, \quad (1.43)$$

where  $\theta$  is a real number. In the case  $\theta = \pi$ , we recover the Fermi-Dirac statistics (minus sign) and in the case  $\theta = 0$ , the Bose-Einstein statistics (plus sign).

Phase factor  $\theta$  can also be viewed as Berry's phase and calculated accordingly to find out the time evolution of a non-degenerate state under adiabatic approximation. When we consider the time evolution of a degenerate state under the same approximation,  $\theta$  doesn't remain a scalar and becomes a matrix,

$$|x_1\sigma_1; x_2\sigma_2\rangle = U_{\sigma_1\sigma_2; \sigma'_1\sigma'_2} |x_2\sigma'_2; x_1\sigma'_1\rangle, \quad (1.44)$$

where  $\sigma$ 's denotes the spin degree of freedom. These kind of quasi-particles are called Non-abelian anyons.

When non-abelian anyons are braided, the transformation of the quantum state of the system depends only on the topological class of the anyonic trajectories which are classified according to the braid group. Therefore, the quantum information which is stored in the state of the system is protected from small errors in the trajectories [29].

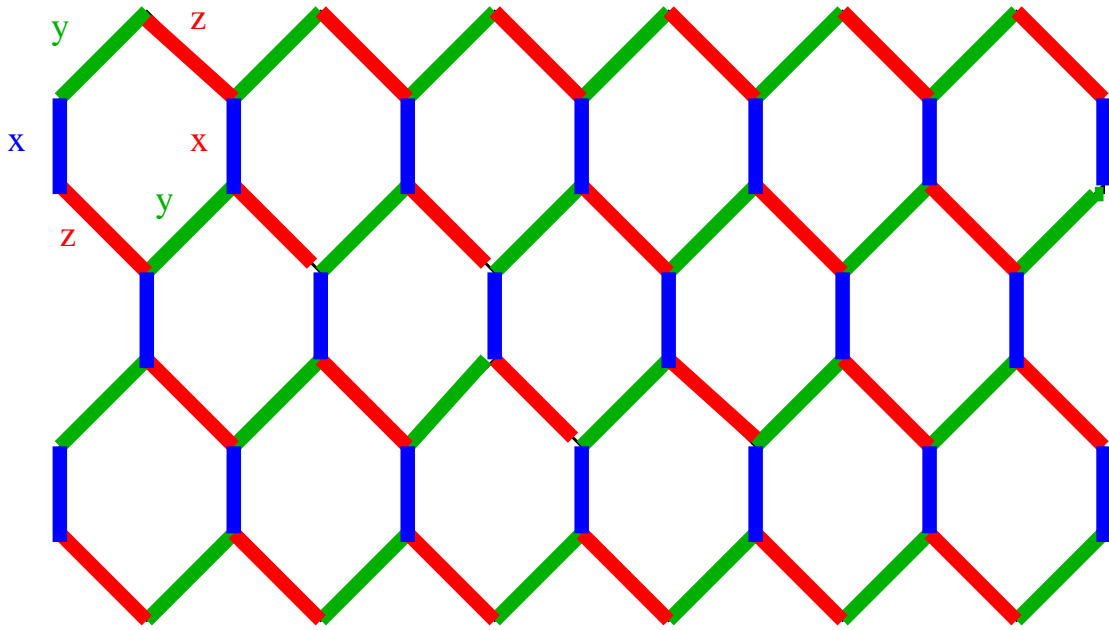


Figure 1.4: The Kitaev Model. The  $x$ ,  $y$  and  $z$  bonds are as indicated.

Non-abelian anyons are theoretically predicted to occur in certain fractional quantum Hall states like  $\nu = 5/2$  [30] and Kitaev's model [2, 31]. There is also theoretical work showing how they could be realised in quantum circuits [32]. Very recently, non-abelian anyons have also been found in various 3 dimensional systems [33, 34].

### 1.6.2 Kitaev Model

In Kitaev's scheme of topological computation, two non-abelian anyons are used as a qubit. He presented a remarkable solvable spin-1/2 model on a honeycomb lattice as shown in figure (1.4) [2], where he could perform braiding operation on a non-abelian anyons.

Kitaev's Hamiltonian is written as follows,

$$H = J_x \sum_{\langle ij \rangle} \sigma_i^x \sigma_j^x + J_y \sum_{\langle ij \rangle} \sigma_i^y \sigma_j^y + J_z \sum_{\langle ij \rangle} \sigma_i^z \sigma_j^z. \quad (1.45)$$

Using the fact that some operators exist which commute with Hamiltonian, Kitaev showed that above Hamiltonian can be solved exactly. In honeycomb model

corresponding to each plaquette  $p$ , one operator  $W_p$  exists,

$$W_p = \sigma_1^x \sigma_2^y \sigma_3^z \sigma_4^x \sigma_5^y \sigma_6^z. \quad (1.46)$$

Because of commuting operators the problem reduces to solving a theory of non-interacting Majorana fermions in the background of static  $Z_2$  gauge field configurations. For the sake of brevity, we will describe all the terminology and machinery of Majorana fermions on a 4 site system in the next section.

Kitaev's honeycomb model can be generalised to a variety of other lattices [35, 36, 37, 38, 39]. The generalised Kitaev models are integrable in the sense that they all reduce to systems of non-interacting Majorana fermions. It can be constructed on any lattice with coordination number three, if all the bonds can be coloured using three colours. It has been shown that all such models can be realised in cold atom systems [40] and using Josephson junction quantum circuits [4] which we will discuss in the another section.

## 1.7 Qubits from Zero mode Majorana Fermions

In the Kitaev model, two non-abelian anyons form a qubit. These two qubits are constructed from two degenerate quantum states of the model. These degenerate states arise because of existence of zero mode solutions in the single particle spectrum. In order to perform braiding operation on non abelian anyons, we should be able to make these zero modes move on the lattice independently. Let us describe the unpairing of these zero modes on a simple 4-site model. The model is shown in figure (1.5).

### 1.7.1 Hamiltonian

Hamiltonian is given by

$$H = J_x (\sigma_1^x \sigma_2^x + \sigma_3^x \sigma_4^x) + J_y (\sigma_1^y \sigma_2^y + \sigma_3^y \sigma_4^y) + J_z (\sigma_2^z \sigma_3^z). \quad (1.47)$$

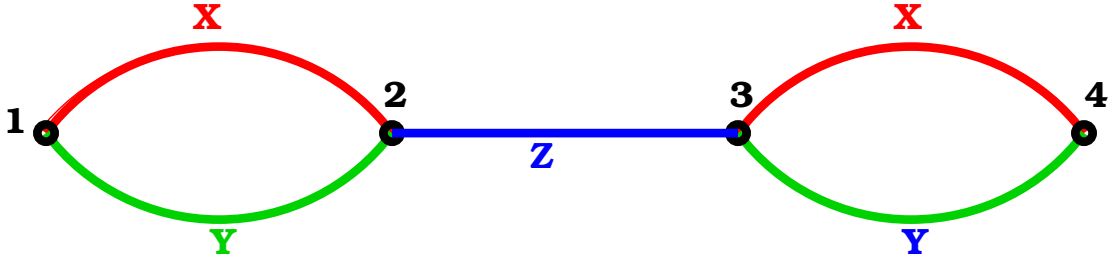


Figure 1.5: The 4 site XY-Ising Model. The  $x, y$  and  $z$  bonds are as indicated.

Commuting operators are

$$\begin{aligned} W_1 &= \sigma_1^z \sigma_2^z \\ \text{and } W_2 &= \sigma_3^z \sigma_4^z. \end{aligned} \quad (1.48)$$

### 1.7.2 Jordan-Wigner Transformation

Let us define Jordan-Wigner Transformation,

$$\begin{aligned} \sigma_j^y &= (c_j^+ + c_j) \exp \left( i\pi \sum_{i < j} c_i^+ c_i \right), \\ \sigma_j^z &= -i(c_j^+ - c_j) \exp \left( i\pi \sum_{i < j} c_i^+ c_i \right) \\ \text{and } \sigma_j^x &= 2c_j^+ c_j - 1 \equiv -(c_j^+ + c_j)(c_j^+ - c_j). \end{aligned} \quad (1.49)$$

where  $c_j^+$  and  $c_j$  are creation and annihilation operators and they follow the usual anti-commutation relation.

We can write the Hamiltonian in Jordan-Wigner basis as follows,

$$\begin{aligned} H &= J_x (c_1^+ + c_1)(c_1^+ - c_1)(c_2^+ + c_2)(c_2^+ - c_2) \\ &+ (c_3^+ + c_3)(c_3^+ - c_3)(c_4^+ + c_4)(c_4^+ - c_4) \\ &+ J_y \left( (c_1^+ - c_1)(c_2^+ + c_2) + (c_3^+ - c_3)(c_4^+ + c_4) \right) \\ &- J_z \left( (c_2^+ + c_2)(c_3^+ - c_3) \right). \end{aligned} \quad (1.50)$$

### 1.7.3 Majorana Fermions

Let us define two hermitian operators called **Majorana operators**,

$$\begin{aligned}\xi_j &= (c_j^\dagger + c_j), \\ \eta_j &= \frac{1}{i}(c_j^\dagger - c_j).\end{aligned}\tag{1.51}$$

It can be checked that  $\xi_j^\dagger = \xi_j$  and  $\eta_j^\dagger = \eta_j$ . Two Majorana operators have to be paired to form a fermionic creation or annihilation operators.

These operators follow the fermion like anti-commutation relations,

$$\begin{aligned}\{\xi_i, \xi_j\} &= 2\delta_{i,j}, \\ \{\eta_i, \eta_j\} &= 2\delta_{i,j}, \\ \text{and } \{\xi_i, \eta_j\} &= 0.\end{aligned}\tag{1.52}$$

In terms of Majorana fermions, Hamiltonian,

$$\begin{aligned}H &= J_x (i\xi_1\eta_1i\xi_2\eta_2 + i\xi_3\eta_3i\xi_4\eta_4) \\ &+ J_y (i\eta_1\xi_2 + i\eta_3\xi_4) \\ &- J_z (i\xi_2\eta_3).\end{aligned}\tag{1.53}$$

Rotating the axis at odd sites,

$$\begin{aligned}\xi_1 &\rightarrow \eta_1, \eta_1 \rightarrow -\xi_1, \\ \xi_3 &\rightarrow \eta_3, \eta_3 \rightarrow -\xi_3.\end{aligned}\tag{1.54}$$

The Hamiltonian then becomes

$$\begin{aligned}H &= - J_x (i\eta_1\eta_2\xi_1i\xi_2 + i\eta_3\eta_4\xi_3i\xi_4) \\ &- J_y (i\xi_1\xi_2 + i\xi_3\xi_4) \\ &+ J_z (i\xi_2\xi_3).\end{aligned}\tag{1.55}$$

In the rotated basis, commuting operators

$$\begin{aligned}\hat{u}_1 &= i\eta_1\eta_2 \\ \text{and } \hat{u}_2 &= i\eta_3\eta_4.\end{aligned}\tag{1.56}$$

Therefore, we can write Hamiltonian as

$$\begin{aligned}H &= -J_x(\hat{u}_1\xi_1i\xi_2 + \hat{u}_2\xi_3i\xi_4) \\ &- J_y(i\xi_1\xi_2 + i\xi_3\xi_4) \\ &+ J_z(i\xi_2\xi_3).\end{aligned}\tag{1.57}$$

As  $\hat{u}_1^2 = 1$  and  $\hat{u}_2^2 = 1$  and  $\hat{u}_1$  and  $\hat{u}_2$  commute with Hamiltonian, these operators can be replaced by their eigenvalues  $u_i = \pm 1$ ,

$$H = -(u_1J_x + J_y)i\xi_1\xi_2 + (u_2J_x + J_y)i\xi_3\xi_4 + J_zi\xi_2\xi_3.\tag{1.58}$$

Thus, the problem reduces to solving a theory of non-interacting Majorana fermions in the background of static  $Z_2$  gauge field configurations.

#### 1.7.4 Zero Mode Majorana Fermions and Unpairing

Being a non-interacting Hamiltonian, it can be written as

$$H = \sum_{i,j} \xi_i^+ h_{i,j} \xi_j.\tag{1.59}$$

To diagonalise Hamiltonian, we substitute

$$\xi_i = \sum_n \phi_i^{n*} \chi^n,\tag{1.60}$$

where  $\phi_i^n$  is found out by solving single particle eigenvalue equation,

$$\sum_j h_{i,j} \phi_j^n = \epsilon_n \phi_i^n.\tag{1.61}$$

The eigenvectors  $\phi_i^n$ 's follow orthogonality and completeness relation,

$$\begin{aligned} \sum_i \phi_i^{m*} \phi_i^n &= \delta_{m,n} \\ \text{and } \sum_n \phi_i^{n*} \phi_j^n &= \delta_{i,j}. \end{aligned} \quad (1.62)$$

Or inversely,

$$\chi^n = \sum_i \phi_i^n \xi_i. \quad (1.63)$$

And h is given by

$$h = \begin{bmatrix} 0 & -i(u_1 J_x + J_y) & 0 & 0 \\ i(u_1 J_x + J_y) & 0 & iJ_z & 0 \\ 0 & -iJ_z & 0 & -i(u_2 J_x + J_y) \\ 0 & 0 & i(u_2 J_x + J_y) & 0 \end{bmatrix}. \quad (1.64)$$

For any non zero  $\epsilon_n$ , we can see that

$$\begin{aligned} h_{i,j}^* \phi_j^{n*} &= \epsilon_n \phi_i^{n*} \\ \text{or } h_{i,j} \phi_j^{n*} &= -\epsilon_n \phi_i^{n*} \end{aligned} \quad (1.65)$$

where we used the fact that  $h^* = -h$ .

Therefore the eigenvalues come in pairs. The wavefunctions  $\phi_i^n$  and  $\phi_i^{*n}$  belong to positive and negative energy modes, peak around same site. This is called pairing of Majorana fermions. Let us consider n=1 and 2, n=3 and 4 are complex conjugate modes. Then one can show from eqn.(1.63),

$$\begin{aligned} \chi^{1\dagger} &= \chi^2, \\ \text{and } \chi^{3\dagger} &= \chi^4. \end{aligned} \quad (1.66)$$

then Hamiltonian in diagonalised space reduces to

$$H = \epsilon_1 (2\chi^{1\dagger} \chi^1 - 1) + \epsilon_3 (2\chi^{3\dagger} \chi^3 - 1). \quad (1.67)$$



Multiparticle eigenstates are

$$|0\rangle, \chi^{1\dagger}|0\rangle, \chi^{3\dagger}|0\rangle, \chi^{1\dagger}\chi^{3\dagger}|0\rangle \quad (1.68)$$

where  $|0\rangle$  is defined by  $\chi^1|0\rangle = 0, \chi^3|0\rangle = 0$ .

Something very interesting happens in single particle eigenequation for  $\epsilon_n = 0$  which is called zero mode solutions. For zero mode, two independent and denenerate solutions  $\phi^{(1)}$  and  $\phi^{(2)}$  exist,

$$\begin{aligned} h\phi^{(1)} &= 0 \\ \text{and } h\phi^{(2)} &= 0. \end{aligned} \quad (1.69)$$

Then, both the eigenvectors  $\phi^{(1)}$  and  $\phi^{(2)}$  belonging to zero mode differ. Hence, probability amplitudes  $|\phi^{(1)}|^2, |\phi^{(2)}|^2$  are different and peak around different sites. This is known as unpairing of zero mode Majorana fermions.

When zero mode eqn.(1.69) is solved for Hamiltonian (1.64), it turns out that zero mode exists for  $J_x = J_y$  for either  $u_1 = -1$  or  $u_2 = -1$ . For example, let us write the zero mode solution for  $u_1 = +1$  and  $u_2 = -1$ ,

$$\phi^{(1)} = \begin{bmatrix} 0 \\ 0 \\ 0 \\ 1 \end{bmatrix}, \phi^{(2)} = \frac{J}{\sqrt{J^2 + J_z^2}} \begin{bmatrix} -\frac{J_z}{J} \\ 0 \\ 1 \\ 0 \end{bmatrix} \quad (1.70)$$

where  $J_x = J_y = J$ .

For zero mode we can redefine  $\phi^{(1)}$  and  $\phi^{(2)}$  by,

$$\begin{aligned} \phi^{(01)} &\rightarrow (\phi^{(1)} + i\phi^{(2)}) \\ \phi^{(02)} &\rightarrow (\phi^{(1)} - i\phi^{(2)}). \end{aligned} \quad (1.71)$$

The Hamiltonian in eqn.(1.67) becomes

$$H = \epsilon_1 (2\chi^{01\dagger}\chi^{01} - 1) + \epsilon_3 (2\chi^{3\dagger}\chi^3 - 1), \quad (1.72)$$

where

$$\chi^{01} = \sum_i \phi_i^{(01)} \xi_i. \quad (1.73)$$

Here, multiparticle states  $|0\rangle, \chi^{01\dagger}|0\rangle$  belong to the degenerate energy states. Let us call them  $|0\rangle$  and  $|1\rangle$  of our proposed qubit.

The non-abelian anyons are realised in the system with these unpaired Majorana modes [41]. In a fermionic system with  $N$  zero energy modes, there are  $2N$  Majorana modes. If these  $2N$  modes can be independently moved around each other, then the geometric phase picked up corresponds to a non-abelian representation of the braid group. The geometric phase picked up is a unitary matrix which represents quantum logic gate operation on the qubit.

## 1.8 Unitary Gate Operation on the Qubit

Let us consider a system where we have four zero modes  $\phi_i^1, \phi_i^2, \phi_i^3$  and  $\phi_i^4$ .

For zero modes we can define  $\chi^{01}$  and  $\chi^{02}$  as

$$\begin{aligned} \chi^{01} &= \sum_i (\phi_i^{1*} + i\phi_i^{2*}) \xi_i \\ &\equiv \frac{1}{2} (\xi^{01} + i\xi^{02}), \\ \chi^{02} &= \sum_i (\phi_i^{3*} + i\phi_i^{4*}) \xi_i \\ &\equiv \frac{1}{2} (\xi^{03} + i\xi^{04}). \end{aligned} \quad (1.74)$$

Then, number operators become,

$$\begin{aligned} \hat{n}_1 &= \chi^{01\dagger} \chi^{01} = \frac{1 + i\xi^{01}\xi^{02}}{2} \\ \text{and } \hat{n}_2 &= \chi^{02\dagger} \chi^{02} = \frac{1 + i\xi^{03}\xi^{04}}{2}, \end{aligned} \quad (1.75)$$

where

$$\begin{aligned}\hat{n}_1|\sigma_1, \sigma_2\rangle &= \sigma_1|\sigma_1, \sigma_2\rangle \\ \text{and } \hat{n}_2|\sigma_1, \sigma_2\rangle &= \sigma_2|\sigma_1, \sigma_2\rangle.\end{aligned}\tag{1.76}$$

In order to perform braiding operation, we interchange modes 1 and 3 keeping 2 and 4 fixed. This is achieved by a unitary transformation which represents quantum logic gate operation on the qubit [42],

$$U = e^{\frac{i\pi}{4}\xi_{01}\xi_{03}} = \frac{1 - \xi_{01}\xi_{03}}{\sqrt{2}}.\tag{1.77}$$

Let us write U in terms of creation and annihilation operators,

$$U = \frac{1}{\sqrt{2}}\{1 - (\chi^{01} + \chi^{01\dagger})(\chi^{02} + \chi^{02\dagger})\}.\tag{1.78}$$

Then,

$$\begin{aligned}U|0, 0\rangle &= \frac{1}{\sqrt{2}}(|0, 0\rangle - |1, 1\rangle), \\ U|0, 1\rangle &= \frac{1}{\sqrt{2}}(|0, 1\rangle - |1, 0\rangle), \\ U|1, 0\rangle &= \frac{1}{\sqrt{2}}(|1, 0\rangle + |0, 1\rangle), \\ U|1, 1\rangle &= \frac{1}{\sqrt{2}}(|1, 1\rangle - |0, 0\rangle).\end{aligned}\tag{1.79}$$

Therefore, in terms of Pauli matrices, U becomes

$$\begin{aligned}U &= \frac{1}{\sqrt{2}}\{I_4 - (\sigma^+ \otimes \sigma^+ + \sigma^- \otimes \sigma^- + \sigma^+ \otimes \sigma^- - \sigma^- \otimes \sigma^+)\} \\ &= \frac{1}{\sqrt{2}}\{I_4 - (\sigma^x \otimes \sigma^x + \sigma^y \otimes \sigma^y + i(\sigma^y \otimes \sigma^x - \sigma^x \otimes \sigma^y))\},\end{aligned}\tag{1.80}$$

which is the unitary gate operation realised by performing exchange operation on Majorana modes.

## 1.9 Josephson Junction Quantum Circuits

In this thesis, we propose an experimental realisation of our model using Josephson junction quantum circuits following J. Q. You *et al.* They devised a way to construct a Quantum computer by realising Kitaev Model by Josephson junction quantum circuits [4]. They proposed a superconducting qubit box as a building block to realise the qubit in Josephson junction quantum circuits as shown in figure (1.6). The superconducting qubit box consists of a superconducting ring

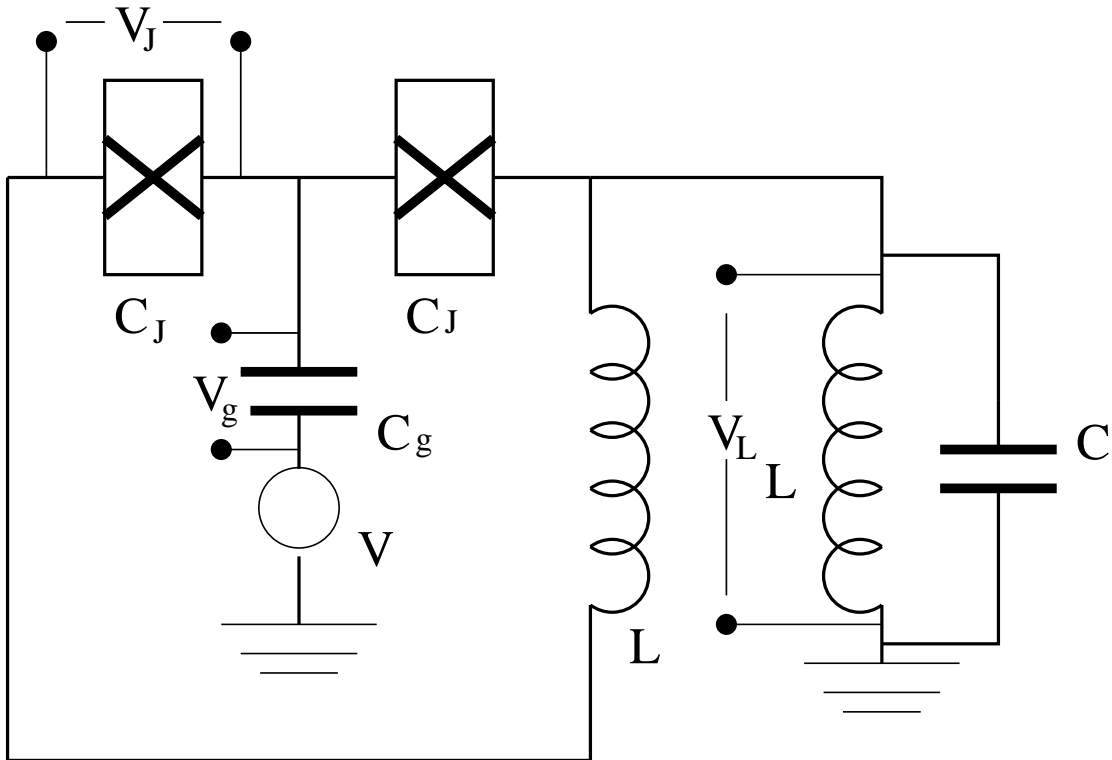


Figure 1.6: The superconducting qubit box.

connected with two identical Josephson junctions (a small box with cross sign) each with coupling energy  $E_J$  and capacitance  $C_J$  (shown by a cross on the box), to form a SQUID loop. The SQUID loop is connected to LC oscillator as shown above. The qubit box is controlled by both a voltage  $V$  (applied via the gate capacitor  $C_g$ ) and a magnetic flux  $\Phi$  passing through the SQUID loop.

Let the voltage across capacitor  $C_g$  be  $V_g$ , voltage across the LC oscillator be  $V_L$  and voltage across Josephson junction be  $V_J$ .

Lagrangian of the system,

$$L = T - U = \frac{1}{2}2C_J V_J^2 + \frac{1}{2}C_g V_g^2 + \frac{1}{2}C V_L^2 + E_J(\Phi) \cos \phi - \frac{\Phi_L^2}{2L}, \quad (1.81)$$

where first term denotes charging energy of Josephson capacitor, second term denotes charging energy of gate capacitor, third term denotes charging energy of LC oscillator, fourth term denotes Josephson coupling energy and fifth and final term denotes potential energy of LC oscillator.

According to Kirchoff's Law,

$$V_g = V - V_J - V_L. \quad (1.82)$$

In Josephson junction, voltage  $V_J$  is related to phase difference  $\phi$  of wavefunction of cooper pair by

$$V_J = \frac{\hbar}{2e} \dot{\phi}. \quad (1.83)$$

According to Faraday's law,

$$V_L = \dot{\Phi}_L \quad (1.84)$$

where  $\Phi_L$  denotes magnetic flux passing through the loop.

Substituting all these value in eqn. (1.81) we get,

$$\begin{aligned} L &= \frac{1}{2}(2C_J + C_g) \left( \frac{\hbar}{2e} \right)^2 \dot{\phi}^2 + C_g \left( \frac{\hbar}{2e} \right) \dot{\phi} (\Phi_L - V) \\ &+ \frac{1}{2}(C + C_g) \dot{\Phi}_L^2 + \frac{1}{2}C_g V^2 - C_g V \dot{\Phi}_L. \end{aligned} \quad (1.85)$$

Therefore, Hamitonian of the system,

$$H = \frac{1}{2C_J + C_g} \left\{ \frac{2ep}{\hbar} - \left( \frac{C_g}{C} P_L - C_g V \right) \right\}^2 + \frac{P_L^2}{2C} - E_J(\Phi) \cos \phi + \frac{\Phi_L^2}{2L}, \quad (1.86)$$

where  $p$  and  $P_L$  are conjugate momentum to  $\phi$  and  $\Phi_L$  respectively.

Let us introduce gauge transformation

$$\tilde{\phi} = \phi - \frac{1}{(2C_J + C_g)} \left( \frac{2e}{\hbar} \right) C_g \Phi_L \quad (1.87)$$

and

$$\tilde{p} = p - \left( \frac{\hbar}{2e} \right) \frac{C_g}{C} \Phi_L, \quad (1.88)$$

then Hamiltonian becomes

$$\begin{aligned} H &= \frac{1}{2(2C_J + C_g)} \left( \frac{2e\tilde{p}}{\hbar} + C_g V \right)^2 + \frac{P_L^2}{2C} \\ &- E_J(\Phi) \cos \left( \tilde{\phi} + \frac{1}{(2C_J + C_g)} \frac{2e}{\hbar} C_g \Phi_L \right) + \frac{\Phi_L^2}{2L}. \end{aligned} \quad (1.89)$$

Fluctuations of  $C_g \Phi_L$  are so weak [43] that

$$\frac{1}{2C_J + C_g} C_g \Phi_L \ll \frac{2e}{\hbar}. \quad (1.90)$$

Then,  $\cos(\phi)$  can be written as

$$\cos(\phi) \approx \cos \tilde{\phi} - \left[ \frac{1}{2C_J + C_g} \left( \frac{2e}{\hbar} \right) C_g \Phi_L \right] \sin \tilde{\phi}. \quad (1.91)$$

Therefore, Hamiltonian finally becomes

$$\begin{aligned} H &= \frac{1}{2(2C_J + C_g)} \left( \frac{2e\tilde{p}}{\hbar} + C_g V \right)^2 + \frac{P_L^2}{2C} - E_J(\Phi) \cos \tilde{\phi} \\ &- \frac{1}{2C_J + C_g} \left( \frac{2e}{\hbar} \right) C_g \Phi_L \sin \tilde{\phi} + \frac{\Phi_L^2}{2L}. \end{aligned} \quad (1.92)$$

Substituting  $Y = E_J(\Phi) \frac{C_g}{2C_J + C_g} \sin \tilde{\phi}$ , Hamiltonian becomes

$$\begin{aligned} H &= \frac{1}{2(2C_J + C_g)} (\tilde{p} + C_g V)^2 + \frac{P_L^2}{2C} - E_J(\Phi) \cos \tilde{\phi} \\ &- \frac{1}{2L} \left( \Phi_L + \frac{2e}{\hbar} LY \right)^2 - \frac{1}{2} \left( \frac{2e}{\hbar} \right)^2 LY^2. \end{aligned} \quad (1.93)$$

The term  $\frac{p_L^2}{2C}$  represents kinetic energy of the LC oscillator and the term  $\frac{(\Phi_L + (\frac{2e}{\hbar}LY))^2}{2L}$  represents potential energy of the oscillator. When the frequency of LC oscillator is much larger than the qubit frequency, the LC oscillator remains in the ground state and, therefore, these terms can be neglected in the hamiltonian [43] to get

$$H = \frac{4e^2}{2(2C_J + C_g)} \left( \frac{\tilde{p}}{\hbar} + \frac{C_g V}{2e} \right)^2 - E_J(\Phi) \cos \tilde{\phi} - \frac{1}{2} \left( \frac{2e}{\hbar} \right)^2 LY^2. \quad (1.94)$$

or, it can be written as,

$$H = E_c(n + n_g)^2 - E_J(\Phi) \cos \tilde{\phi} - \frac{1}{2} \left( \frac{2e}{\hbar} \right)^2 LY^2. \quad (1.95)$$

Here,  $n = \frac{\tilde{p}}{\hbar}$  represents number of extra cooper pairs in the box and  $E_c = \frac{4e^2}{2(2C_J + C_g)}$  and  $n_g = \frac{C_g V}{2e}$ .

At low temperature, only lowest energy eigenstates of a superconducting circuit element are involved in the dynamics. As low energy eigenstates are mixtures of zero and one extra cooper pair in the box, these two charge states can be considered as two level quantum system. Then, canonically conjugate variable  $n$  and  $\phi$  obey following commutation relation:

$$[\hat{n}, \hat{\phi}] = i\hbar. \quad (1.96)$$

In eqn. (1.95), the term  $Y^2 \equiv \sin^2 \tilde{\phi}$  is also removed because they are reduced to the identity operators in the qubit subspace.

Therefore, the Hamiltonian in eqn. (1.95) becomes

$$H = E_c(n + n_g)^2 - E_J(\Phi) \cos \tilde{\phi}. \quad (1.97)$$

In the Hamiltonian for  $E_c \gg E_J$ , we can tune  $n_g$  via  $C_g$  to make the quantum state  $n=0$  and  $n=1$  degenerate which happens at  $n_g = -\frac{1}{2}$ . Therefore, Hamiltonian in eqn. (1.98) becomes,

$$H = E_c \left( n - \frac{1}{2} \right)^2. \quad (1.98)$$

Let us label our quantum state by  $|n\rangle$  where  $n=0,1$  represents charge of zero, one extra cooper pair. Then,

$$\begin{aligned}
 e^{i\hat{\phi}}|n\rangle &= e^{i\hat{\phi}} \int d\phi |\phi\rangle \langle \phi|n\rangle \\
 &= \int d\phi e^{i\hat{\phi}} |\phi\rangle e^{in\phi} \\
 &= \int d\phi e^{i\phi} |\phi\rangle e^{in\phi} \\
 &= \int d\phi |\phi\rangle e^{i(n+1)\phi} \\
 &= |n+1\rangle.
 \end{aligned}$$

Thus,

$$e^{i\hat{\phi}}|n\rangle = |n+1\rangle. \quad (1.99)$$

Similarly,

$$e^{-i\hat{\phi}}|n\rangle = |n-1\rangle. \quad (1.100)$$

As we have projected to a two level quantum system,  $e^{i\phi}$  or  $e^{-i\phi}$  cannot raise or lower the states indefinitely, so we get only

$$\begin{aligned}
 \langle 1|e^{i\hat{\phi}}|0\rangle &= 1 \\
 \text{and } \langle 0|e^{-i\hat{\phi}}|1\rangle &= 1
 \end{aligned} \quad (1.101)$$

and all other matrix elements of  $e^{i\hat{\phi}}$  and  $e^{-i\hat{\phi}}$  vanish.

So  $e^{i\hat{\phi}}$  and  $e^{-i\hat{\phi}}$  acting like spin raising and lowering ladder operators  $\hat{\sigma}^+$  and  $\hat{\sigma}^-$ . So  $\cos \hat{\phi}$  and  $\sin \hat{\phi}$  acts like  $\hat{\sigma}^x$  and  $\hat{\sigma}^y$  operators.

Further,

$$\begin{aligned}
 (2\hat{n} - 1)|0\rangle &= -|0\rangle \\
 (2\hat{n} - 1)|1\rangle &= +|1\rangle,
 \end{aligned} \quad (1.102)$$



which is like  $\sigma^z$  operator.

Therefore, in the low energy limit, the system variables of qubit space can be mapped on to spin space,

$$\begin{aligned}\cos \hat{\phi} &= \sigma^x, \\ \sin \hat{\phi} &= \sigma^y, \\ 2\hat{n} - 1 &= \sigma^z.\end{aligned}\tag{1.103}$$

Therefore, x, y and z bond of the model can be realised if we can engineer following terms in the Hamiltonian,

$$\begin{aligned}\sigma_1^x \sigma_2^x &= \cos \hat{\phi}_1 \cos \hat{\phi}_2, \\ \sigma_1^y \sigma_2^y &= \sin \hat{\phi}_1 \sin \hat{\phi}_2, \\ \sigma_1^z \sigma_2^z &= (2\hat{n}_1 - 1)(2\hat{n}_2 - 1).\end{aligned}\tag{1.104}$$

To design x-bond, circuit is made up of two superconducting qubit box coupled by a mutual inductance as shown in figure 1.7. The Hamiltonian for the circuit

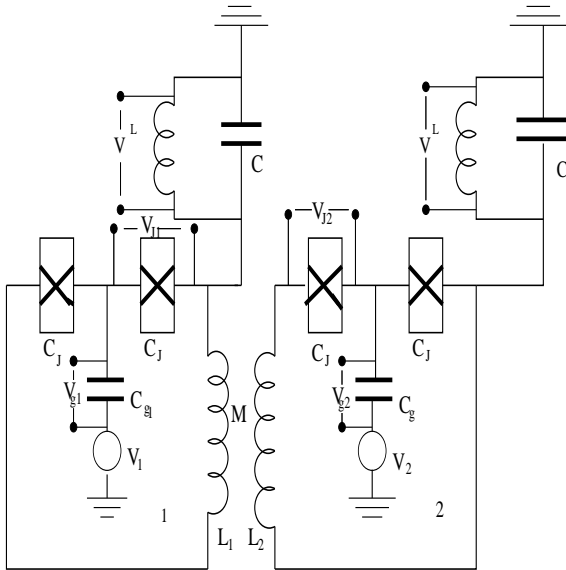


Figure 1.7: Josephson junction quantum circuit to realise x bond

shown in figure (1.7) to be,

$$H_x = H_1 + H_2 + J_x \cos \tilde{\phi}_1 \cos \tilde{\phi}_2, \quad (1.105)$$

$$\begin{aligned} \text{where } H_i &= E_c \left( n_i - \frac{1}{2} \right)^2 \\ \text{and } J_x &= -MI_c^2 \sin \Phi_1 \sin \Phi_2. \end{aligned} \quad (1.106)$$

To design y-bond, circuit is made up of two superconducting qubit box connected by wire shown in figure (1.8).

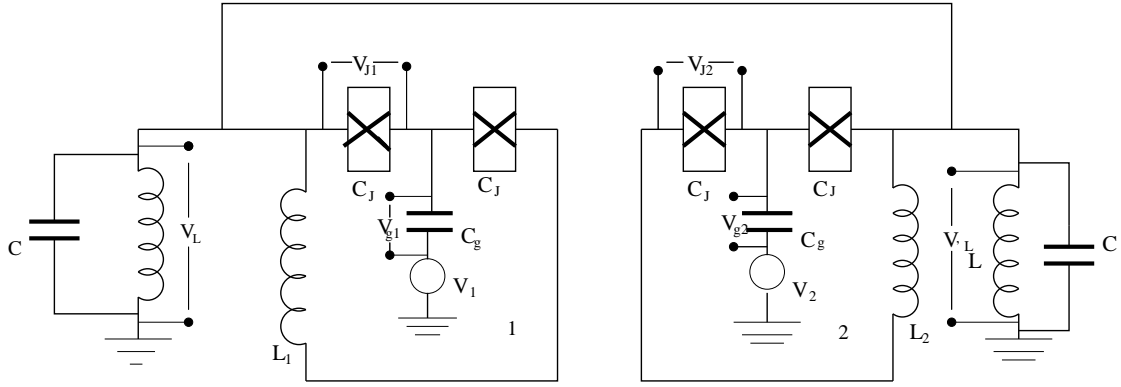


Figure 1.8: Josephson junction quantum circuit to realise y bond

The Hamiltonian for circuit shown in figure (??),

$$H_y = H_1 + H_2 + J_y \sin \tilde{\phi}_1 \sin \tilde{\phi}_2, \quad (1.107)$$

where  $J_y = -4 \left[ \frac{eLC_gC_\Sigma}{\hbar\Lambda} \right]^2 E_{J_1}(\Phi_1)E_{J_2}(\Phi_2)$ .

Finally, we make a circuit for z-bond using two superconducting qubit box connected by a capacitor as shown in figure (1.9),

and the Hamiltonian for the circuit,

$$H_z = H_1 + H_2 + J_z (\tilde{n}_1 + C_g V_1) (\tilde{n}_2 + C_g V_2) \quad (1.108)$$

where  $C_\Sigma = 2C_J + C_g + C_m$ ,  $\Lambda = C_\Sigma^2 - C_m^2$  and  $J_z = \frac{4e^2 C_m}{\Lambda}$ .

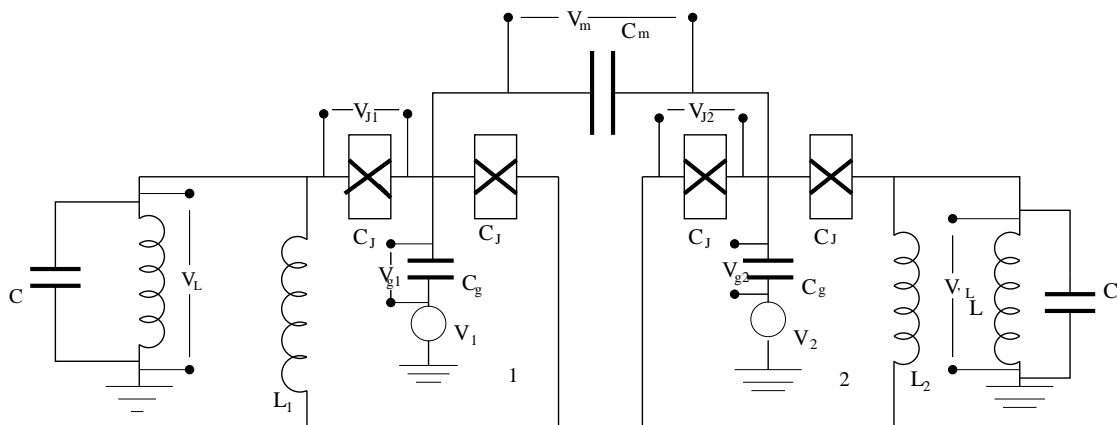


Figure 1.9: Josephson junction quantum circuit to realise z bond

Therefore, Hamiltonian in eqn.(1.105), eqn.(1.107) and eqn.(1.108) becomes

$$\begin{aligned}
 H_x &= H_1 + H_2 + J_x \sigma_1^x \sigma_2^x, \\
 H_y &= H_1 + H_2 + J_y \sigma_1^y \sigma_2^y, \\
 H_z &= H_1 + H_2 + J_z \sigma_1^z \sigma_2^z.
 \end{aligned} \tag{1.109}$$

Here, we can see that  $J_x$  and  $J_y$  are tunable by external magnetic field  $\Phi_i$  and  $J_z$  is tunable via coupling capacitor  $c_m$ . And,  $H_1$  and  $H_2$  are constant term in the Hamiltonian. Following these results Nori *et al* placed a superconducting qubit box at each node of a honeycomb lattice. But, designing the 6-spin commuting operators (1.48) in the Kitaev model to manipulate the Majorana fermions is not possible. Therefore, we proposed another model "XY-Ising model" where we could design Hamiltonian altogether with commuting operators.

## 1.10 Organisation of the thesis

In chapter 2, we design a Tetrahedral model where zero energy modes can be studied analytically. Further, we show that by tuning flux configuration, we could manipulate the zero mode wavefunction. but experimental realisation of 3-spin commuting operators does not seem to be possible.

In chapter 3, we study another model XY-Ising model because experimental realisation of 2-spin commuting operators is possible. We solve the XY-Ising model

exactly and find the ground state. We study the nature of low energy excitations.

In chapter 4, we show that XYZ-Ising model can also be solved using the Kitaev's trick even if it's not a Kitaev type model. We study zero temperature phase diagram of the XYZ-Ising model for all  $J$  and  $J_z$  numerically. We study the ground state of the model analytically in extreme limits.

In chapter 5, we take XY-Ising model where we have a qubit with two degenerate ground states of the model. We show that this qubit is protected from decoherence by environmental perturbations. Finally, we discuss a possible physical realisation of XY-Ising model by Josephson junction quantum circuits.

We present the summary and outlook of the thesis in chapter 6.

# 2

## Tetrahedral Model

In this chapter, we present a one dimensional generalisation of the Kitaev honeycomb model which we call the Tetrahedral Chain (TC). In this model we study the zero energy Unpaired Majorana Fermions (UMF) modes analytically. One dimensional models with (UMF) at the edges have been studied earlier [44, 45]. The new feature of our model is that the wavefunctions of the UMF not necessarily peak at the edges of the chain but can peak anywhere in the bulk. As we will show, they are trapped to kink and anti-kink flux configurations and can be moved by tuning the flux configuration. Further, by tuning the coupling constants, their wavefunctions, which we obtain analytically, can also be tuned.

### 2.1 The Hamiltonian

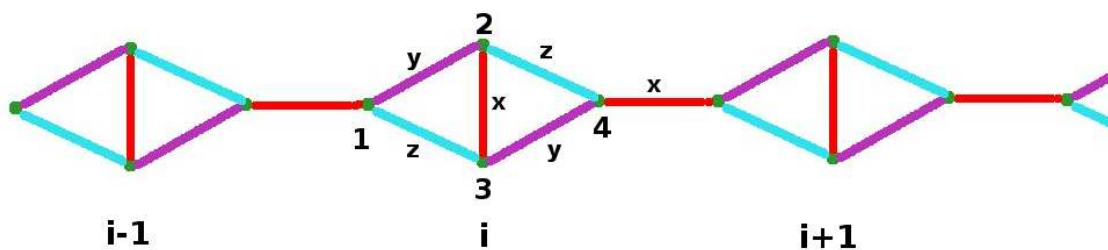


Figure 2.1: The tetrahedral chain. There are four sites per unit cell. The  $x$ ,  $y$  and  $z$  bonds are as indicated.

The chain we define our model on is shown in figure (2.1).

The Hamiltonian,

$$\begin{aligned}
H = & \sum_i \left( J_x (\sigma_{i-1,4}^x \sigma_{i,1}^x + \sigma_{i,2}^x \sigma_{i,3}^x) \right. \\
& + J_y (\sigma_{i,1}^y \sigma_{i,2}^y + \sigma_{i,3}^y \sigma_{i,4}^y) \\
& \left. + J_z (\sigma_{i,1}^z \sigma_{i,3}^z + \sigma_{i,2}^z \sigma_{i,4}^z) \right). \tag{2.1}
\end{aligned}$$

There are two triangular plaquettes operators in each unit cell and a conserved  $Z_2$  flux associated with each of them. The operators are,

$$W_i^L = \sigma_{i,1}^x \sigma_{i,2}^z \sigma_{i,3}^y \quad W_i^R = \sigma_{i,4}^x \sigma_{i,3}^z \sigma_{i,2}^y. \tag{2.2}$$

For future reference we define an operator  $W_i$ ,

$$W_i \equiv W_i^L W_i^R = \sigma_{i,1}^x \sigma_{i,2}^x \sigma_{i,3}^x \sigma_{i,4}^x. \tag{2.3}$$

As in Kitaev's honeycomb model, these quantities are conserved as a consequence of a local spin rotation symmetry of the model, namely, a  $\pi$  rotation on each site of a plaquette about the direction of the outgoing bond.

Apart from these local commuting operators there are also three global operators which are conserved as a consequence the fact that a global  $\pi$  rotation about each of the three axes is a symmetry of the model. We denote these by,

$$\Sigma^a \equiv e^{i\frac{\pi}{2} \sum_{i,a} \sigma_{i,\alpha}^a}. \tag{2.4}$$

Therefore,  $\Sigma^x$  is the product of the all the plaquette operators,

$$\Sigma^x = \prod_i (W_i^L W_i^R). \tag{2.5}$$

## 2.2 Fermionisation

We express the Hamiltonian in terms of Majorana fermions using the Jordan-Wigner transformation. We choose the Jordan-Wigner path to go along the  $x$  and the  $y$  bonds from left to right. At every site we have two bonds that are tangential to the path. We denote the incoming bond by  $t_1$ . This is the  $x$ -bond on the

sublattices 1, 3 and  $y$ -bond on sublattices 2,4. The outgoing bond, corresponding to  $y$  on sublattices 1, 3 and  $x$  on sublattices 2,4, is denoted by  $t_2$ . The third bond on each site which is normal to the path, is denoted by  $n$  with the sign defined by  $\hat{n} = \hat{t}_1 \times \hat{t}_2$ . With our choice of path, the normal bond is  $z$  for sublattices 1,3 and  $-z$  for sublattices 2,4.

The Hamiltonian,

$$\begin{aligned}
 H = & \sum_i J_x (\sigma_{i-1,4}^{t_2} \sigma_{i,1}^{t_1} + \sigma_{i,2}^{t_2} \sigma_{i,3}^{t_1}) \\
 & + J_y (\sigma_{i,1}^{t_2} \sigma_{i,2}^{t_1} + \sigma_{i,3}^{t_2} \sigma_{i,4}^{t_1}) \\
 & - J_z (\sigma_{i,1}^n \sigma_{i,3}^n + \sigma_{i,2}^n \sigma_{i,4}^n).
 \end{aligned} \tag{2.6}$$

Let us define the two Majorana fermions  $\xi_{i,\alpha}$  and  $\eta_{i,\alpha}$  at each site,

$$\begin{aligned}
 \xi_{i,\alpha} &= \sigma_{i,\alpha}^{t_1} \prod_{j<i} \left( \prod_{\beta<\alpha} \sigma_{j,\beta}^n \right), \\
 \eta_{i,\alpha} &= \sigma_{i,\alpha}^{t_2} \prod_{j<i} \left( \prod_{\beta<\alpha} \sigma_{j,\beta}^n \right).
 \end{aligned} \tag{2.7}$$

It can be shown that  $\xi_i$  and  $\eta_i$  follow anti commutation relation,

$$\{\xi_i, \xi_j\} = 2\delta_{i,j}; \{\eta_i, \eta_j\} = 2\delta_{i,j}; \{\xi_i, \eta_j\} = 0. \tag{2.8}$$

The Hamiltonian, then, can be expressed in terms of the Majorana operators,

$$\begin{aligned}
 H = & \sum_i^N J_x (i\xi_{i-1,4}\xi_{i,1} + i\xi_{i,2}\xi_{i,3}) \\
 & + J_y (i\xi_{i,1}\xi_{i,2} + i\xi_{i,3}\xi_{i,4}) \\
 & + J_z \left( -i\hat{u}_i^L \xi_{i,1}\xi_{i,3} + i\hat{u}_i^R \xi_{i,2}\xi_{i,4} \right),
 \end{aligned} \tag{2.9}$$

where the link fields,  $\hat{u}_i^{L(R)}$ , are defined as,

$$\hat{u}_i^L \equiv i\eta_{i,3}\eta_{i,1} \quad \text{and} \quad \hat{u}_i^R \equiv i\eta_{i,2}\eta_{i,4}. \tag{2.10}$$

It is easy to see that the link operators  $u_i^{L,(R)}$  are conserved quantities. Thus,

as expected for a generalised Kitaev model, the theory gets written in terms of Majorana fermions with nearest neighbour hopping in the background of conserved  $Z_2$  gauge fields, with the gauge fixing condition that the gauge fields on  $x$  and  $y$  bonds are equal to  $+1$ . The gauge fields on the  $z$  bonds are equal to  $\pm 1$ . It is easy to check that the two plaquette operators, or say, flux operators  $W_i^L, W_i^R$ , are nothing but link operators in the transformed basis,

$$\hat{u}_i^L = i\eta_{i,3}\eta_{i,1} \equiv W_i^L \quad \text{and} \quad \hat{u}_i^R = i\eta_{i,2}\eta_{i,4} \equiv W_i^R. \quad (2.11)$$

Let us express the three global conserved quantities,  $\Sigma^{x,y,z}$  in terms of the fermionic variables. We have,

$$\begin{aligned} \Sigma^x &= \prod_i (\eta_{i,1}\eta_{i,2}\eta_{i,3}\eta_{i,4}), \\ \Sigma^y &= \prod_i (\xi_{i,1}\xi_{i,2}\xi_{i,3}\xi_{i,4}) \\ \text{and } \Sigma^z &= \Sigma^x \Sigma^y. \end{aligned} \quad (2.12)$$

We will refer to  $\Sigma^x$  as the flux number and  $\Sigma^y$  as the Majorana number.

## 2.3 Diagonalisation

The Hamiltonian can be diagonalised in the standard way. We write the eigenstates as direct products of states in the  $\eta$  fermion sector,  $|\mathcal{G}\rangle$ , which we refer to as the gauge sector and states in the  $\xi$  fermion sector,  $|\mathcal{M}\rangle$ , which we call the matter sector. We choose the states in the gauge sector to be the simultaneous eigenstates of the  $Z_2$  flux operators, i.e,

$$|\mathcal{G}\rangle = |\{u_i^L, u_i^R\}\rangle, \text{ where}$$

$$\hat{u}_i^{L(R)} |\{u_i^L, u_i^R\}\rangle = u_i^{L(R)} |\{u_i^L, u_i^R\}\rangle. \quad (2.13)$$

We then have,

$$H [\hat{u}_i^L, \hat{u}_i^R] |\mathcal{M}\rangle |\{u_i^L, u_i^R\}\rangle = H [u_i^L, u_i^R] |\mathcal{M}\rangle |\{u_i^L, u_i^R\}\rangle. \quad (2.14)$$

The problem reduces to finding the eigenstates of the quadratic Hamiltonian of



the  $\xi$  fermions in the background of the gauge field configuration  $\{u_i^L, u_i^R\}$ . The Hamiltonian can be written as,

$$H = \sum_{i,j} \xi_i h_{i,j} \xi_j. \quad (2.15)$$

To diagonalise the Hamiltonian, we substitute

$$\xi_i = \sum_n \phi_i^{n*} \chi^n, \quad (2.16)$$

where normal modes  $\phi_i^n$  is found out by solving single particle eigenvalue equation

$$\sum_j h_{i,j} \phi_j^n = \epsilon_n \phi_i^n. \quad (2.17)$$

Here,  $h = T + V$  is a purely imaginary anti-symmetric matrix,

$$T_{i,j} = iJ_x \begin{pmatrix} 0 & 0 & 0 & -\delta_{i-1,j} \\ 0 & 0 & 0 & 0 \\ 0 & 0 & 0 & 0 \\ \delta_{i+1,j} & 0 & 0 & 0 \end{pmatrix} \quad (2.18)$$

and

$$V_{i,j} = i\delta_{i,j} \begin{pmatrix} 0 & J_y & -J_z u_i^L & 0 \\ -J_y & 0 & J_x & J_z u_i^R \\ J_z u_i^L & -J_x & 0 & J_y \\ 0 & -J_z u_i^R & -J_y & 0 \end{pmatrix}. \quad (2.19)$$

As we have shown the eigenvalues of antisymmetric matrix come in pairs. Therefore, for every positive eigenvalue,  $h$  has one negative eigenvalue and the eigenvectors corresponding to the positive and negative eigenvalues are complex conjugates of each other. If, in equation (2.16), the summation index  $n$  runs only over modes

of the positive energy, then we can expand the  $\xi$  fermions as,

$$\xi_{i,\alpha} = \sum_n \phi_{i,\alpha}^{n*} \chi^n + \phi_{i,\alpha}^n \chi^{n\dagger}. \quad (2.20)$$

In equation (2.16),  $\chi^n$  and  $\chi^{n\dagger}$  are fermionic operators and follow the commutation relation,

$$[\chi^{m\dagger}, \chi^n] = \delta_{m,n}. \quad (2.21)$$

The diagonal form of the hamiltonian is then,

$$H = \sum_n \epsilon_n (2\chi^{n\dagger} \chi^n - 1). \quad (2.22)$$

Therefore, the ground state energy is,

$$E_0 = - \sum_n \epsilon_n. \quad (2.23)$$

### 2.3.1 Boundary Conditions

Now, we analyse the system with Periodic (PBC) and Open Boundary Conditions (OBC).

Under open boundary condition the fermionic Hamiltonian (2.9) have to be solved with the boundary condition,

$$\phi_{0,1} = \phi_{N+1,1} = 0. \quad (2.24)$$

Under periodic boundary condition, the term in the Hamiltonian for the link  $i = N$  to  $i = 1$  is,

$$H_{N,1} = J_x \sigma_{N,4}^x \sigma_{1,1}^x. \quad (2.25)$$

After Jordan-Wigner Transformation it becomes,

$$H_{N,1} = J_x \Sigma^z i \xi_{N,4} \xi_{1,1}. \quad (2.26)$$

$\Sigma^z$  is a conserved quantity and can hence be chosen to be diagonal. Thus, the spin Hamiltonian (2.1) becomes fermionic hamiltonian with periodic boundary conditions for  $\Sigma^z = -1$  and antiperiodic boundary conditions for  $\Sigma^z = +1$ . We can express it in terms of wavefunctions,

$$\phi_{N+1,\alpha} = p\phi_{1,\alpha}, \quad (2.27)$$

where  $p = \pm 1$  is the eigenvalue of  $\Sigma^z$ .

## 2.4 The Degeneracy of the States

We have also found that each eigenstate of the spectrum is  $2^N$  fold degenerate including the ground state for all values of the parameters. We observed that this degeneracy comes from dependence of the single particle spectrum only on the values of the product,  $u_i \equiv u_i^L u_i^R$ , and not on their individual values,  $u_i^L$  and  $u_i^R$ . In this section, we give an analytic proof of this  $2^N$  fold degeneracy of all the states.

This degeneracy is related to, but not the same as, the  $4^N$  degeneracy in the simple one dimensional Kitaev chain, the  $J_z = 0$  limit of our model. In this case the degeneracy is easy to understand. The gauge fields do not occur at all in the Hamiltonian and, therefore, the model is equivalent to a system of non-interacting fermions with nearest neighbour hopping. Thus, each state is  $4^N$  degenerate corresponding to all the states in the gauge sector ( $\eta$  fermion sector). The extra  $z$ -bond terms in our model lift this degeneracy partially.

At  $J_y = J_z$ , the degeneracy can be explained easily in terms of a local symmetry. It consists of interchanging the spins at sublattice 2 and 3 in any unit cell and then performing a  $\pi/2$  rotation about the  $x$ -axis on all the spins in that unit cell. The operator that implements this transformation is,

$$P_i \equiv \left( \frac{\vec{\sigma}_{i2} \cdot \vec{\sigma}_{i3} + 1}{2} \right) e^{i\frac{\pi}{4} \sum_{\alpha=1}^4 \sigma_{i\alpha}^x}. \quad (2.28)$$

Further, we can see that

$$P_i W_i^{L(R)} P_i = -W_i^{L(R)}, \quad P_i W_i^L W_i^R P_i = W_i^L W_i^R. \quad (2.29)$$

Thus, it changes the flux configuration while leaves the total flux operator through the unit cell invariant. Since the  $P_i$ 's commute with the Hamiltonian, it does not also change the energy eigenvalue. Therefore, every eigenstate of the hamiltonian is  $2^N$  fold degenerate.

However, we numerically observe that the degeneracy persists even when  $J_y \neq J_z$ . We now give a proof for the degeneracy which is valid at all couplings. We note that in equation (2.17),  $\phi_{i,2}$  and  $\phi_{i,3}$  couple only to sites within the unit cell. We express them in terms of  $\phi_{i,1}$  and  $\phi_{i,4}$  and obtain an eigenvalue equation for these quantities. We are then able to show that the eigenvalues depend only on  $u_i = u_i^L u_i^R$ .

We define the two component column vectors,

$$\chi_i \equiv \begin{pmatrix} \phi_{i,1} \\ \phi_{i,4} \end{pmatrix} \quad \psi_i \equiv \begin{pmatrix} \phi_{i,2} \\ \phi_{i,3} \end{pmatrix} \quad (2.30)$$

and the matrices,

$$\begin{aligned} T_{ij} &= i\delta_{i-1,j} \begin{pmatrix} 0 & -J_x \\ 0 & 0 \end{pmatrix} + i\delta_{i+1,j} \begin{pmatrix} 0 & 0 \\ J_x & 0 \end{pmatrix} \\ \text{and } U_{ij} &= i\delta_{i,j} \begin{pmatrix} J_y & J_z u_i^L \\ J_z u_i^R & -J_y \end{pmatrix} \end{aligned} \quad (2.31)$$

The eigenvalue equations (2.17) can then be written as,

$$\begin{pmatrix} T & U \\ U^\dagger & J_x \tau^2 \end{pmatrix} \begin{pmatrix} \chi \\ \psi \end{pmatrix} = \epsilon \begin{pmatrix} \chi \\ \psi \end{pmatrix} \quad (2.32)$$

where  $\tau^a$ ,  $a = 1, 2, 3$  are the Pauli matrices.

Eliminating  $\psi$  from the eqn. (2.32) we get,

$$\left( T + U \frac{1}{\epsilon - J_x \tau^2} U^\dagger \right) \chi = \epsilon \chi. \quad (2.33)$$

Substituting the components of column vectors of  $\chi_i$ , the equations can be explic-

itly written as,

$$\begin{aligned} -iJ_x\phi_{i-1,4} + c_i e^{i\alpha_i} \phi_{i,4} &= \lambda\phi_{i,1} \\ \text{and } iJ_x\phi_{i+1,1} + c_i e^{-i\alpha_i} \phi_{i,1} &= \lambda\phi_{i,4}, \end{aligned} \quad (2.34)$$

where

$$\begin{aligned} c_i &= \sqrt{\frac{J_x^2(J_y^2 + J_z^2)^2 + 2J_z^2 J_y^2 (\epsilon^2 - J_x^2)(1 - u_i)}{(\epsilon^2 - J_x^2)^2}}, \\ \alpha_i &= \tan^{-1} \left( \frac{\epsilon J_y J_z}{J_x (J_y^2 + J_z^2 u_i)} (u_i^R - u_i^L) \right), \\ \lambda &= \epsilon \left( 1 - \frac{J_y^2 + J_z^2}{\epsilon^2 - J_x^2} \right). \end{aligned} \quad (2.35)$$

When these equations are solved for  $\lambda$ , they will give an equation for  $\epsilon$ . We now make a transformation to get rid of phases in eqn (2.34),

$$\begin{aligned} \phi_{i,1} &\rightarrow e^{i\theta_i} \phi_{i,1}, \\ \phi_{i,4} &\rightarrow e^{i\theta_{i+1}} \phi_{i,4} \\ \text{and } \theta_i &= -\sum_{j<i} \left( \alpha_j + \frac{\pi}{2} \right) \end{aligned} \quad (2.36)$$

which become finally,

$$\begin{aligned} -iJ_x\phi_{i-1,4} - ic_i\phi_{i,4} &= \lambda\phi_{i,1}, \\ iJ_x\phi_{i+1,1} + ic_i\phi_{i,1} &= \lambda\phi_{i,4}. \end{aligned} \quad (2.37)$$

Since  $c_i$  depends only on  $u_i$  and not on  $u_i^L, u_i^R$  individually,  $\lambda$  and, hence,  $\epsilon$  depends only on the  $u_i$ . Thus, the energy eigenvalues depend only on the total flux passing through the unit cell.

This result is true for all values of  $J_x, J_y$  and  $J_z$ . Note that when  $J_z = 0$ , eqn. (2.35) implies that  $c_i$  is independent of  $u_i$  too. Thus, the  $4^N$  fold degeneracy of the simple Kitaev chain is recovered in this limit.

## 2.5 The Ground States and gaps

The translationally invariant fluxes through the unit cells, namely,  $u_i^L = -1$  and  $u_i^R = -1$  is the ground state sector of the model. We call it defect free sector. We can show analytically that energy of  $u_i = 1$  (defect free) configuration is less than that of  $u_i = -1$  i.e.  $u_i^L = 1$  and  $u_i^R = -1$  (defect full) sector.

We can solve the Hamiltonian for translationally invariant flux sector  $u_i^L$  and  $u_i^R$  using Fourier transform,

$$\xi_{i,a} = \frac{1}{\sqrt{N}} \sum_k \xi_{k,a} e^{-ikR_i}. \quad (2.38)$$

Substituting Fourier transform in the eqns. (2.37), we get

$$\begin{aligned} -iJ_x \phi_{k,4} e^{ika} - ic_i \phi_{k,4} &= \lambda \phi_{k,1}, \\ iJ_x \phi_{k,1} e^{-ika} + ic_i \phi_{k,1} &= \lambda \phi_{k,4}. \end{aligned} \quad (2.39)$$

If  $u_i = u$ , then  $c_i$  in eqn. (2.39) is independent of  $i$ ,  $c_i = c$ ,

$$\begin{aligned} -iJ_x \phi_{k,4} e^{ika} - ic \phi_{k,4} &= \lambda \phi_{k,1}, \\ iJ_x \phi_{k,1} e^{-ika} + ic \phi_{k,1} &= \lambda \phi_{k,4}. \end{aligned} \quad (2.40)$$

Eigenvalue  $\lambda$  is then given by,

$$\lambda = \pm \sqrt{c^2 + J_x^2 + 2cJ_x \cos k}. \quad (2.41)$$

Along with eqn. ((2.35)), this calculation confirms that the  $u_i = +1$  (defect free) sector has a lower ground state energy than the  $u_i = -1$  (defect full) sector.

This can be shown analytically since the expression in eqn. (2.35) simplifies considerably at  $u_i = 1$ . Let us substitute  $u_i = 1$  in eqn. (2.35) to get,

$$c = \sqrt{\frac{J_x^2 (J_y^2 + J_z^2)^2}{(\epsilon^2 - J_x^2)^2}}. \quad (2.42)$$

Now substituting  $c$  from above eqn. and  $\lambda$  from eqn. (2.35),

$$\begin{aligned} \epsilon^2 \left( 1 - \frac{J_y^2 + J_z^2}{\epsilon^2 - J_x^2} \right)^2 &= \frac{J_x^2 (J_y^2 + J_z^2)^2}{(\epsilon^2 - J_x^2)^2} + J_x^2 + \frac{2J_x^2 (J_y^2 + J_z^2)}{\epsilon^2 - J_x^2} \cos(k) \\ \epsilon^2 - 2\epsilon^2 \frac{(J_y^2 + J_z^2)}{\epsilon^2 - J_x^2} + \epsilon^2 \frac{(J_y^2 + J_z^2)^2}{(\epsilon^2 - J_x^2)^2} &= \frac{J_x^2 (J_y^2 + J_z^2)^2}{(\epsilon^2 - J_x^2)^2} + J_x^2 + \frac{2J_x^2 (J_y^2 + J_z^2)}{\epsilon^2 - J_x^2} \cos(k) \\ \text{or, } (\epsilon^2 - J_x^2) - 2 \frac{(\epsilon^2 + J_x^2 \cos(k)) (J_y^2 + J_z^2)}{(\epsilon^2 - J_x^2)} + (\epsilon^2 - J_x^2) \frac{(J_y^2 + J_z^2)}{(\epsilon^2 - J_x^2)^2} &= 0 \\ \text{or, } (\epsilon^2 - J_x^2)^2 - 2(\epsilon^2 + J_x^2 \cos(k))(J_y^2 + J_z^2) + (J_y^2 + J_z^2)^2 &= 0 \end{aligned} \quad (2.43)$$

and finally,

$$\epsilon = \sqrt{(J_x^2 + J_y^2 + J_z^2)} \pm 2J_x (J_y^2 + J_z^2) \cos\left(\frac{k}{2}\right). \quad (2.44)$$

The fermionic gap denoted by  $\Delta$  is twice the value of the lowest single particle energy eigenvalue. The gap is, therefore, given by

$$\Delta = 2|\sqrt{J_y^2 + J_z^2} - J_x|. \quad (2.45)$$

The circle in the parameter space,  $J_x^2 = J_y^2 + J_z^2$  is, therefore, gapless. This is shown in figure (2.2) where the iso-gap contours are plotted in the  $J_y - J_z$  plane. Another way this can be confirmed is by numerically evaluating the gap and plotting it as a function of  $J \equiv \sqrt{J_y^2 + J_z^2}$ . All the points fall on the straight line as shown in figure (2.3).

## 2.6 Zero modes

As we have stated earlier, solutions belonging to  $\epsilon = 0$  are called zero mode solutions. The zero modes are given by the solution of the single particle eigenvalue equation,

$$\sum_{j\beta} h_{i\alpha, j\beta} \phi_{j\beta}^n = 0. \quad (2.46)$$

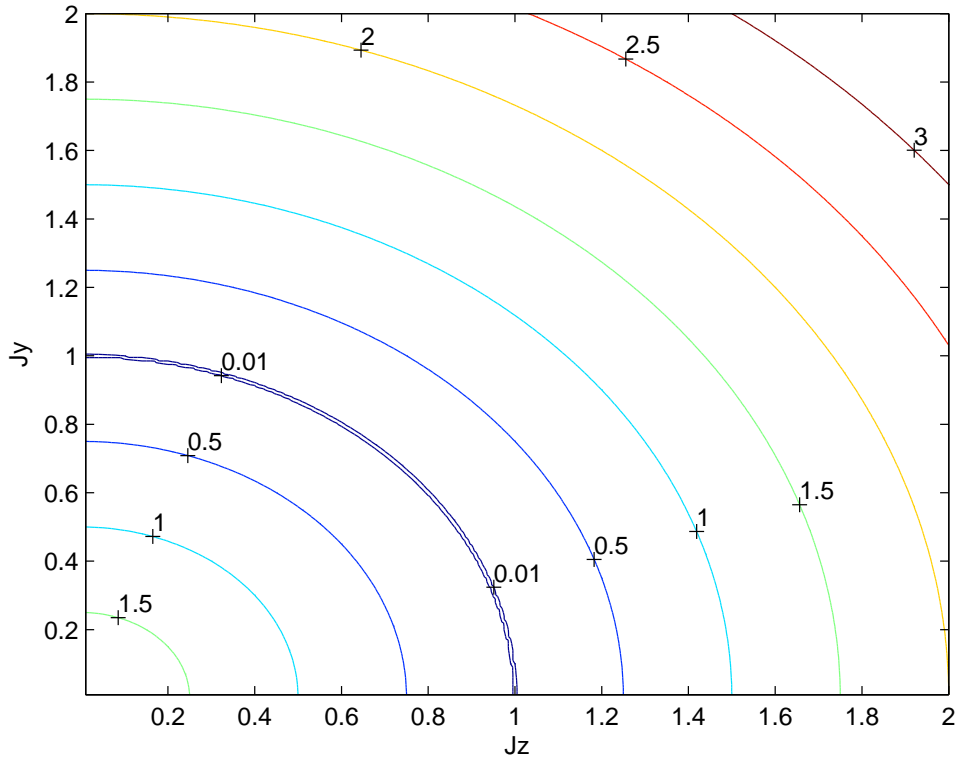


Figure 2.2: The contours of equal gap in the defect free flux sector plotted in the  $J_y - J_z$  plane at  $J_x = 1$  for a 100 a site system. It can be seen that the contours are circular with the unit circle being gapless.

The independent degenerate zero mode solutions peak around different sites. This is known as unpairing of zero mode eigenvectors.

Let us find out the condition in which zero modes exist in our model. For  $\epsilon = 0$  or  $\lambda = 0$ , eqn. (2.37) become,

$$\begin{aligned}
 J_x \phi_{i+1,1} + \frac{J_y^2 + u_i J_z^2}{J_x} \phi_{i,1} &= 0, \\
 J_x \phi_{i-1,4} + \frac{J_y^2 + u_i J_z^2}{J_x} \phi_{i,4} &= 0.
 \end{aligned}
 \tag{2.47}$$



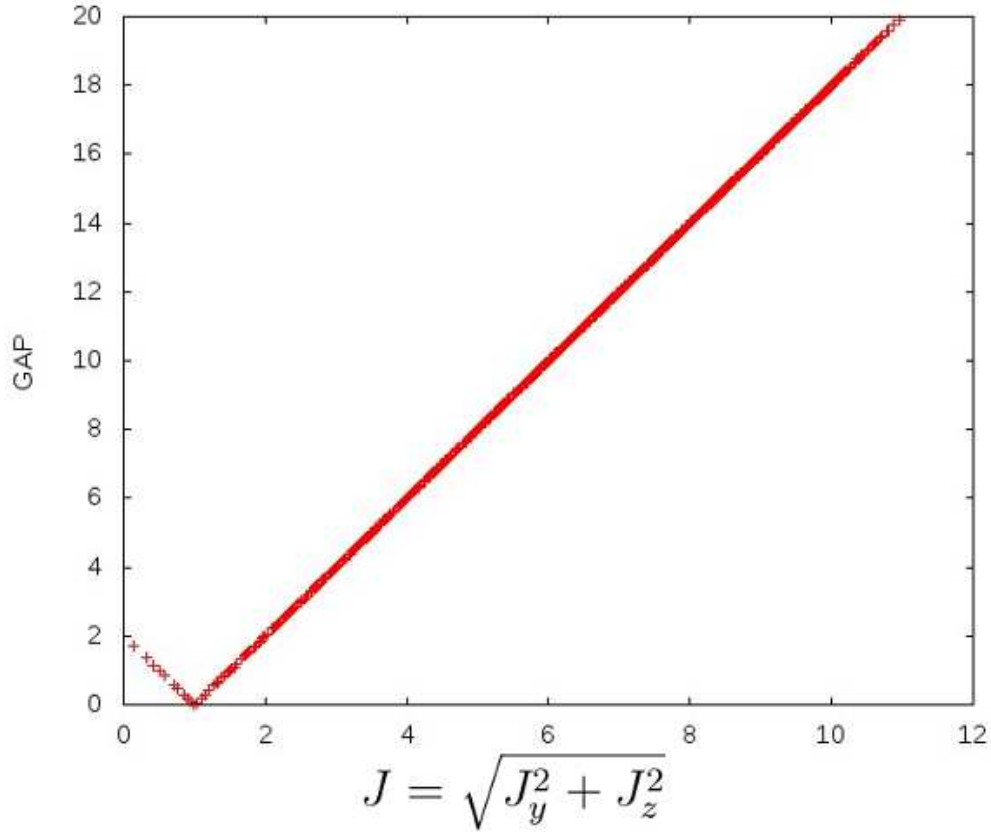


Figure 2.3: The gap in the defect free flux sector plotted against  $J \equiv \sqrt{J_y^2 + J_z^2}$  for a 100 site system. The points fall on straight lines with slopes  $\pm 2$ .

Solving these recursion relations we get,

$$\begin{aligned} \phi_{i,1} &= \prod_{j<i} \left( \frac{J_y^2 + u_j J_z^2}{J_x^2} \right) \phi_1 \\ \text{and } \phi_{i,4} &= \prod_{j>i} \left( \frac{J_y^2 + u_j J_z^2}{J_x^2} \right) \phi_4, \end{aligned} \quad (2.48)$$

where  $\phi_{1(4)}$  are arbitrary constants. Thus, there are two formal solutions for every set of values of the parameters and every flux configuration. One with  $\phi_{i,1} \neq 0$  and  $\phi_{i,4} = 0$ , which we denote by  $\phi^+$ , and the other with  $\phi_{i,1} = 0$  and  $\phi_{i,4} \neq 0$ , which we denote by  $\phi^-$ .

Analytic solutions are not easy for the non-translationally invariant flux sectors. While strong coupling and other techniques exist to study these sectors in certain

parameter ranges [46, 47, 48], a detailed analysis of the zero energy modes is generally not possible. However, the boundary conditions that the modes have to satisfy will pick out certain flux configurations for each point in the parameter space. We now analyse the situation for the cases of open boundary condition (OBC) and periodic boundary condition (PBC).

### 2.6.1 Periodic Boundary Condition

We consider a chain with  $N$  unit cells. As discussed in eqn. (2.27), PBC will imply that,

$$\phi_{N+1,1} = p\phi_{1,1}. \quad (2.49)$$

So, for zero modes to exist eqns. (3.90) and (2.49) imply,

$$\prod_{i=1}^N \left( \frac{J_y^2 + u_i J_z^2}{J_x^2} \right) = p. \quad (2.50)$$

Let us consider the general case where  $M \leq N$  of the  $u_i$ 's are equal to  $-1$  and  $N - M$  of them are  $+1$ . We refer to such configurations as  $M$ -defect configurations. Eqn. (2.50) can then be written as,

$$\left( \frac{J_y^2 - J_z^2}{J_y^2 + J_z^2} \right)^M = p \left( \frac{J_x^2}{J_y^2 + J_z^2} \right)^N. \quad (2.51)$$

Thus, for zero modes to exist for  $M = 0$  or ground state flux configuration,

$$p \left( \frac{J_x^2}{J_y^2 + J_z^2} \right)^N = 1. \quad (2.52)$$

We only have solutions on the circle of radius  $J_x$  in the  $J_y - J_z$  plane when  $p$  is positive. Thus, this result implies that the model is gapless only on the circle, in accordance with eqn. (2.45).

When  $M > 0$

$$\left( \frac{J_y^2 - J_z^2}{J_y^2 + J_z^2} \right)^M < 1. \quad (2.53)$$

Therefore,

$$\left(\frac{J_x^2}{J_y^2 + J_z^2}\right)^N < 1. \quad (2.54)$$

Thus, zero modes does not exist within the circle of radius  $J_x$ .

Outside the circle,

$$\left(\frac{J_x^2}{J_y^2 + J_z^2}\right)^N > 1. \quad (2.55)$$

So, for zero mode to exist,

$$\left(\frac{J_y^2 - J_z^2}{J_y^2 + J_z^2}\right)^M > p. \quad (2.56)$$

For every even  $M$ , eqn. (2.52) is satisfied for both  $J_y > J_z$  and  $J_z > J_y$  for  $p = +1$ . For odd  $M$ , the  $J_y > J_z$  solution exists for  $p = +1$  and the  $J_y < J_z$  solution exists for  $p = -1$ .

Thus, for every  $N$ , there is a discrete set of points outside the circle which support zero energy modes. In the thermodynamic limit of  $N \rightarrow \infty$ ,  $N/M$  can take all values from 1 to  $\infty$ . In this limit, all the points outside the circle in the range,  $J_x^2 \leq |J_y^2 - J_z^2| \leq 0$  support zero energy modes. This region is shown for  $J_x = 1$  in figure (2.4).

Let us consider the cases when the  $M$  defects are in adjoining unit cells, say from  $i = 1$  to  $i = M$ . We call this a kink-antikink configuration. We define polar coordinates in the  $J_y - J_z$  plane,

$$J \equiv \sqrt{J_y^2 + J_z^2}, \quad \gamma = \tan^{-1} \left( \frac{J_z}{J_y} \right). \quad (2.57)$$

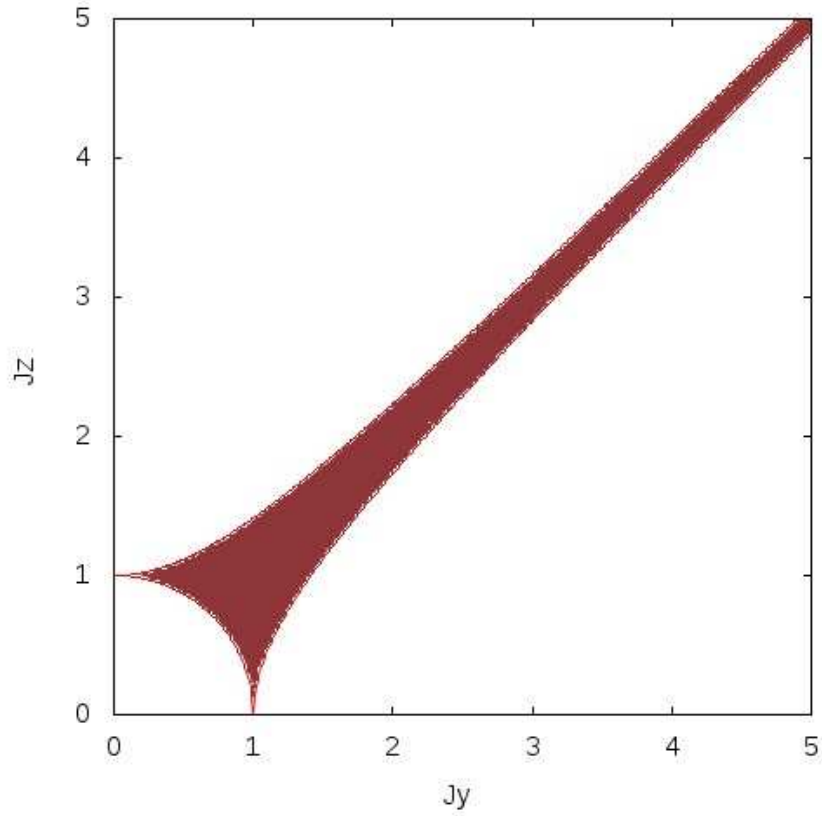


Figure 2.4: The region in the  $J_y - J_z$  plane at  $J_x = 1$  that supports zero energy modes in sectors with defects.

Then, the unnormalised wave functions of the two zero modes are given by,

$$\begin{aligned}
 \phi_{i,1}^+ &= J^{2(i-1)} (\cos 2\gamma)^{i-1} & i \leq M+1 \\
 &= J^{2(i-1)} (\cos 2\gamma)^{i-1-M} & i > M+1, \\
 \phi_{i,4}^+ &= 0 & (2.58)
 \end{aligned}$$

and

$$\begin{aligned}
 \phi_{i,4}^- &= J^{-2(i-1)} (\cos 2\gamma)^{-(i-1)} & i \leq M+1, \\
 &= J^{-2(i-1)} (\cos 2\gamma)^{-(i-1-M)} & i > M+1, \\
 \phi_{i,1}^- &= 0. & (2.59)
 \end{aligned}$$

$\phi_{i,2}^\pm$  and  $\phi_{i,3}^\pm$  are given in terms of  $\phi_{i,1}^\pm$  and  $\phi_{i,4}^\pm$ ,

$$\phi_{i,2}^\pm = \frac{1}{J_x} (J_y \phi_{i,1}^\pm - u_i^R J_z \phi_{i,4}^\pm), \quad (2.60)$$

$$\phi_{i,3}^\pm = \frac{1}{J_x} (u_i^L J_z \phi_{i,1}^\pm + J_y \phi_{i,4}^\pm). \quad (2.61)$$

It can be seen that  $\phi^+$  peaks at  $i=M$  and is minimum at  $i=1$  whereas  $\phi^-$  peaks at  $i=1$  and has a minimum at  $i = M$ . Thus, we have one Majorana mode localised at the location of the kink and another at the location of the antikink. When  $M$  is large these are well separated. If the flux configuration can be manipulated, then so can the Majorana modes trapped in them.

## 2.6.2 Open Boundary Condition

Let us now consider the Hamiltonian under open boundary condition with  $N$  unit cells. We then need to solve eqns. (2.47) with the boundary conditions (2.24). From the solutions in eqn. (2.48), we see that the above boundary condition has non trivial solutions if and only if atleast one of the factors in the products on the RHS of the eqn. (2.48) is zero. This is only possible when  $|J_y| = |J_z|$  and at least one  $u_i = -1$ . We can make unpaired majorana fermions to move along the chain tuning flux configuration as shown in figure (2.6).

In OBC the zero mode wavefunctions can be made to vanish in the region between the kink and the antikink. For example, if we consider a flux configuration with  $u_i = -1$ ,  $i_1 \leq i < i_1 + M$ , then the wavefunctions are given by,

$$\begin{aligned} \phi_{i,1}^+ &= J^{2(i-1)} \quad i \leq i_1, \\ &= 0 \quad i > i_1, \\ \phi_{i,4}^+ &= 0 \end{aligned} \quad (2.62)$$

$$\begin{aligned} \text{And } \phi_{i,4}^- &= J^{-2(i-1)} \quad i > i_1 + M, \\ &= 0 \quad i > M + 1, \\ \phi_{i,1}^- &= 0 \end{aligned} \quad (2.63)$$

and  $\phi_{i,2}^\pm$  and  $\phi_{i,3}^\pm$  are given in terms of  $\phi_{i,1}^\pm$  and  $\phi_{i,4}^\pm$  as before. These wavefunctions are shown in figure (2.5) for  $N = 25$  and  $M = 7$ .

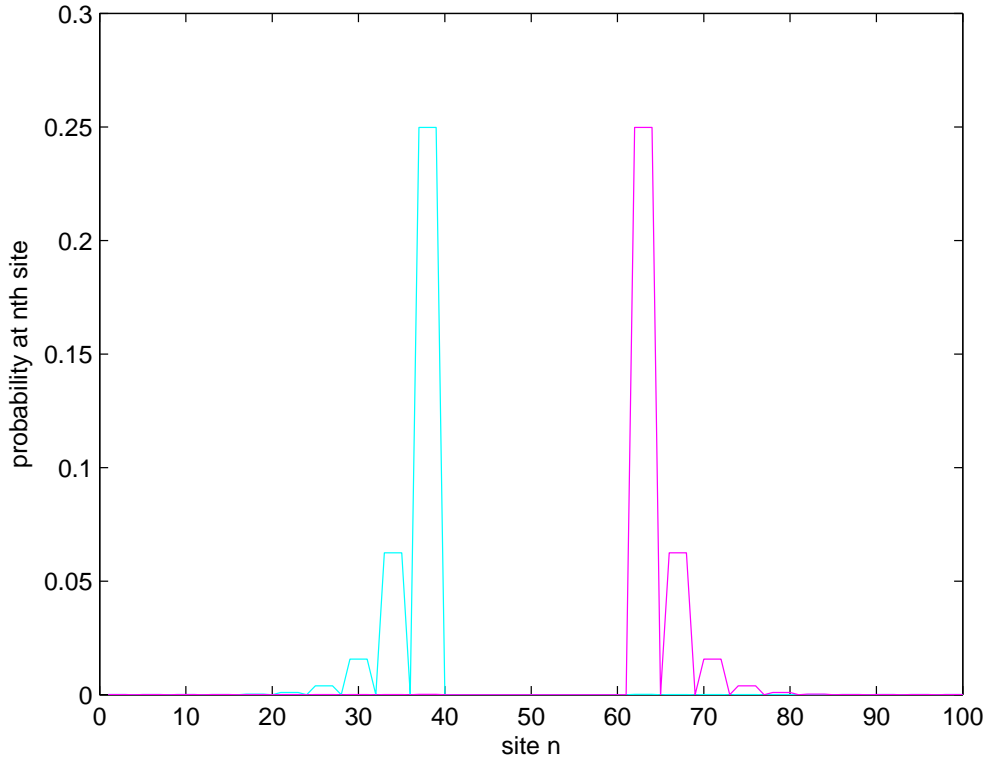


Figure 2.5: The wavefunctions of the two Majorana zero modes for  $N = 25$ ,  $M = 7$  with open boundary conditions.

### 2.6.3 Inhomogenous chains

The solutions for the zero mode eqn. (2.47) hold even for the case of inhomogenous chains where the coupling constants  $J_y$  and  $J_z$  depend on  $i$ . The equations then become,

$$\begin{aligned}
 J_x \phi_{i+1,1} + \frac{J_{y_i}^2 + u_i J_{z_i}^2}{J_x} \phi_{i,1} &= 0, \\
 J_x \phi_{i-1,4} + \frac{J_{y_i}^2 + u_i J_{z_i}^2}{J_x} \phi_{i,4} &= 0.
 \end{aligned}
 \tag{2.64}$$

The solutions of these recursion relations are exactly the same as these in the case of the homogenous chain with 'i' dependent  $J_{y(z)}$ .

$$\begin{aligned}\phi_{i,1} &= \prod_{j<i} \left( \frac{J_{yj}^2 + u_j J_{zj}^2}{J_x^2} \right) \phi_1, \\ \phi_{i,4} &= \prod_{j>i} \left( \frac{J_{yj}^2 + u_j J_{zj}^2}{J_x^2} \right) \phi_4.\end{aligned}\tag{2.65}$$

It is clear that by tuning the values of the site dependent couplings, a large variety of zero mode wavefunctions can be engineered.

### 2.6.4 The Qubit

As  $\phi_i^n$ 's obey the orthogonality and completeness relation, we can define inversely from eqn.(2.16),

$$\chi^n = \sum_i \phi_i^n \xi_i,\tag{2.66}$$

where we take  $\phi^1$  and  $\phi^2$  to be two independent degenerate zero modes.

We redefine  $\chi^1$  and  $\chi^2$  as  $\chi^{01}$  and  $\chi^{01\dagger}$  by,

$$\begin{aligned}\chi^{01} &= (\chi^1 + i\chi^2), \\ \chi^{01\dagger} &= (\chi^1 - i\chi^2).\end{aligned}\tag{2.67}$$

If the vacuum  $|0\rangle$  is defined by  $\chi^n|0\rangle = 0, \forall n$ , then the lowest level degenerate multiparticle states

$$\begin{aligned}|0\rangle, \\ \chi^{01\dagger}|0\rangle\end{aligned}$$

are the  $|0\rangle$  and  $|1\rangle$  of the proposed qubit.

### 2.6.5 Tuning the flux configuration

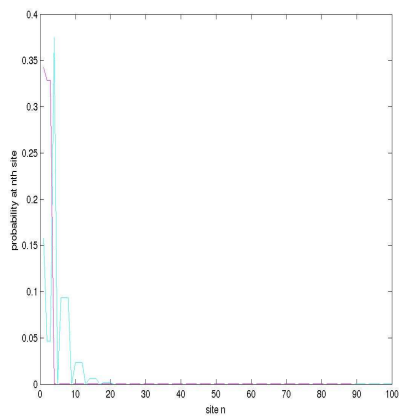
We can add the following “chemical potential” term for the plaquette operators,

$$H_\mu = \sum_i (\mu_i^L W_i^L + \mu_i^R W_i^R). \quad (2.68)$$

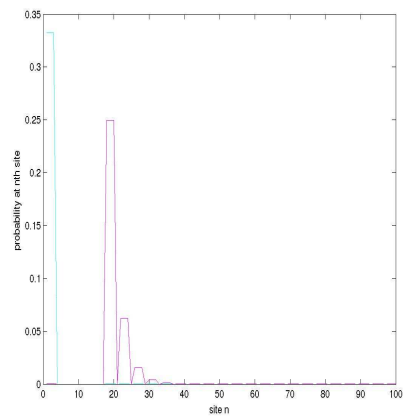
This term is commuting with the Hamiltonian, adding it into the hamiltonian will not change the eigenstates but will change the energy eigenvalues. If the  $\mu_i^{L(R)}$  can be tuned, then any particular flux configurations can be made the ground state.

However, it is still not known how to engineer these 3-spin operators in the physical realisation of the model in quantum circuits. Therefore, we propose another model in the next chapter 3 where commuting operators are 2-spin operators. In the chapter 5, we show how to realise this model and its commuting operators.

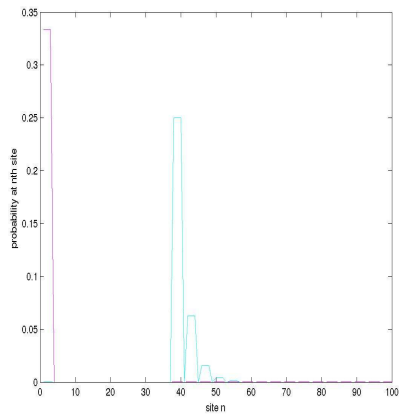




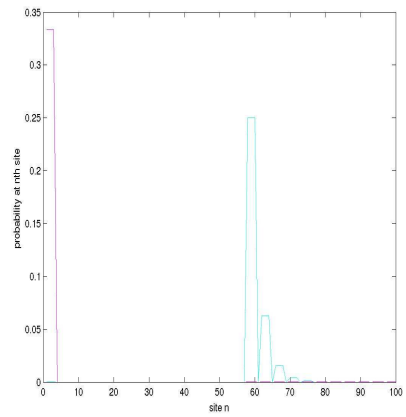
(a)



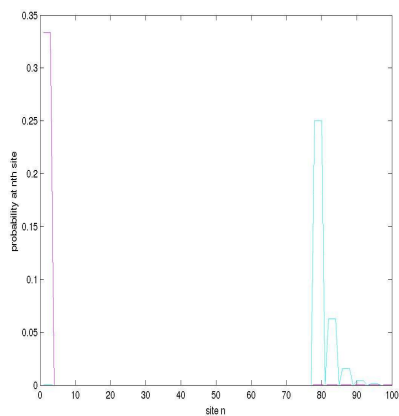
(b)



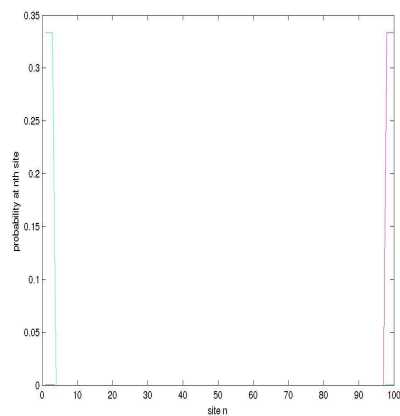
(c)



(d)



(e)



(f)

Figure 2.6: Unpairing with 1, 5, 10, 15, 20 and 25 defects in figure (a), (b), (c), (d), (e) and (f) respectively. The defects have been put from the left end of the chain of 25 unit cells.

# 3

## XYZ-Ising Model: Exact Solutions

In this chapter, we will describe a simpler version of Tetrahedron Model which we call XYZ-Ising Model. The Tetrahedron model has localised unpaired Majorana modes which we can move around the lattice by tuning the defects using three-spin commuting operators. The same thing can be achieved in the XYZ-Ising model. The main motivation to study this model is that the unpaired Majorana modes can be moved around using two-spin commuting operators. We solve the model using the Kitaev's method and reproduce their results. We further bring out the topological nature of the excitations of the model.

### 3.1 The Hamiltonian

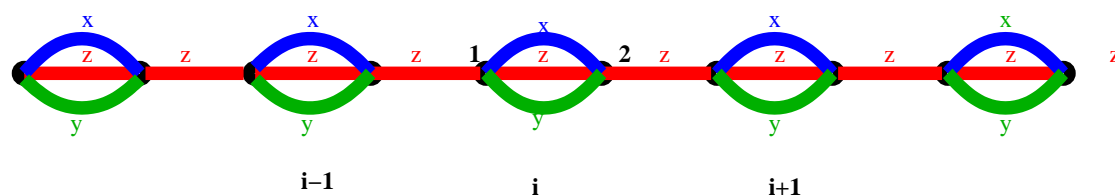


Figure 3.1: The XYZ-Ising chain. There are two sites per unit cell. The  $x$ ,  $y$  and  $z$  bonds are as indicated.

The Hamiltonian,

$$H = \sum_i^N (J_x \sigma_{i,1}^x \sigma_{i,2}^x + J_y \sigma_{i,1}^y \sigma_{i,2}^y + J_z \sigma_{i,1}^z \sigma_{i,2}^z + \sigma_{i,2}^z \sigma_{i+1,1}^z). \quad (3.1)$$

Leib, Schultz and Mattis have studied the model for  $J_x = J_y = J_z$  [49].

The periodic boundary condition (PBC) is given by,

$$\sigma_{N+1,1}^z = \sigma_{1,1}^z. \quad (3.2)$$

In each unit cell there is a commuting operator  $W_i$ ,

$$W_i = \sigma_{i,1}^z \sigma_{i,2}^z. \quad (3.3)$$

Apart from these local conserved operators there are also three global operators which are conserved as a consequence the fact that a global  $\pi$  rotation about each of the three axes is a symmetry of the model. We denote these by,

$$\Sigma^a \equiv e^{i\frac{\pi}{2} \sum_{i,a} \sigma_{i,a}^a}. \quad (3.4)$$

It can be verified that  $\Sigma^z$  is the product of the fluxes of all the bond operators,

$$\Sigma^z = \prod_i (W_i). \quad (3.5)$$

The XYZ-Ising model Hamiltonian can also be written as

$$H = \sum_i^N (J_x \sigma_{i,1}^x \sigma_{i,2}^x + J_y \sigma_{i,1}^y \sigma_{i,2}^y + J_z W_i + \sigma_{i,2}^z \sigma_{i+1,1}^z). \quad (3.6)$$

Therefore, the eigenstates of the model are independent of  $J_z$ . In this chapter, we will focus on  $J_z = 0$  which we call XY-Ising model. The chain we define our model

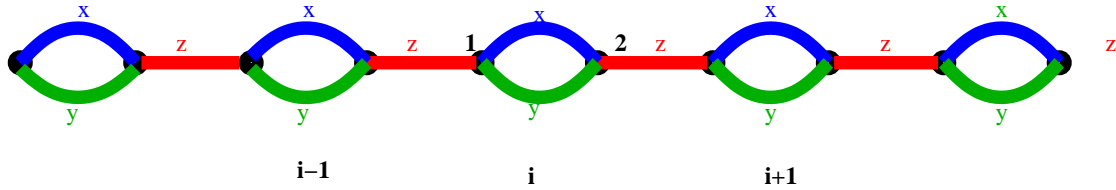


Figure 3.2: The XY-Ising chain. There are two sites per unit cell. The  $x$ ,  $y$  and  $z$  bonds are as indicated.

on, is shown in figure (3.2).

The Hamiltonian is,

$$H = \sum_{i=1}^N (J_x (\sigma_{i,1}^x \sigma_{i,2}^x) + J_y (\sigma_{i,1}^y \sigma_{i,2}^y) + (\sigma_{i,2}^z \sigma_{i+1,1}^z)). \quad (3.7)$$

## 3.2 Fermionisation

We choose the Jordan-Wigner path to go along the  $y$  and the  $z$  bonds from left to right. At every site we have two bonds that are tangential to the path. We denote the incoming bond by  $t_1$  and the outgoing bond by  $t_2$ . The third bond on each site which is normal to the path is denoted by  $n$  with the sign defined by  $\hat{n} = \hat{t}_1 \times \hat{t}_2$ . With our choice of path,

$$\begin{aligned} \sigma_{i,1}^x &\rightarrow -\sigma_{i,1}^n \\ \sigma_{i,2}^x &\rightarrow \sigma_{i,2}^n \\ \sigma_{i,1}^y &\rightarrow \sigma_{i,1}^{t_2} \\ \sigma_{i,2}^y &\rightarrow \sigma_{i,2}^{t_1} \\ \sigma_{i,1}^z &\rightarrow \sigma_{i,1}^{t_1} \\ \sigma_{i,2}^z &\rightarrow \sigma_{i,2}^{t_2}. \end{aligned} \quad (3.8)$$

So, Hamiltonian can be written as

$$H = \sum_{i=1}^N (-J_x (\sigma_{i,1}^n \sigma_{i,2}^n) + J_y (\sigma_{i,1}^{t_2} \sigma_{i,2}^{t_1}) + (\sigma_{i,2}^{t_2} \sigma_{i+1,1}^{t_1})). \quad (3.9)$$

with periodic boundary condition,

$$\sigma_{N+1,1}^{t_1} \equiv \sigma_{1,1}^{t_1}. \quad (3.10)$$

The commuting operator becomes,

$$W_i = \sigma_{i,1}^{t_1} \sigma_{i,2}^{t_2}. \quad (3.11)$$

We express the Hamiltonian in terms of Majorana fermions using the Jordan-Wigner transformation. The two Majorana operators at each site are defined as,

$$\begin{aligned}\xi_{i,\alpha} &= \sigma_{i,\alpha}^{t_1} \prod_{j<i} \left( \prod_{\beta<\alpha} \sigma_{j,\beta}^n \right), \\ \eta_{i,\alpha} &= \sigma_{i,\alpha}^{t_2} \prod_{j<i} \left( \prod_{\beta<\alpha} \sigma_{j,\beta}^n \right).\end{aligned}\quad (3.12)$$

$\xi_i$  and  $\eta_i$  operators follow anti commutation relation,

$$\{\xi_i, \xi_j\} = 2\delta_{i,j}; \quad \{\eta_i, \eta_j\} = 2\delta_{i,j}; \quad \{\xi_i, \eta_j\} = 0. \quad (3.13)$$

The Hamiltonian can be expressed in terms of the Majorana operators as defined above,

$$\begin{aligned}H &= \sum_{i=1}^N (J_y - J_x \hat{u}_i) i\xi_{i,1}\xi_{i,2} + \sum_{i=1}^{N-1} i\xi_{i,2}\xi_{i+1,1} \\ &+ i \prod_i^n (i\xi_{i,1}\xi_{i,2}) \prod_i^N (\hat{u}_i) i\xi_{N,2}\xi_{1,1},\end{aligned}\quad (3.14)$$

where the link fields,  $\hat{u}_i$  are defined as,

$$\hat{u}_i \equiv i\eta_{i,1}\eta_{i,2}. \quad (3.15)$$

The commuting operator  $W_i$  becomes

$$W_i = -i\eta_{i,1}\eta_{i,2}. \quad (3.16)$$

It is easy to see that the link fields are commuting operators. As  $\hat{u}_i^2 = 1$ ,  $\hat{u}_i$  has two eigenvalues  $\pm 1$ . We can interpret it as flux passing through x-y bond and denote it by  $u_i$ . Thus, the interacting Hamiltonian of spin half operators transforms into a non-interacting Hamiltonian of Majorana operators with nearest neighbour hopping in the background of conserved  $Z_2$  gauge fields with the gauge fixing condition that the gauge fields on the  $y$  and  $z$  bonds are equal to  $+1$ .

We can express the three global conserved quantities,  $\Sigma^a$  in terms of the

fermionic variables,

$$\begin{aligned}
 \Sigma^z &= \prod_i^N (-i\eta_{i,1}\eta_{i,2}) = \prod_i^N \hat{u}_i, \\
 \Sigma^y &= \prod_i^N (i\xi_{i,1}\xi_{i,2}), \\
 \text{and } \Sigma^x &= \Sigma^y \Sigma^z = \prod_i^N (i\xi_{i,1}\xi_{i,2}) \prod_i^N \hat{u}_i.
 \end{aligned} \tag{3.17}$$

We refer to  $\Sigma^z$  as the flux number and  $\Sigma^y$  as the Majorana number.

From eqn. (3.17), we can write

$$H = \sum_{i=1}^N (J_y - J_x \hat{u}_i) i\xi_{i,1}\xi_{i,2} + \sum_{i=1}^{N-1} i\xi_{i,2}\xi_{i+1,1} + i\Sigma^x \xi_{N,2}\xi_{1,1}, \tag{3.18}$$

where  $\prod_i^N (i\xi_{i,1}\xi_{i,2}) \prod_i^N \hat{u}_i = \Sigma^x$  is a conserved quantity. Hence, Hamiltonian can be diagonalised in the basis of  $\Sigma^x$ .

Thus, the spin Hamiltonian gets converted into the fermionic hamiltonian with periodic boundary condition with  $\Sigma^x = +1$  and with anti-periodic boundary conditions for states with  $\Sigma^x = -1$ .

### 3.3 Diagonalisation

The Hamiltonian can be diagonalised in the standard way. We write the eigenstates as direct products of states  $|\mathcal{G}\rangle$  in the  $\eta$  fermion sector and states  $|\mathcal{M}\rangle$  in the  $\xi$  fermion sector. We will refer to states belonging to  $\eta$  fermion sector as the gauge sector and states belonging to  $\xi$  fermion sector as matter sector. We choose the states in the gauge sector to be the simultaneous eigenstates of the  $Z_2$  flux operators, i.e  $|\mathcal{G}\rangle = |\{u_i\}\rangle$ , where

$$\hat{u}_i |\{u_i\}\rangle = u_i |\{u_i\}\rangle. \tag{3.19}$$

We then have

$$H[\hat{u}_i]|\mathcal{M}\rangle|\{u_i\}\rangle = H[u_i]|\mathcal{M}\rangle|\{u_i\}\rangle. \quad (3.20)$$

Therefore, the problem reduces to finding the eigenstates of the quadratic Hamiltonian of the  $\xi$  fermions in the background of the gauge field configuration  $\{u_i\}$ .

We can write the Hamiltonian as

$$H = \sum_{i,\alpha} \sum_{j,\beta} \xi_{i,\alpha} h_{i\alpha,j\beta} \xi_{i,\beta}. \quad (3.21)$$

To diagonalise the Hamiltonian, we substitute

$$\xi_{i,a} = \sum_n \phi_{i,a}^{*n} \chi_n, \quad (3.22)$$

where normal modes  $\phi_i^{n,a}$  are found out by solving single particle eigenvalue equation,

$$\sum_{j,\beta} h_{i\alpha,j\beta} \phi_{j,\beta}^n = \epsilon_n \phi_{i,\alpha}^n, \quad (3.23)$$

where  $h$  is a purely imaginary hermitian matrix. For every positive eigenvalue, single particle Hamiltonian  $h$  has one negative eigenvalue and the eigenvectors corresponding to the positive and negative eigenvalues are complex conjugates of each other.

The normal modes  $\phi_i^{n,a}$ 's obey orthogonality and completeness relation.

$$\begin{aligned} \sum_i \phi_{i,a}^{m*} \phi_{i,a}^n &= \delta_{m,n}, \\ \sum_n \phi_{i,a}^n \phi_{j,a}^{n*} &= \delta_{i,j}. \end{aligned} \quad (3.24)$$

In eqn. (3.22),  $\chi^n$  and  $\chi^{n\dagger}$  are fermionic operators and follow the commutation relation,

$$\{\chi^{m\dagger}, \chi^n\} = \delta_{m,n}. \quad (3.25)$$

The diagonal form of the Hamiltonian is then,

$$H = \sum_n \epsilon_n (2\chi^{n\dagger}\chi^n - 1). \quad (3.26)$$

Therefore, ground state energy  $E_0$  can be written as,

$$E_0 = - \sum_n \epsilon_n. \quad (3.27)$$

### 3.4 Exact Solution for all Sectors

The Hamiltonian for special case  $J_x = J_y = \frac{J}{2}$  is,

$$H = \sum_{i=1}^N \left( \frac{J}{2} (1 - u_i) i\xi_{i,1}\xi_{i,2} \right) + \sum_{i=1}^{N-1} (i\xi_{i,2}\xi_{i+1,1}) + i\xi_{N,2}\xi_{1,1}\Sigma_x. \quad (3.28)$$

The Hamiltonian for special case  $J_x = J_y = \frac{J}{2}$  can be solved exactly for all sectors because whenever  $u_i = +1$ , at the  $i$ th unit cell, the chain is cut at that unit cell. Let us call  $u_i = -1$ , for all  $i$ , the defect free state and refer to every  $u_i = +1$  as a defect.

#### 3.4.1 The 0-defect sector

With the notation introduced above, the defect free sector corresponds to a Majorana fermions with nearest neighbour hopping on a closed chain of  $2N$  sites,

$$H = \sum_{i=1}^N (iJ\xi_{i,1}\xi_{i,2}) + \sum_{i=1}^{N-1} (i\xi_{i,2}\xi_{i+1,1}) + i\xi_{N,2}\xi_{1,1}\Sigma_x. \quad (3.29)$$

The defect free sector consists of two sectors corresponding to periodic or anti-periodic boundary conditions for  $\Sigma_x = +1$  and  $\Sigma_x = -1$  respectively.

We can write the Hamiltonian as

$$H = \sum_{i=1}^N (iJ\xi_{i,1}\xi_{i,2} + i\xi_{i,2}\xi_{i+1,1}), \quad (3.30)$$



with boundary condition

$$\xi_{1,1} = \pm \xi_{N+1,1}, \quad (3.31)$$

where +1 corresponds to (PBC) and -1 corresponds to Anti-(PBC).

The single particle eigenvalue equation in the zero defect sector is,

$$\begin{aligned} \frac{-i}{2}\phi_{i-1,2} + \frac{iJ}{2}\phi_{i,2} &= \epsilon\phi_{i,1} \\ \text{and } \frac{-iJ}{2}\phi_{i,1} + \frac{i}{2}\phi_{i+1,1} &= \epsilon\phi_{i,2}, \end{aligned} \quad (3.32)$$

with boundary conditions

$$\phi_{1,1} = \phi_{N+1,1}. \quad (3.33)$$

We use Fourier transform to solve this equation,

$$\phi_{i,a} = \frac{1}{\sqrt{N}} \sum_k \phi_{k,a} e^{-ikR_i}, \quad (3.34)$$

$$(3.35)$$

then, single particle energy eigenvalue equation becomes,

$$\begin{aligned} \frac{(-ie^{ika} + iJ)}{2}\phi_{k,2} &= \epsilon(k)\phi_{k,1} \\ \text{and } \frac{(-iJ + ie^{-ika})}{2}\phi_{k,1} &= \epsilon(k)\phi_{k,2}. \end{aligned} \quad (3.36)$$

The boundary condition implies that

$$e^{ikNa} = \pm 1. \quad (3.37)$$

Therefore,

$$ka = \frac{(2m - a)\pi}{N}, \quad (3.38)$$

where  $m = 1, 2, 3 \dots N$  and  $a = 0, 1$  for PBC and anti-PBC respectively.

So, Hamiltonian becomes

$$H = \sum_{k=1}^N \left( \frac{iJ - ie^{ika}}{2} \right) \xi_{k,1}^+ \xi_{k,2} + h.c., \quad (3.39)$$

$$\text{or, } H = \sum_{k=1}^N \begin{bmatrix} \xi_{k,1}^+ \xi_{k,2} \end{bmatrix} \begin{bmatrix} 0 & \frac{i}{2} \epsilon_k e^{i\alpha_k} \\ -\frac{i}{2} \epsilon_k e^{-i\alpha_k} & 0 \end{bmatrix} \begin{bmatrix} \xi_{k,1} \\ \xi_{k,2} \end{bmatrix}, \quad (3.40)$$

$$\text{where } \epsilon_k e^{i\alpha_k} = J - e^{ika}$$

Solving the Hamiltonian, we get

$$H = \sum_k (\epsilon_1(k) \chi_{k,1}^+ \chi_{k,1} + \epsilon_2(k) \chi_{k,2}^+ \chi_{k,2}), \quad (3.41)$$

where  $\epsilon_{1,2}(k)$  is given by,

$$\epsilon_{1,2}(k) = \pm \sqrt{J^2 - 2J \cos(ka) + 1}, \quad (3.42)$$

and  $\chi_{k,1}$  and  $\chi_{k,2}$  is given by,

$$\begin{bmatrix} \chi_{k,1} \chi_{k,2} \end{bmatrix} = \begin{bmatrix} 1 & 1 \\ ie^{-i\alpha_k} & -ie^{i\alpha_k} \end{bmatrix} \begin{bmatrix} \xi_{k,1} \\ \xi_{k,2} \end{bmatrix}. \quad (3.43)$$

### 3.4.2 The 1-defect sector

Without any loss of generality, we can choose  $u_N = 1$  and all other  $u_i = -1$ . The eqn. (3.28) then becomes,

$$H = \sum_{i=1}^{N-1} (iJ \xi_{i,1} \xi_{i,2} + i \xi_{i,2} \xi_{i+1,1}) + i \xi_{N,2} \xi_{1,1} \Sigma_x. \quad (3.44)$$

We redefine  $\xi_{N,2}\Sigma_x \rightarrow \xi_{N,2}$ . The Hamiltonian then becomes,

$$H = \sum_{i=1}^{N-1} (iJ\xi_{i,1}\xi_{i,2} + i\xi_{i,2}\xi_{i+1,1}) + i\xi_{N,2}\xi_{1,1}. \quad (3.45)$$

This corresponds to the fermions on an open chain with N sites.

Let us relabel the site and replace  $\xi_{N,2}$  by  $\xi_{0,2}$  so that we can express the Hamiltonian in a concise form,

$$H = \sum_{i=1}^{N-1} iJ\xi_{i,1}\xi_{i,2} + \sum_{i=0}^{N-1} i\xi_{i,2}\xi_{i+1,1}. \quad (3.46)$$

The boundary condition is,

$$\begin{aligned} \xi_{0,1} &= 0 \\ \text{and } \xi_{N,2} &= 0. \end{aligned} \quad (3.47)$$

We can write the Hamiltonian as,

$$H = \sum_{i,\alpha} \sum_{j,\beta} \xi_{i,\alpha} h_{i\alpha,j\beta} \xi_{i,\beta}. \quad (3.48)$$

The single particle eigenvalue equation in one defect sector is,

$$\sum_{j,\beta} h_{i\alpha,j\beta} \phi_{j,\beta} = \epsilon \phi_{i,\alpha}. \quad (3.49)$$

Therefore,

$$\begin{aligned} \frac{-i}{2} \phi_{i-1,2} + \frac{iJ}{2} \phi_{i,2} &= \epsilon \phi_{i,1} \\ \text{and } \frac{-iJ}{2} \phi_{i,1} + \frac{i}{2} \phi_{i+1,1} &= \epsilon \phi_{i,2}, \end{aligned} \quad (3.50)$$

with boundary conditions

$$\begin{aligned} \phi_{0,1} &= 0 \\ \text{and } \phi_{N,2} &= 0. \end{aligned} \quad (3.51)$$

We use now the standing waves transform to solve this open chain problem,

$$\phi_{i,a} = \frac{1}{\sqrt{2N}} \sum_k \phi_{k,a} e^{ikR_i} + \phi_{-k,a} e^{-ikR_i}. \quad (3.52)$$

Substituting  $\phi_{i,1}$  and  $\phi_{i,2}$  in eqn. (3.50) and equating  $e^{ikR_i}$  and  $e^{-ikR_i}$ , we get

$$\begin{aligned} \frac{(-ie^{ika} + iJ)}{2} \phi_{k,2} &= \epsilon \phi_{k,1} \\ \frac{(-iJ + ie^{-ika})}{2} \phi_{k,1} &= \epsilon \phi_{k,2}. \end{aligned} \quad (3.53)$$

$$\text{or, } \begin{bmatrix} -\epsilon & \frac{i}{2} \epsilon_k e^{i\alpha_k} \\ -\frac{i}{2} \epsilon_k e^{-i\alpha_k} & -\epsilon \end{bmatrix} \begin{bmatrix} \phi_{k,1} \\ \phi_{k,2} \end{bmatrix} = 0, \quad (3.54)$$

where we substitute

$$J - e^{ika} = \epsilon_k e^{i\alpha_k}. \quad (3.55)$$

The relation  $J - e^{ika} = \epsilon_k e^{i\alpha_k}$  has been shown in the Argand plane in the figure (3.3) and figure (3.4).

$\alpha_k$  is given by,

$$\tan \alpha_k = \frac{-\sin(ka)}{J - \cos(ka)}. \quad (3.56)$$

For non trivial solution,

$$\begin{vmatrix} -\epsilon & \frac{i\epsilon_k e^{i\alpha_k}}{2} \\ \frac{-i\epsilon_k e^{-i\alpha_k}}{2} & -\epsilon \end{vmatrix} = 0. \quad (3.57)$$

Therefore,  $\epsilon(k)$  is given by

$$\epsilon_{1,2}(k) = \pm \epsilon_k = \pm \frac{1}{2} \sqrt{J^2 - 2J \cos(ka) + 1}, \quad (3.58)$$

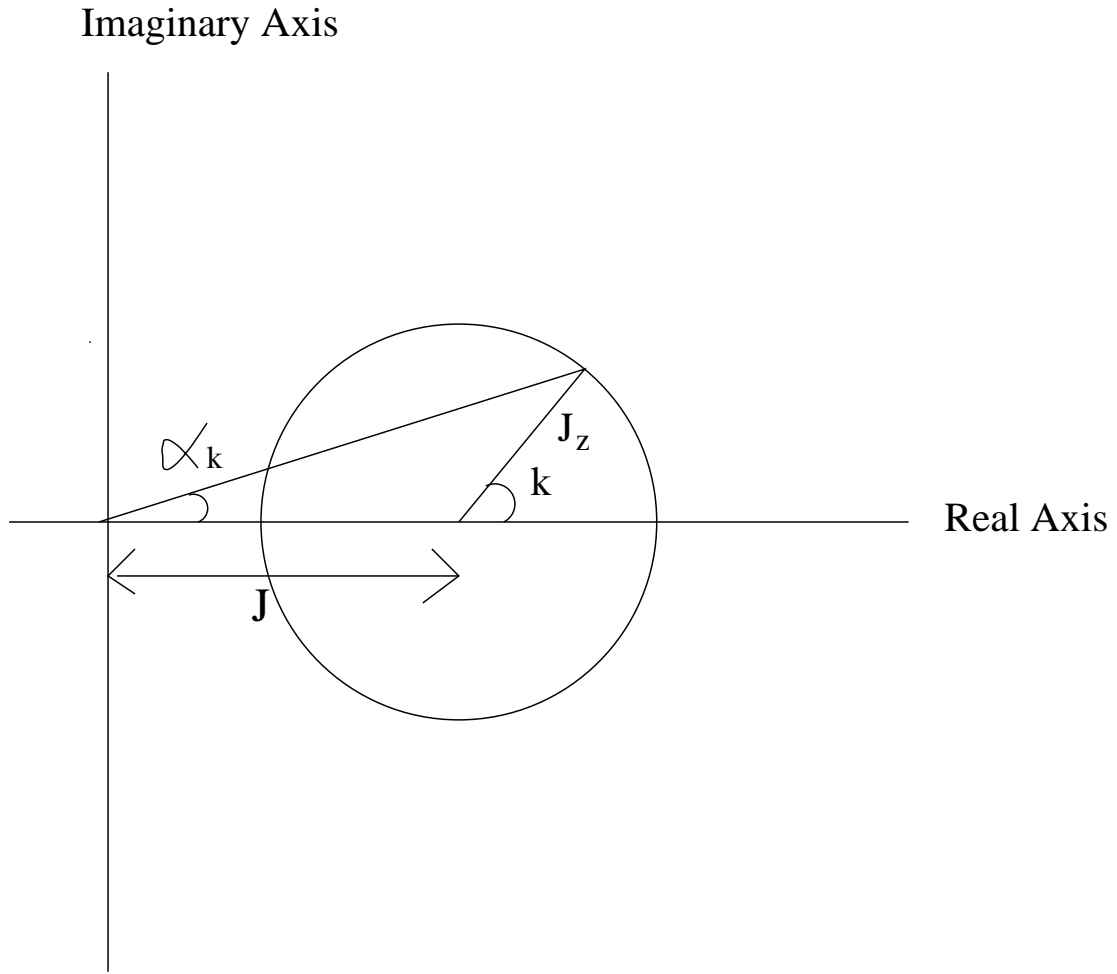


Figure 3.3:  $J - e^{ika} = \epsilon_k e^{i\alpha_k}$  in Argand plane. For  $J > 1$ ,  $\alpha(0) = 0$  and  $\alpha(\pi) = 0$ .

and phase factors  $\phi_{k,1}$  and  $\phi_{k,2}$  are,

$$\phi_{k,1} = \pm i e^{\alpha_k} \phi_{k,2}. \quad (3.59)$$

The boundary condition  $\phi_{0,1} = 0$  and  $\phi_{N,2} = 0$  from eqn. (3.52) implies that

$$\phi_{k,1} = -\phi_{-k,1} \quad (3.60)$$

$$\phi_{k,2} = -\phi_{-k,2} e^{-2i(N+1)ka}, \quad (3.61)$$

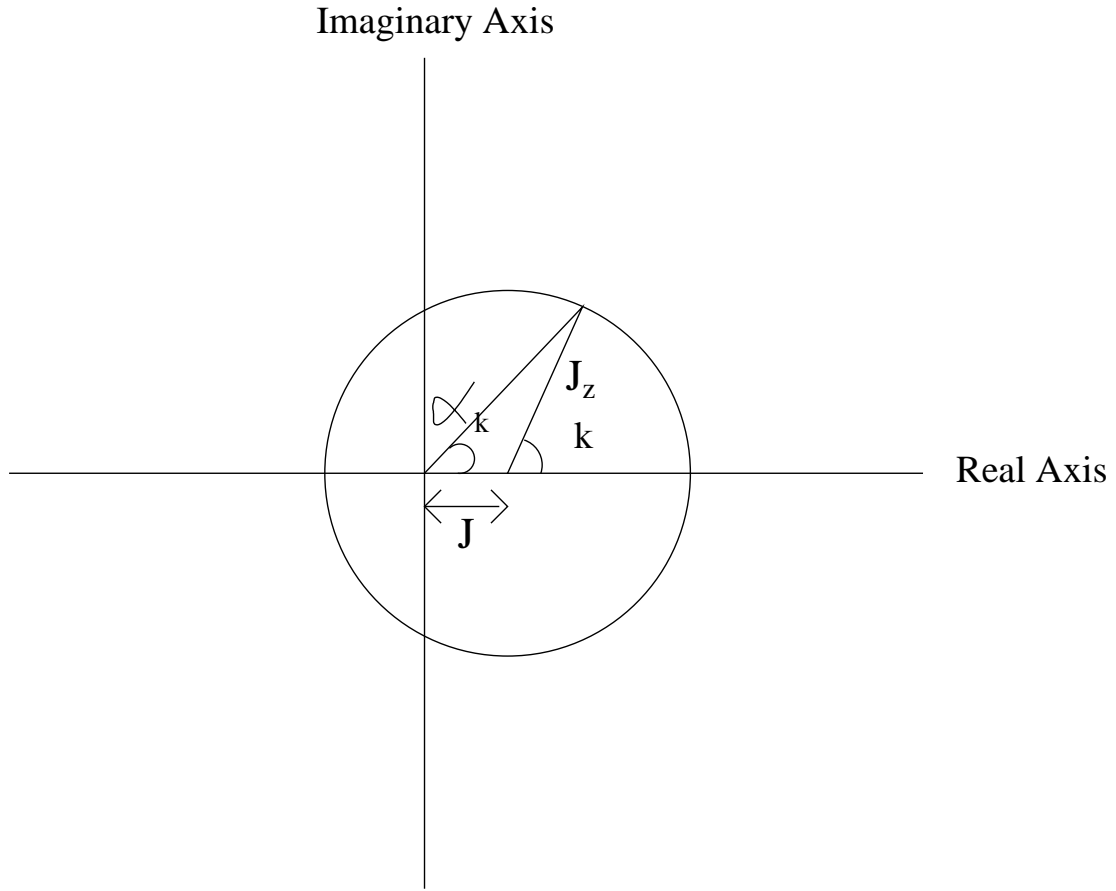


Figure 3.4:  $J - e^{ika} = \epsilon_k e^{i\alpha_k}$  in Argand plane. For  $J < 1$ ,  $\alpha(0) = 0$  and  $\alpha(\pi) = \pi$ .

and substituting  $\phi_{k,1}$  and  $\phi_{-k,1}$  from eqn. (3.59) in eqn. (3.60),

$$\phi_{-k,2} = -e^{2i\alpha_k} \phi_{k,2}. \quad (3.62)$$

Using eqn. (3.61), above eqn. becomes,

$$e^{2i\alpha_k} = e^{2i(N+1)ka}. \quad (3.63)$$

The solution of this eqn. gives the values of  $k$ ,

$$ka = \frac{n\pi}{N+1} + \frac{\alpha_k}{N+1}, \quad (3.64)$$

where  $n$  goes to 1 to  $N$ .

Thus, one defect sector Hamiltonian has been solved.

Here, we have solved eqn. (3.56) and eqn. (3.64) numerically for  $N=10$  and plotted  $k$  versus  $n$  for  $J > 1$  and  $J < 1$  as shown in figure 3.5. In this figure,

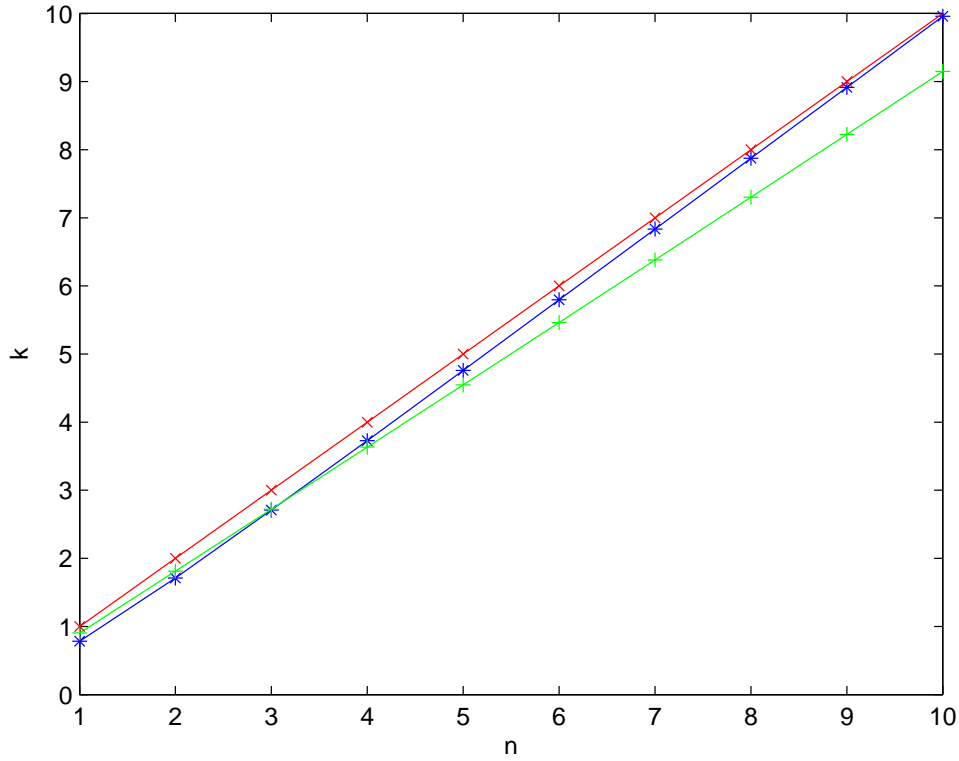


Figure 3.5: The red line shows the plot between  $k$  and  $n$  without the correction  $\alpha_k$ . The green and blue line shows the plot between  $k$  and  $n$  for  $J < 1$  and for  $J > 1$  respectively.

one can see that for  $J < 1$  number of allowed values of  $k$  for  $N$  ( $N=10$ ) is  $N$ . But for  $J > 1$  number of allowed values of  $k$  (for  $N=10$ ) is  $N-1$ . The missing one mode is zero mode of the model. Since the appearance of the zero mode depends on the topology of parameters of Hamiltonian as shown in figure (3.3) and (3.4), therefore, zero mode of the Hamiltonian is robust.

### 3.4.3 The $n_D$ -defect sector

If we define,

$$H_L = \sum_{i=1}^{L-1} (iJ\xi_{i,1}\xi_{i,2} + i\xi_{i,2}\xi_{i+1,1}) + i\xi_{L,2}\xi_{1,1}, \quad (3.65)$$

then the one defect sector hamiltonian is,

$$H = H_L. \quad (3.66)$$

The two defect sector hamiltonian is,

$$H = H_{L_1} + H_{L_2}, \quad L_1 + L_2 = N, L_{1(2)} \geq 1 \quad (3.67)$$

and, similarly,  $n_D$  sector hamiltonian is,

$$H = \sum_{n=1}^{n_D} H_{L_n}, \quad (3.68)$$

$$\text{where } \sum_{n=1}^{n_D} L_n = N, L_n \geq 1.$$

Thus, the one defect sector Hamiltonian is equivalent to open chain Hamiltonian and  $n_D$  defect sector Hamiltonian is equivalent to  $n_D$  open chain Hamiltonian. So, if we can solve one open chain Hamiltonian we can solve the Hamiltonian in all sectors.

## 3.5 Ground State and Gap

In this section, we prove that zero defect sector is the ground state sector of XY-Ising Hamiltonian.

For Hamiltonian with (PBC),

$$H = \sum_{i=1}^N \left( \frac{J}{2} (1 - u_i) i\xi_{i,1}\xi_{i,2} \right) + \sum_{i=1}^{N-1} (i\xi_{i,2}\xi_{i+1,1}) + i\xi_{N,2}\xi_{1,1}\Sigma_x. \quad (3.69)$$



In order to prove the statement, first we show that the ground state energy of zero defect sector is less than that of one defect sector for large  $N$ . Then, we prove that ground state energy of one defect sector is less than that of two defect sector, and so on.

So, let us first show that the ground state energy of zero defect sector is less than that of one defect sector.

Let us consider the ground state energy  $GSE_{zds}$  of zero defect sector,

$$GSE_{zds} = - \sum_{k=1}^N f\left(\frac{2k\pi}{N}\right), \quad (3.70)$$

where  $f(k) = \sqrt{J^2 - 2J \cos(ka) + 1}$ .

The ground state energy  $GSE_{ods}$  of one defect sector,

$$GSE_{ods} = - \sum_{k=1}^N f\left(\frac{k\pi}{N+1} + \frac{\alpha(k\pi/N+1)}{N+1}\right), \quad (3.71)$$

where  $f(k) = \sqrt{J^2 - 2J \cos(ka) + 1}$ .

In Appendix of this chapter, we have shown that ground state energy of zero defect sector,

$$GSE_{zds} = -\frac{N}{\pi} \int_0^\pi f(y) dy, \quad (3.72)$$

and ground state energy of one defect sector,

$$\begin{aligned} GSE_{ods} &= -\frac{N}{\pi} \int_0^\pi f(y) dy \\ &\quad - \frac{1}{\pi} \int_0^\pi dy \frac{J^2 - J \cos(y)}{\sqrt{J^2 - 2J \cos(y) + 1}} + J. \end{aligned} \quad (3.73)$$

Therefore, we can always write

$$GSE_{ods} = GSE_{zds} - \frac{1}{\pi} \int_0^\pi dy \frac{J^2 - J \cos(y)}{\sqrt{J^2 - 2J \cos(y) + 1}} + J. \quad (3.74)$$

Now let us take the last part of above expression,

$$\begin{aligned}
 & \frac{1}{\pi} \int_0^\pi dy \frac{J^2 - J \cos(y)}{\sqrt{J^2 - 2J \cos(y) + 1}} \\
 &= \frac{1}{\pi} \int_0^\pi dy \frac{J(J - \cos(y))}{\sqrt{J^2 - 2J \cos(y) + 1}} \\
 &= \frac{1}{\pi} \int_0^\pi dy J \sqrt{\frac{J^2 - 2J \cos(y) + \cos^2(y)}{J^2 - 2J \cos(y) + 1}} \\
 &< \frac{1}{\pi} \int_0^\pi dy J
 \end{aligned} \tag{3.75}$$

and show that

$$-\frac{1}{\pi} \int_0^\pi dy \frac{J^2 - J \cos(y)}{\sqrt{J^2 - 2J \cos(y) + 1}} + J > 0. \tag{3.76}$$

Therefore, using eqn. (3.74), we can write finally,

$$GSE_{ods} > GSE_{zds}. \tag{3.77}$$

Thus, the ground state energy of zero defect sector is less than the ground state energy of one defect sector.

Now, we prove that ground state energy for one defect sector is less than that of for two defect sector.

In order to show this we split the Hamiltonian into three parts,

$$H_{L_1+L_2} = H_{L_1} + H_{L_2} + H_{12}, \tag{3.78}$$

where  $H$  is the Hamiltonian for one defect sector,  $H_{L_1}$  and  $H_{L_2}$  are Hamiltonians of lengths  $L_1$  and  $L_2$  respectively,  $H_{12}$  is the link bond between  $H_{L_1}$  and  $H_{L_2}$ .

From variational principle,

$$\epsilon_G(L_1 + L_2) \leq \langle \psi_0 | H | \psi_0 \rangle, \tag{3.79}$$

where  $\epsilon_G(L_1 + L_2)$  is the ground state energy of Hamiltonian for one defect sector and  $\psi_0$  is the simultaneous ground state of Hamiltonian  $H_{L_1}$  and  $H_{L_2}$ . We can write

$\psi_0$  as direct product of ground state of Hamiltonian  $H_{L_1}$  and  $H_{L_2}$ ,

$$|\psi_0\rangle = |\psi_{L_1}\rangle|\psi_{L_2}\rangle \quad (3.80)$$

and

$$H_{L_1}|\psi_{L_1}\rangle = \epsilon_G(L_1)|\psi_{L_1}\rangle \quad (3.81)$$

$$H_{L_2}|\psi_{L_2}\rangle = \epsilon_G(L_2)|\psi_{L_2}\rangle. \quad (3.82)$$

If we substitute H in eqn. (3.79) from eqn. (3.78) , we get

$$\epsilon_G(L_1 + L_2) \leq \langle \psi_0 | H_{L_1} + H_{L_2} + H_{12} | \psi_0 \rangle. \quad (3.83)$$

Now, let us substitute  $|\psi_0\rangle$  from eqn. (3.80),

$$\begin{aligned} \epsilon_G(L_1 + L_2) &\leq \langle \psi_{L_1} | \langle \psi_{L_2} | H_{L_1} + H_{L_2} + H_{12} | \psi_{L_2} \rangle | \psi_{L_1} \rangle \\ \epsilon_G(L_1 + L_2) &\leq \langle \psi_{L_1} | H_{L_1} | \psi_{L_1} \rangle + \langle \psi_{L_2} | H_{L_2} | \psi_{L_2} \rangle \\ &\quad + \langle \psi_{L_1} | \langle \psi_{L_2} | H_{12} | \psi_{L_2} \rangle | \psi_{L_1} \rangle \\ \epsilon_G(L_1 + L_2) &\leq \epsilon_G(L_1) + \epsilon_G(L_2) + \langle \psi_{L_1} | \langle \psi_{L_2} | H_{12} | \psi_{L_2} \rangle | \psi_{L_1} \rangle. \end{aligned} \quad (3.84)$$

Now, let us calculate  $\langle \psi_{L_1} | \langle \psi_{L_2} | H_{12} | \psi_{L_1} \rangle | \psi_{L_2} \rangle$ . Let us consider the link Hamiltonian  $H_{12} = i\xi_n\xi_{n+1}$ , where  $\xi_n$  belongs to the Hamiltonian  $H_{L_1}$  because  $n$  is last site of  $H_{L_1}$  and  $\xi_{n+1}$  belongs to the Hamiltonian  $H_{L_2}$  because  $n+1$  is first site of  $H_{L_2}$ . Therefore,

$$\langle \psi_{L_1} | \langle \psi_{L_2} | i\xi_n\xi_{n+1} | \psi_{L_1} \rangle | \psi_{L_2} \rangle = i\langle \psi_{L_1} | \xi_n | \psi_{L_1} \rangle \langle \psi_{L_2} | \xi_{n+1} | \psi_{L_2} \rangle. \quad (3.85)$$

Now, expectation value of single  $\xi_n$  operator in the ground state is always zero. Therefore, eqn. (3.83) becomes

$$\epsilon_G(L_1 + L_2) \leq \epsilon_G(L_1) + \epsilon_G(L_2), \quad (3.86)$$

where  $\epsilon_G(L_1) + \epsilon_G(L_2)$  is nothing but ground state energy of two defect sector. Therefore, the ground state energy of one defect sector is less than the ground state energy of two defect sector. Similarly, we can prove for three defect sector

and so on.

**Therefore, ground state of zero defect sector is the ground state of the model.**

As we have solved the Hamiltonian for zero defect sector using Fourier transform being translationally invariant flux sector  $u_i = -1$  and get energy eigenspectrum  $\epsilon_k$ ,

$$\epsilon_k = \pm \frac{1}{2} \sqrt{J^2 - 2J \cos(ka) + 1}. \quad (3.87)$$

Now, we can calculate the fermionic gap  $\Delta$ , which is twice the value of the lowest single particle energy eigenvalue. The gap is given by

$$\Delta = |(1 - J)|. \quad (3.88)$$

Therefore, model is gapless for  $J = 1$ .

### 3.5.1 Nature of low energy excitations

The low temperature behaviour of any system depends mostly on ground state and the first excited state of the model. We proved that ground state of zero defect sector, namely,  $u_i = -1$ , is the ground state of the model.

Numerically we have shown that **first excited state of ground state sector** is the first excited state of the model for  $J=0.75$  to  $J=1.17$  (Assuming  $J_z=1$ ). **The ground state energy of the one defect sector** is the first excited state of the model for  $J=0$  to  $J=0.74$  and for  $J=1.17$  onwards. We have plotted first excited state energy of zero defect sector (red line) with  $J$  and ground state energy of one defect sector (green line) with  $J$  shown in figure (3.6). (While plotting all the energies, ground state of zero defect sector has been taken as reference point).

### 3.5.2 Zero modes

The solutions belonging to  $\epsilon = 0$  are called zero mode solutions. As we have seen earlier that degenerate and independent zero mode solutions peak around different sites which is called unpairing of zero mode eigenvectors. The single

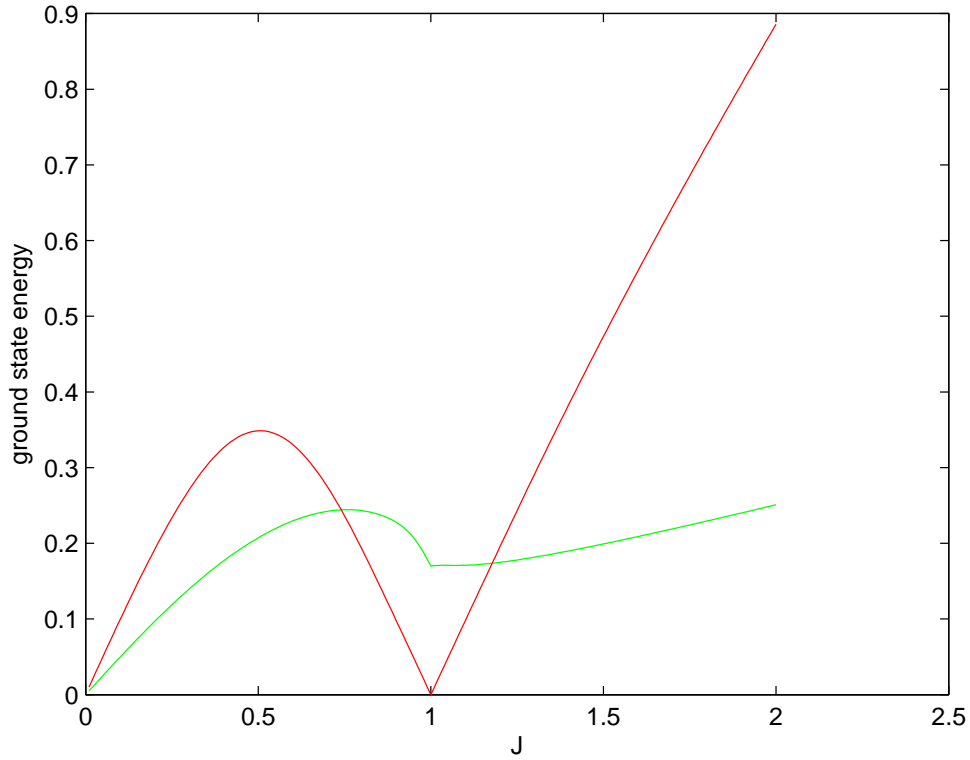


Figure 3.6: First excitation in XY-Ising Model

particle eigenvalue equation for zero energy is

$$\begin{aligned}
 -\frac{J(1-u_i)}{2}\phi_{i,1} + \phi_{i+1,1} &= 0 \\
 \text{and } -\phi_{i-1,2} + \frac{J(1-u_i)}{2}\phi_{i,2} &= 0.
 \end{aligned} \tag{3.89}$$

Solving these recursion relations we get,

$$\begin{aligned}
 \phi_{i,1} &= \prod_{j=1}^i \left( \frac{J(1-u_j)}{2} \right) \phi_{1,1} \\
 \text{and } \phi_{i,2} &= \prod_{j=i}^N \left( \frac{2}{J(1-u_j)} \right) \phi_{N,2}.
 \end{aligned} \tag{3.90}$$

In zero defect sector the zero mode equation (3.89) becomes,

$$\begin{aligned} -J\phi_{i,1} + \phi_{i+1,1} &= 0 \\ \text{and } -\phi_{i-1,2} + J\phi_{i,2} &= 0. \end{aligned} \quad (3.91)$$

Therefore,  $\phi_{i,1}$  and  $\phi_{i,2}$  can be expressed as

$$\begin{aligned} \phi_{i,1} &= J^{i-1}\phi_{1,1} \\ \text{and } \phi_{i,2} &= \left(\frac{1}{J}\right)^{i-1}\phi_{N,2}. \end{aligned} \quad (3.92)$$

In zero defect sector, imposing boundary condition  $\phi_{1,1} = \phi_{N+1,1}$  we find that the zero mode exists for zero defect sector only at the gapless point  $J = 1$ .

We will show that in one defect sector, zero mode does exist in the model. In one defect sector, the zero mode equation is same as that of zero defect sector but with boundary condition,

$$\phi_{0,1} = \phi_{N,2} = 0. \quad (3.93)$$

In this case,  $\phi_{i,1}$  and  $\phi_{i,2}$  can be expressed as,

$$\begin{aligned} \phi_{i,1} &= J^i\phi_{1,0} \\ \text{and } \phi_{i,2} &= \left(\frac{1}{J}\right)^{i-1}\phi_{N,2}. \end{aligned} \quad (3.94)$$

Non-trivial solutions for  $\phi$ 's exist only in infinite chain for  $J > 1$ . This zero mode is topologically protected about with we have discussed earlier.

From eqn. (3.89) we can see that zero modes exist in finite chain in two or more defect sector for all values of  $J$ .

## Appendix

The ground state energy  $GSE_{zds}$  of zero defect sector is,

$$GSE_{zds} = -\sum_{k=1}^N f\left(\frac{2k\pi}{N}\right), \quad (3.95)$$

where  $f(k) = \sqrt{J^2 - 2J \cos(ka) + 1}$ .

To evaluate the summation series, we convert it into integral using Euler-Maclaurin formula,

$$\sum_{x=1}^n f(x) = \int_0^n f(x) dx + B_1[f(0) - f(n)] + \sum_{k=1}^p \frac{B_{2k}}{(2k)!} (f^{(2k-1)}(n) - f^{(2k-1)}(0)) \quad (3.96)$$

where  $B_1 = -1/2, B_2 = 1/6, B_3 = 0, B_4 = -1/30, B_5 = 0, B_6 = 1/42 \dots$  are the Bernoulli numbers.

The expression for ground state energy for zero defect sector eqn. (3.99) becomes,

$$\begin{aligned} GSE_{zds} = - \sum_{k=1}^N f\left(\frac{2k\pi}{N}\right) &= - \int_0^{2\pi} f\left(k\frac{2\pi}{N}\right) dk + \frac{1}{2}[f(0) - f(N\frac{2\pi}{N})] \\ &- \frac{1}{12}[f'(N\frac{2\pi}{N}) - f'(0)] + \dots \end{aligned} \quad (3.97)$$

Substituting  $y = \frac{2k\pi}{N}$  and  $dx = \frac{N}{2\pi} dy$  we get,

$$\begin{aligned} GSE_{zds} = - \frac{N}{2\pi} \int_0^{2\pi} f(y) dy + \frac{1}{2}[f(0) - f(2\pi)] \\ - \frac{1}{12} \frac{2\pi}{N} [f'(N\frac{2\pi}{N}) - f'(0)] + \dots \end{aligned} \quad (3.98)$$

At thermodynamic limit,  $N \rightarrow \infty$ , only first two terms survive in the equation,

$$GSE_{zds} = - \frac{N}{2\pi} \int_0^{2\pi} f(y) dy + \frac{1}{2}[f(0) - f(2\pi)]. \quad (3.99)$$

We can take  $f(y) = f(\cos(y))$  and try to show for  $N \rightarrow \infty$ ,

$$\frac{N}{2\pi} \int_0^{2\pi} f(\cos y) dy = \frac{N}{\pi} \int_0^{\pi} f(\cos y) dy. \quad (3.100)$$

LHS of eqn. (3.100) is,

$$\frac{N}{2\pi} \int_0^{2\pi} f(\cos y) dy = \frac{N}{2\pi} \int_0^{\frac{\pi}{2}} f(\cos y) dy + \frac{N}{2\pi} \int_{\frac{\pi}{2}}^{\frac{3\pi}{2}} f(\cos y) dy \quad (3.101)$$

$$+ \frac{N}{2\pi} \int_{\frac{3\pi}{2}}^{2\pi} f(\cos y) dy. \quad (3.102)$$

It can be easily shown that

$$\int_{\frac{\pi}{2}}^{\frac{3\pi}{2}} f(\cos y) dy = 2 \int_0^{\frac{\pi}{2}} f(-\cos y) dy \quad (3.103)$$

$$\int_{\frac{3\pi}{2}}^{2\pi} f(\cos y) dy = \int_0^{\frac{\pi}{2}} f(\cos y) dy. \quad (3.104)$$

Therefore,

$$\frac{N}{2\pi} \int_0^{2\pi} f(\cos y) dy = 2 \frac{N}{2\pi} \int_0^{\frac{\pi}{2}} f(\cos y) dy + 2 \frac{N}{2\pi} \int_0^{\frac{\pi}{2}} f(-\cos y) dy. \quad (3.105)$$

Let us take RHS of eqn. (3.100),

$$\frac{N}{\pi} \int_0^{\pi} f(\cos y) dy = \frac{N}{\pi} \int_0^{\frac{\pi}{2}} f(\cos y) dy + \frac{N}{\pi} \int_{\frac{\pi}{2}}^{\pi} f(-\cos y) dy. \quad (3.106)$$

Hence,

$$\frac{N}{2\pi} \int_0^{2\pi} f(\cos y) dy = \frac{N}{\pi} \int_0^{\pi} f(\cos y) dy. \quad (3.107)$$

Thus, from eqn. (3.99),

$$GSE_{zds} = -\frac{N}{\pi} \int_0^{\pi} f(\cos y) dy + \frac{1}{2}[f(0) - f(2\pi)]. \quad (3.108)$$

We know that  $f(0) = f(2\pi) = J + 1$ . Therefore, finally we can write

$$GSE_{zds} = -\frac{N}{\pi} \int_0^{\pi} f(y) dy. \quad (3.109)$$



The ground state energy  $GSE_{ods}$  of one defect sector is,

$$GSE_{ods} = - \sum_{k=1}^N f \left( \frac{k\pi}{N+1} + \frac{\alpha(k\pi/N+1)}{N+1} \right) \quad (3.110)$$

where  $f(k) = \sqrt{J^2 - 2J \cos(ka) + 1}$ . To evaluate the summation series we again convert it into integral using Euler-Maclaurin formula and neglect last terms containing  $(N+1)$  in the denominator in limit  $N \rightarrow \infty$ ,

$$\begin{aligned} GSE_{ods} &= - \int_0^N f \left( \frac{k\pi}{N+1} + \frac{\alpha(k\pi/N+1)}{N+1} \right) dk \\ &+ \frac{1}{2} \left[ f \left( \frac{\alpha(0)}{N+1} \right) - f \left( \frac{N\pi}{N+1} + \frac{\alpha(N\pi/N+1)}{N+1} \right) \right]. \end{aligned} \quad (3.111)$$

Let us evaluate  $f \left( \frac{\alpha(0)}{N+1} \right)$ ,

$$f \left( \frac{\alpha(0)}{N+1} \right) = f(0) + \frac{\alpha(0)}{N+1} f'(0) + \dots = f(0), \quad (3.112)$$

where, again, we neglected terms containing  $(N+1)$  in the denominator in limit  $N \rightarrow \infty$ .

Let us evaluate

$$\begin{aligned} &f \left( \frac{N\pi}{N+1} + \frac{\alpha(N\pi/N+1)}{N+1} \right) \\ &= f \left( \pi - \frac{\pi}{N+1} + \frac{\alpha(\pi - \pi/N+1)}{N+1} \right) \\ &= f \left( \pi - \frac{\pi}{N+1} + \frac{\alpha(\pi - \pi/N+1)}{N+1} \right) \\ &= f \left( \pi - \frac{\pi}{N+1} + \frac{\alpha(\pi) - (\pi/N+1)\alpha'(\pi) + \dots}{N+1} \right) \end{aligned}$$

$$\begin{aligned}
 &= f\left(\pi - \frac{\pi}{N+1} + \frac{\alpha(\pi)}{N+1} - \frac{\pi}{(N+1)^2}\alpha'(\pi) + \dots\right) \\
 &= f\left(\pi - \frac{1}{N+1}\left(\pi + \alpha(\pi) - \frac{\pi}{(N+1)}\alpha'(\pi) + \dots\right)\right) \\
 &= f(\pi) - \frac{1}{N+1}\left(\pi + \alpha(\pi) - \frac{\pi}{N+1}\alpha'(\pi) + \dots\right) \\
 &= f(\pi),
 \end{aligned} \tag{3.113}$$

where we neglected last terms containing  $(N+1)$  in the denominator in limit  $N \rightarrow \infty$ .

Substituting all these values in eqn. (3.111) we get,

$$GSE_{ods} = - \int_0^N f\left(\frac{k\pi}{N+1} + \frac{\alpha(k\pi/N+1)}{N+1}\right) dk + \frac{1}{2}[f(0) - f(\pi)]. \tag{3.114}$$

Let us substitute  $y = \frac{k\pi}{N+1}$  then  $dy = \frac{dk\pi}{N+1}$ .

At  $k=0$ ,  $y=0$  and at  $k=N$ ,  $y=\frac{N\pi}{N+1}$  above expression for ground state energy for one defect sector then becomes

$$GSE_{ods} = -\frac{N+1}{\pi} \int_0^{\frac{N\pi}{N+1}} f\left(y + \frac{\alpha(y)}{N+1}\right) dy + \frac{1}{2}[f(0) - f(\pi)]. \tag{3.115}$$

Using Taylor expansion,

$$\begin{aligned}
 GSE_{ods} &= -\frac{N+1}{\pi} \int_0^{\frac{N\pi}{N+1}} \left(f(y) + \frac{\alpha(y)}{N+1}f'(y) + \dots\right) dy \\
 &\quad + \frac{1}{2}[f(0) - f(\pi)] \\
 &= -\frac{N+1}{\pi} \int_0^{\frac{N\pi}{N+1}} f(y)dy - \frac{1}{\pi} \int_0^{\frac{N\pi}{N+1}} (\alpha(y)f'(y)) dy \\
 &\quad + \text{terms containing } \frac{1}{N+1} + \frac{1}{2}[f(0) - f(\pi)].
 \end{aligned} \tag{3.116}$$

Negelecting terms containing  $\frac{1}{N+1}$  in thermodynamic limit  $N \rightarrow \infty$ ,

$$\begin{aligned}
 GSE_{ods} &= -\frac{N+1}{\pi} \int_0^{\frac{N\pi}{N+1}} f(y)dy - \frac{1}{\pi} \int_0^{\frac{N\pi}{N+1}} \alpha(y)f'(y)dy \\
 &\quad + \frac{1}{2}[f(0) - f(\pi)].
 \end{aligned} \tag{3.117}$$

Using integration by parts,

$$\begin{aligned}
 GSE_{ods} = & - \frac{N+1}{\pi} \int_0^{\frac{N\pi}{N+1}} f(y) dy - \frac{1}{\pi} [\alpha(y)f(y)]_0^{\frac{N\pi}{N+1}} \\
 & + \frac{1}{\pi} \int_0^{\frac{N\pi}{N+1}} \alpha'(y)f(y) dy + \frac{1}{2} [f(0) - f(\pi)]. \quad (3.118)
 \end{aligned}$$

Using eqn. (3.56), we evaluate  $\alpha'(y)$ ,

$$\frac{d\alpha(y)}{dy} = - \frac{J \cos(y) - 1}{J^2 - 2J \cos(y) + 1}, \quad (3.119)$$

and we already know that  $f(y) = \sqrt{J^2 - 2J \cos(y) + 1}$ .

Therefore,

$$\int_0^{\frac{N\pi}{N+1}} \alpha'(y)f(y) dy = - \int_0^{\frac{N\pi}{N+1}} \frac{J \cos(y) - 1}{\sqrt{J^2 - 2J \cos(y) + 1}} dy. \quad (3.120)$$

So, eqn. (3.118) becomes,

$$\begin{aligned}
 GSE_{ods} = & - \frac{N+1}{\pi} \int_0^{\frac{N\pi}{N+1}} f(y) dy - \frac{1}{\pi} \left[ \alpha\left(\frac{N\pi}{N+1}\right)f\left(\frac{N\pi}{N+1}\right) - \alpha(0)f(0) \right] \\
 & - \frac{1}{\pi} \int_0^{\frac{N\pi}{N+1}} \frac{J \cos(y) - 1}{\sqrt{J^2 - 2J \cos(y) + 1}} dy + \frac{1}{2} [f(0) - f(\pi)]. \quad (3.121)
 \end{aligned}$$

Now, let us simplify first term in the above equation,

$$\begin{aligned}
 \int_0^{\frac{N\pi}{N+1}} f(y) dy &= \int_0^{\pi - \frac{\pi}{N+1}} f(y) dy \\
 &= \int_0^{\pi} f(y) dy - \int_{\pi - \frac{\pi}{N+1}}^{\pi} f(y) dy \\
 &= \int_0^{\pi} f(y) dy - \frac{\pi}{(N+1)} f(\pi) \quad (3.122)
 \end{aligned}$$

Therefore,

$$\begin{aligned}
 GSE_{ods} = & - \frac{N+1}{\pi} \int_0^\pi f(y) dy + f(\pi) - \frac{1}{\pi} \left[ \alpha \left( \frac{N\pi}{N+1} \right) f \left( \frac{N\pi}{N+1} \right) - \alpha(0)f(0) \right] \\
 & - \frac{1}{\pi} \int_0^{\frac{N\pi}{N+1}} dy \frac{J \cos(y) - 1}{\sqrt{J^2 - 2J \cos(y) + 1}} + \frac{1}{2} [f(0) - f(\pi)]. \quad (3.123)
 \end{aligned}$$

Now, we take the thermodynamic limit,

$$\begin{aligned}
 GSE_{ods} = & - \frac{N+1}{\pi} \int_0^\pi f(y) dy + f(\pi) - \frac{1}{\pi} [\alpha(\pi)f(\pi) - \alpha(0)f(0)] \\
 & - \frac{1}{\pi} \int_0^\pi dy \frac{J \cos(y) - 1}{\sqrt{J^2 - 2J \cos(y) + 1}} + \frac{1}{2} [f(0) - f(\pi)]. \quad (3.124)
 \end{aligned}$$

Finally,

$$\begin{aligned}
 GSE_{ods} = & - \frac{N}{\pi} \int_0^\pi f(y) dy + \frac{1}{\pi} \int_0^\pi dy \frac{J \cos(y) - J^2}{\sqrt{J^2 - 2J \cos(y) + 1}} \\
 & + \frac{1}{2} [f(0) + f(\pi)] - \frac{1}{\pi} [\alpha(\pi)f(\pi) - \alpha(0)f(0)]. \quad (3.125)
 \end{aligned}$$

Here,

$$\begin{aligned}
 f(0) &= J + 1 \\
 f(\pi) &= J - 1 \text{ when } J > 1 \\
 f(\pi) &= 1 - J \text{ when } J < 1 \\
 \alpha(0) &= 0 \\
 \alpha(\pi) &= 0 \text{ when } J > 1 \\
 \alpha(\pi) &= \pi \text{ when } J < 1. \quad (3.126)
 \end{aligned}$$

We show that for both cases  $J > 1$  and  $J < 1$  ground state energy of one defect

sector is the same. For  $J > 1$ ,

$$\begin{aligned}
 GSE_{ods} &= -\frac{N}{\pi} \int_0^\pi f(y) dy + \frac{1}{\pi} \int_0^\pi dy \frac{J \cos(y) - J^2}{\sqrt{J^2 - 2J \cos(y) + 1}} \\
 &\quad + \frac{1}{2} [(J+1) + (J-1)] - \frac{1}{\pi} [0 - 0] \\
 &= -\frac{N}{\pi} \int_0^\pi f(y) dy + \frac{1}{\pi} \int_0^\pi dy \frac{J \cos(y) - J^2}{\sqrt{J^2 - 2J \cos(y) + 1}} \\
 &\quad + J.
 \end{aligned} \tag{3.127}$$

For  $J < 1$ ,

$$\begin{aligned}
 GSE_{ods} &= -\frac{N}{\pi} \int_0^\pi f(y) dy + \int_0^\pi dy \frac{J \cos(y) - J^2}{\sqrt{J^2 - 2J \cos(y) + 1}} \\
 &\quad + \frac{1}{2} [(J+1) + (1-J)] - \frac{1}{\pi} [\pi(1-J) - 0] \\
 &= -\frac{N}{\pi} \int_0^\pi f(y) dy + \frac{1}{\pi} \int_0^\pi dy \frac{J \cos(y) - J^2}{\sqrt{J^2 - 2J \cos(y) + 1}} \\
 &\quad + J.
 \end{aligned} \tag{3.128}$$

# 4

## XYZ-Ising Model: Phase Diagram

In this chapter, we study the phases of XYZ-Ising model at zero temperature as a function of coupling constants of Hamiltonian. Lieb, Schultz and Mattis studied this model where the interactions are alternately Ising and isotropic Heisenberg interactions [49]. They solved the model exactly in the sense that the ground state, all the elementary excitations and the free energy has been found.

### 4.1 The Hamiltonian

As we have mentioned in the chapter 3, the Hamiltonian is,

$$H = \sum_i^N (J_x \sigma_{i,1}^x \sigma_{i,2}^x + J_y \sigma_{i,1}^y \sigma_{i,2}^y + J_z \sigma_{i,1}^z \sigma_{i,2}^z + \sigma_{i,2}^z \sigma_{i+1,1}^z) \quad (4.1)$$

with  $\sigma_{N+1,1}^z = \sigma_{1,1}^z$ .

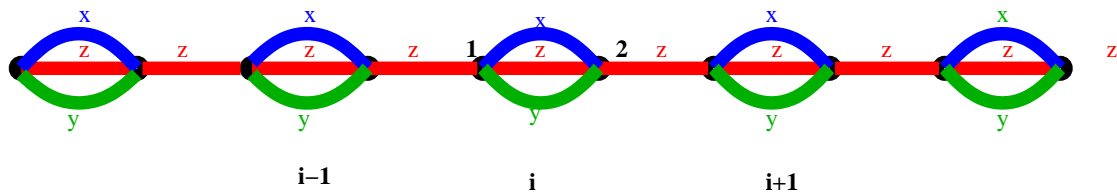


Figure 4.1: The XYZ-Ising chain. There are two sites per unit cell. The  $x, y$  and  $z$  bonds are as indicated.

The fermionised Hamiltonian,

$$\begin{aligned}
 H &= \sum_{i=1}^N ((J_y - J_x u_i) i \xi_{i,1} \xi_{i,2} + J_z u_i) \\
 &+ \sum_{i=1}^{N-1} (i \xi_{i,2} \xi_{i+1,1}) + i \xi_{N,2} \xi_{1,1} \Sigma_x.
 \end{aligned} \tag{4.2}$$

The XYZ-Ising model can be exactly solved as XY-Ising model has been solved for  $J_x = J_y = J/2$  in the last section.

## 4.2 Ground State in Extreme Limit of Coupling Constants

Let us discuss the ground state of XYZ-Ising model in extreme limits. When  $J_z$  is large then the Hamiltonian is expressed as

$$H = J_z \sum_i^N \sigma_{i,1}^z \sigma_{i,2}^z = J_z \sum_i^N W_i. \tag{4.3}$$

For large and positive (negative)  $J_z$ , the Hamiltonian is minimum at  $W_i = -1(+1)$ . Then, Hamiltonian becomes

$$H = -(+)N J_z. \tag{4.4}$$

Therefore, for large and positive (negative)  $J_z$  the ground state belongs to  $W_i = -1(+1)$  sector as shown in figure 4.2.

Now let us consider the another limit large  $J$ . In this limit, the Hamiltonian is written as

$$\begin{aligned}
 H &= \frac{J}{2} \sum_i^N (\sigma_{i,1}^x \sigma_{i,2}^x + \sigma_{i,1}^y \sigma_{i,2}^y) \\
 \text{or, } H &= \frac{J}{4} \sum_i^N (\sigma_{i,1}^+ \sigma_{i,2}^- + \sigma_{i,1}^- \sigma_{i,2}^+).
 \end{aligned} \tag{4.5}$$

The eigenstates are

$$\begin{aligned}
 & |\uparrow\uparrow\rangle, \\
 & |\uparrow\downarrow\rangle + |\downarrow\uparrow\rangle, \\
 & |\uparrow\downarrow\rangle - |\downarrow\uparrow\rangle, \\
 & \text{and } |\downarrow\downarrow\rangle
 \end{aligned} \tag{4.6}$$

with eigenvalues  $0, \frac{J}{2}, -\frac{J}{2}, 0$ .

Therefore, spin singlet is the ground state of the model for large and positive  $J$  and spin triplet is the ground state for large and negative  $J$  as shown in figure (4.2).

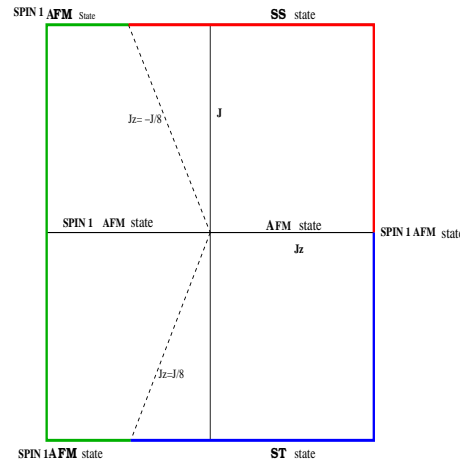


Figure 4.2: The phase diagram of XYZ-Ising Model in  $J - J_z$  plane. The boundary of the figure indicates the extreme limits of  $J$  and  $J_z$ . The blue, red and green line of the figure shows the range for large  $J$  and  $J_z$  in which the spin triplet (ST) state, spin singlet (SS) state and spin 1 antiferromagnetic (SPIN 1 AFM) state is the ground state respectively.

Let us find out the ground state in the limit of large  $J$  and  $J_z$ . The Hamiltonian in this limit can be written as,

$$\begin{aligned}
 H &= \frac{J}{2} \sum_i^N \sigma_{i,1}^x \sigma_{i,2}^x + \sigma_{i,1}^y \sigma_{i,2}^y \\
 &+ J_z \sum_i^N \sigma_{i,1}^z \sigma_{i,2}^z.
 \end{aligned} \tag{4.7}$$



The same eigenstates written in eqn.(4.6) are the eigenstates of the above Hamiltonian with eigenvalues  $J_z, -J_z + \frac{J}{4}, -J_z - \frac{J}{4}$  and  $J_z$  respectively.

We have shown the zero temperature phase diagram of the model in figure 4.2 in extreme limit. In the first quadrant of figure (4.2) where  $J > 0, J_z > 0$ , spin singlet state is the ground state for large  $J, J_z$  as shown in figure (4.2). In the second quadrant of figure (4.2) where  $J > 0$  and  $J_z < 0$ , spin one antiferromagnet,

$$|\uparrow\uparrow\downarrow\downarrow\uparrow\uparrow\rangle,$$

is the ground state for  $|J_z| > \frac{|J|}{8}$  for large  $J$  and  $J_z$  and spin singlet state is ground state for  $|J_z| > \frac{|J|}{8}$  for large  $J$  and  $J_z$ . In the third quadrant of figure (4.2) where  $J < 0$  and  $J_z < 0$ , spin triplet state is the ground state for  $|J_z| < \frac{|J|}{8}$  for large  $J$  and  $J_z$  and spin one antiferromagnetic state is ground state for  $|J_z| > \frac{|J|}{8}$  for large  $J$  and  $J_z$ . In the fourth quadrant of figure (4.2) where  $J < 0$  and  $J_z > 0$ , spin triplet is the ground state for large  $J$  and  $J_z$ .

### 4.3 The Ground States in all defect sectors

As we have shown in the last chapter the zero defect sector of Hamiltonian consists of both periodic and anti-periodic boundary condition. The ground state energy of zero defect sector  $GSE_{zds}$  under anti-periodic and periodic boundary condition is given by,

$$GSE_{zds} = -NJ_z - \sum_{n=1}^N \sqrt{J^2 + 1 - 2J \cos\left(\frac{(2n + \alpha)\pi}{N}\right)}, \quad (4.8)$$

where  $\alpha = 1$  and  $0$  belongs to anti-periodic and periodic boundary condition respectively.

Using this expression, we calculated numerically the ground state energy of zero defect sector under anti-periodic and periodic boundary condition for  $J$  and  $J_z$  from -100 to 100, as shown in figure 4.3(a) and figure 4.3(c). The ground state energy under anti-periodic or periodic boundary condition is minimum for small  $J$  and large positive  $J_z$  and large  $|J|$ . In figure 4.3(b) and figure 4.3(d) the sign of ground state energy has been shown under anti-periodic and periodic boundary condition.

It was already shown in the last chapter, closed chain becomes  $n_D$  decoupled

open chain for  $n_D$  defect sectors. There can be various partitions of  $N$  for  $n_D$  defect sectors. Therefore, instead of finding the ground state energy of  $n_D$  defect sector we calculate the ground state energy for each partition of  $N$ . Let us consider  $\{L_i\}$  as the partition of  $N$  belonging to  $n_D$  defect sectors. Then,

$$\sum_{i=1}^{n_D} L_i = N \quad (4.9)$$

Then, the ground state energy  $GSE_{\{L_i\}}$  of partition  $\{L_i\}$  is given by

$$GSE_{\{L_i\}} = -(N - 2n_D)J_z - \sum_{i=1}^{n_D} \sum_{n=1}^{L_i} \sqrt{J^2 + 1 - 2J \cos\left(\frac{n\pi}{L_i + 1}\right)} \quad (4.10)$$

The ground state energy of various defect sectors is plotted in  $J - J_z$  plane for  $J$  and  $J_z$  from -100 to 100 for  $N=10$  unit cells. There are 42 partitions for various defect sectors of 10 unit cells.

The ground state energy of zero defect sector under periodic and anti-periodic boundary condition are equal.

The ground state energy of 1 defect sector for partition 10 is shown in the figure 4.3(e). The ground state energy is minimum at large negative  $J_z$  and large  $|J|$ .

The ground state energy of 2 defect sector for the partitions (9, 1), (8, 2), (7, 3), (6, 4) and (5, 5) is shown in the figure 4.4(a) and 4.4(b). The ground state energy is minimum at large positive  $J_z$  and large  $|J|$  for all partitions of 2 defect sector.

The ground state energy of 3 defect sector for the partitions (8, 1, 1), (7, 2, 1), (6, 3, 1), (6, 2, 2), (5, 4, 1), (5, 3, 2), (4, 4, 2) and (4, 3, 3) is shown in the figure 4.4(b), 4.5(a) and 4.5(b). The ground state energy is minimum at large positive  $J_z$  and large  $J$  for first, second and third partitions. For fourth, fifth, sixth, seventh partitions, the ground state energy is minimum at large positive  $J$  and  $J_z$ . For last partition (4, 3, 3), the ground state energy is minimum at large positive  $J_z$  and large  $|J|$ .

The ground state energy of 4 defect sector for the partitions (7, 1, 1, 1), (6, 2, 1, 1), (5, 3, 1, 1), (5, 2, 2, 1), (4, 4, 1, 1), (4, 3, 2, 1), (4, 2, 2, 2), (3, 3, 3, 1) and (3, 3, 2, 2) is shown in the figure 4.5(b), 4.6(a) and figure 4.6(b). The ground state energy is minimum at large positive  $J_z$  and large  $J$  for first 7 partitions. For

other partitions  $(3, 3, 3, 1)$  and  $(3, 3, 2, 2)$ , the ground state energy is minimum for large positive  $J$  and  $J_z$ .

The ground state energy of 5 defect sector for the partitions  $(6, 1, 1, 1, 1)$ ,  $(5, 2, 1, 1, 1)$ ,  $(4, 3, 1, 1, 1)$ ,  $(4, 2, 2, 1, 1)$ ,  $(3, 3, 2, 1, 1)$ ,  $(3, 2, 2, 2, 1)$  and  $(2, 2, 2, 2, 2)$  is shown in the figure 4.6(b), 4.7(a) and 4.7(b). The ground state energy is minimum at large positive  $J$  for first two partitions. For all other partitions of 5 defect sectors, ground state is minimum at large  $|J|$ .

The ground state energy of 6 defect sector for the partitions  $(5, 1, 1, 1, 1, 1)$ ,  $(4, 2, 1, 1, 1, 1)$ ,  $(3, 3, 1, 1, 1, 1)$ ,  $(3, 2, 2, 1, 1, 1)$ ,  $(2, 2, 2, 2, 1, 1)$  is shown in the figure 4.7(b) and 4.8(a). The ground state energy is minimum at large negative  $J_z$  and large  $J$  for first three partitions. For other partitions of 6 defect sector, the ground state energy is minimum for large negative  $J_z$  and large positive  $J$ .

The ground state energy of 7 defect sector for the partitions  $(4, 1, 1, 1, 1, 1, 1)$ ,  $(3, 2, 1, 1, 1, 1, 1)$  and  $(2, 2, 2, 1, 1, 1, 1)$  is shown in the figure 4.8(a) and 4.8(b). The ground state energy is minimum at large negative  $J_z$  and large positive  $J$  for first and second partitions. For third partition, the ground state is minimum at large negative  $J_z$  and large  $|J|$ .

The ground state energy of 8 defect sector for the partitions  $(3, 1, 1, 1, 1, 1, 1, 1)$  and  $(2, 2, 1, 1, 1, 1, 1, 1)$  is shown in the figure 4.8(b). The ground state energy is minimum at large negative  $J_z$  and large  $|J|$  for both partitions of 8 defect sector.

The ground state energy of 9 defect sector for the partition  $(2, 1, 1, 1, 1, 1, 1, 1, 1)$  is shown in the figure 4.8(b). The ground state energy is minimum at large negative  $J_z$  and large  $|J|$ .

The ground state energy of 10 or full defect sector for the partition  $(1, 1, 1, 1, 1, 1, 1, 1, 1, 1)$  is shown in the figure 4.9(a). The ground state energy of full defect sector is minimum at large negative  $J_z$  and large  $|J|$ . In the figure 4.9(b), the sign of ground state energy is plotted for  $J$  and  $J_z$  from -100 to 100.

**Among all these ground states of various defect sectors, we find that the ground state energy of zero defect sector is minimum for positive  $J_z$ .**

## 4.4 Zero Temperature Phase Diagram

For each  $J$  and  $J_z$ , we calculate the ground state numerically in all partitions of the model and plot the zero temperature phase diagram as shown in figure (4.4). In order to plot the phase diagram, we found out the minimum energy for each partition for each  $J$  and  $J_z$  and calculated numerically the first order derivative of  $E$  with respect to  $J$  for each  $J$  and  $J_z$ . For all those values of  $J$  and  $J_z$ , wherever we found a discontinuity in the first derivative of ground state energy, we plot those values of  $J$  and  $J_z$  in  $J - J_z$  plane. For  $J_z < 0$ , we find that the system undergoes through a first order phase transition and for  $J_z > 0$ , the system undergoes through topological phase transition in the model because it is characterised by winding number. The fact that zero defect sector is ground state sector for  $J_z > 0$  makes it easier to analyse the phase transition for  $J_z > 0$ .

In order to show that the system has a first order phase transition we plot the ground state energy versus  $J$  for  $J_z = -2$  and  $J_z = -4$  as shown in figure (4.10). The ground state energy has two kinks which indicates that first order derivative is discontinuous.

In order to show that the system has a topological phase transition for  $J_z > 0$ , we compute winding number. In order to compute the winding number we calculate Berry's phase. The winding number  $\nu$  is related to Berry's phase  $\phi$  by

$$\nu = \frac{\phi}{\pi}. \quad (4.11)$$

The Berry's phase for Hamiltonian  $H(\mathbf{R})$  is given by

$$\phi = \phi_t - \phi_0 = \int_{R(0)}^{R(t)} \langle \Psi^\dagger | i \partial_{\mathbf{R}} | \Psi \rangle . d\mathbf{R}, \quad (4.12)$$

where parameters  $R_1, R_2, \dots, R_N$  are components of a vector  $\mathbf{R}$ .

For our case, Hamiltonian  $H$  is function of only one parameter  $k$  which runs from 0 to  $\pi$  as we have mentioned in chapter 3. Therefore,

$$\phi = \int_0^\pi \langle \Psi^\dagger | i \partial_k | \Psi \rangle . dk \quad (4.13)$$

From eqn. (3.40) in chapter 3 we write the two component wave function,

$$|\Psi_{k,1}\rangle = \begin{bmatrix} e^{i\alpha_k} \\ 1 \end{bmatrix} \quad (4.14)$$

$$\text{and } |\Psi_{k,2}\rangle = \begin{bmatrix} 1 \\ e^{-i\alpha_k} \end{bmatrix}. \quad (4.15)$$

The integrand  $\langle \Psi^\dagger | i\partial_k | \Psi \rangle$  is then given by,

$$\langle \Psi^\dagger | i\partial_k | \Psi \rangle = \begin{bmatrix} e^{-i\alpha_k} & 1 \end{bmatrix} i\partial_k \begin{bmatrix} e^{i\alpha_k} \\ 1 \end{bmatrix} = -\frac{\partial\alpha_k}{\partial k}. \quad (4.16)$$

Therefore, the berry's phase is given by,

$$\begin{aligned} \phi &= -\int_0^\pi \frac{\partial\alpha_k}{\partial k} \cdot dk \\ &= -\int_0^\pi d\alpha_k \\ &= -(\alpha(\pi) - \alpha(0)). \end{aligned} \quad (4.17)$$

In chapter 3, we have shown in figure (3.3) and (3.4) that  $\alpha(0) = 0$  and  $\alpha(\pi) = 0$  for  $|J| > 1$  and  $\alpha(0) = 0$  and  $\alpha(\pi) = \pi$  for  $|J| < 1$ . Therefore, the Berry's phase  $\phi$  is given by,

$$\begin{aligned} \phi &= 0 \quad \text{for } |J| > 1 \\ \text{and } \phi &= -\pi \quad \text{for } |J| < 1. \end{aligned} \quad (4.18)$$

Now, we calculate the winding number from eqn. (4.11),

$$\begin{aligned} \nu &= 0 \quad \text{for } |J| > 1, \\ \nu &= -1 \quad \text{and for } |J| < 1. \end{aligned} \quad (4.19)$$

Therefore, the winding number takes different values for both cases  $|J| > 1$  and  $|J| < 1$  which characterises the phase transition shown in figure (4.4).

For  $J_z > 0$ , the zero defect sector is the ground state sector of the Hamiltonian.

So, for  $J_z > 0$ , we can calculate first order derivative substituting  $E_G = GSE_{zds}$  from eqn. (4.10). From eqn. (4.10), we can write,

$$\begin{aligned}\frac{\partial E_G}{\partial J} &= -\frac{1}{N} \sum_{n=1}^N \frac{J - \cos(\frac{2n\pi}{N})}{\sqrt{J^2 + 1 - 2J \cos(\frac{2n\pi}{N})}} \\ \frac{\partial^2 E_G}{\partial J^2} &= -\frac{1}{N} \sum_{n=1}^N \frac{\sin^2(\frac{2n\pi}{N})}{\{J^2 + 1 - 2J \cos(\frac{2n\pi}{N})\}^{3/2}}.\end{aligned}\quad (4.20)$$

We can show analytically that at  $J = 1$ , the second order derivative blows up. At  $J=1$ , the eqn. (4.20) becomes,

$$\begin{aligned}\frac{\partial^2 E_G}{\partial J^2} &= -\frac{1}{N} \sum_{n=1}^N \frac{\sin^2(\frac{2n\pi}{N})}{\{4 \sin^2(\frac{n\pi}{N})\}^{3/2}} \\ &= -\frac{1}{N} \sum_{n=1}^N \frac{4 \sin^2(\frac{n\pi}{N}) \cos^2(\frac{n\pi}{N})}{\{8 \sin^3(\frac{n\pi}{N})\}} \\ &= -\frac{1}{N} \sum_{n=1}^N \frac{\cos^2(\frac{n\pi}{N})}{\{2 \sin(\frac{n\pi}{N})\}} \\ &= \infty\end{aligned}\quad (4.21)$$

because at  $n = N$ , the denominator becomes zero.

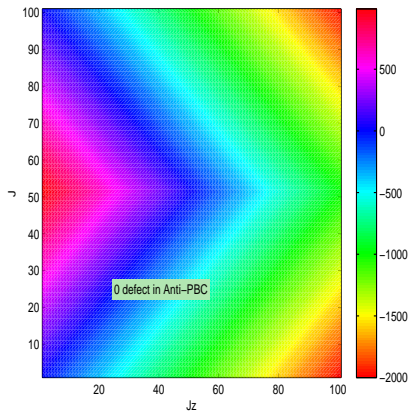
Similarly, we can show that at  $J=-1$  also, the second order derivative of ground state energy blows up. At  $J=-1$ , the eqn. (4.20) becomes,

$$\begin{aligned}\frac{\partial^2 E_G}{\partial J^2} &= -\frac{1}{N} \sum_{n=1}^N \frac{\sin^2(\frac{2n\pi}{N})}{\{4 \cos^2(\frac{n\pi}{N})\}^{3/2}} \\ &= -\frac{1}{N} \sum_{n=1}^N \frac{4 \sin^2(\frac{n\pi}{N}) \cos^2(\frac{n\pi}{N})}{\{8 \cos^3(\frac{n\pi}{N})\}} \\ &= -\frac{1}{N} \sum_{n=1}^N \frac{\sin^2(\frac{n\pi}{N})}{\{2 \cos(\frac{n\pi}{N})\}} \\ &= \infty\end{aligned}\quad (4.22)$$

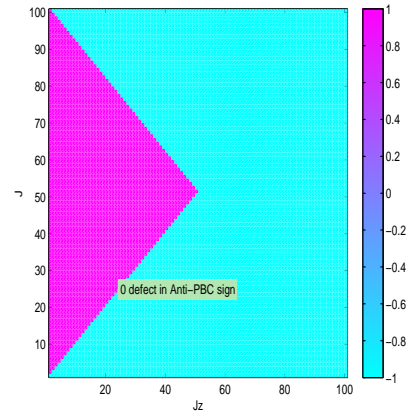
because at  $n = N/2$ , the denominator becomes zero.

Thus, at  $J = \pm 1$ , the model has second order phase transition for  $J_z > 0$ . In

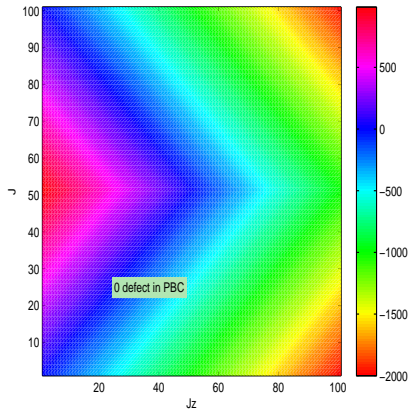
figure (4.12), we plot the first order and second order derivative of energy versus  $J$  for  $J=-2$  to  $2$ .



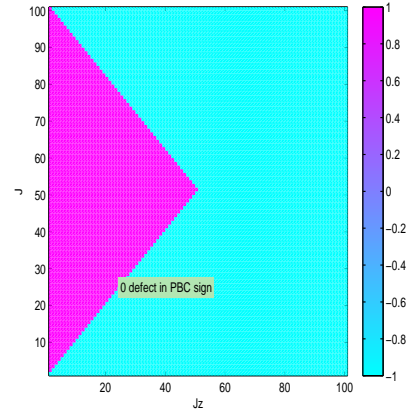
(a) The color variation shows the magnitude of ground state energy of zero defect sector in  $J - J_z$  plane under anti-periodic boundary condition.



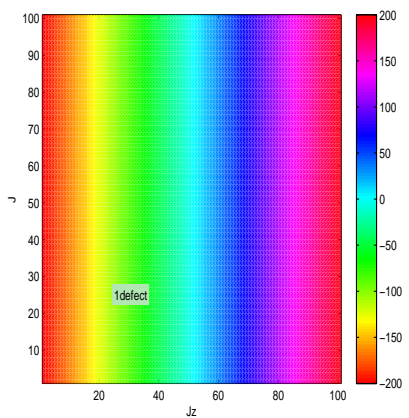
(b) The color variation shows the sign of ground state energy of zero defect sector in  $J - J_z$  plane under anti-periodic boundary condition.



(c) The color variation shows the magnitude of ground state energy of zero defect sector in  $J - J_z$  plane under periodic boundary condition.



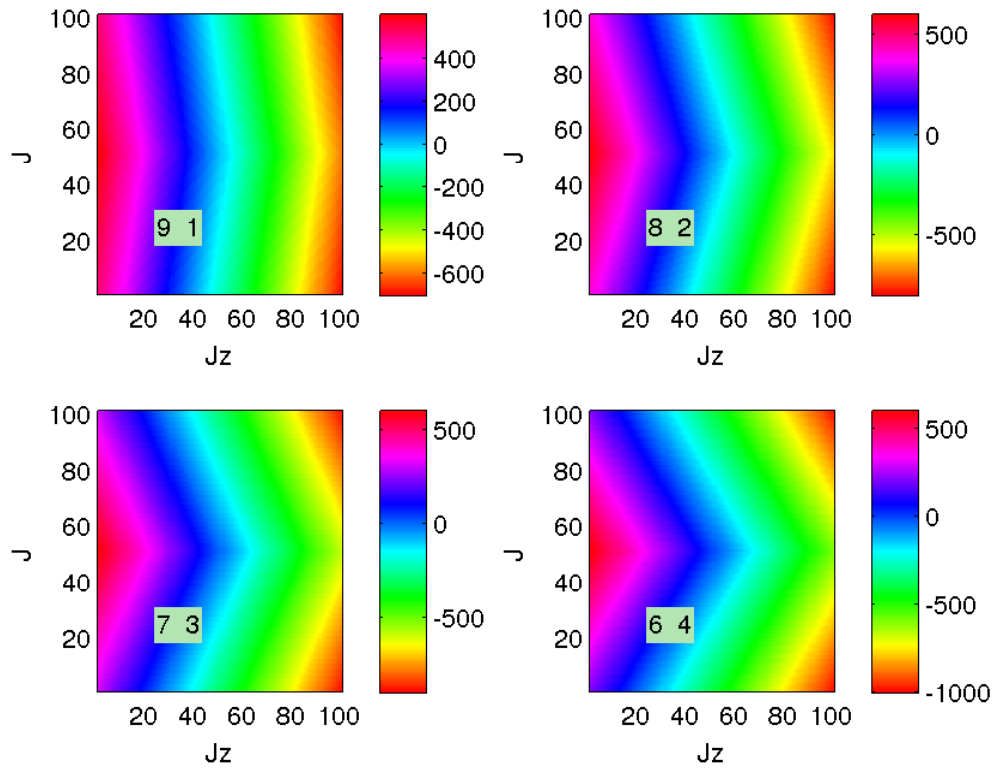
(d) The color variation shows the magnitude of ground state energy of zero defect sector in  $J - J_z$  plane under periodic boundary condition.



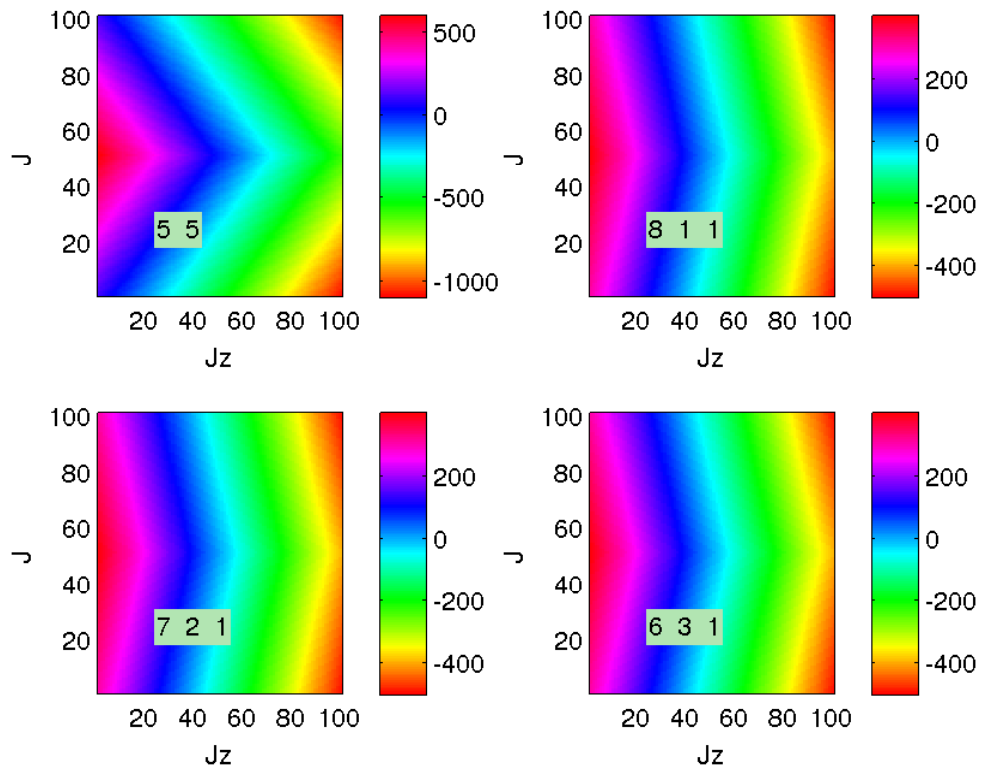
(e) The color variation shows the magnitude of ground state energy of one defect sector in  $J - J_z$  plane .

Figure 4.3:



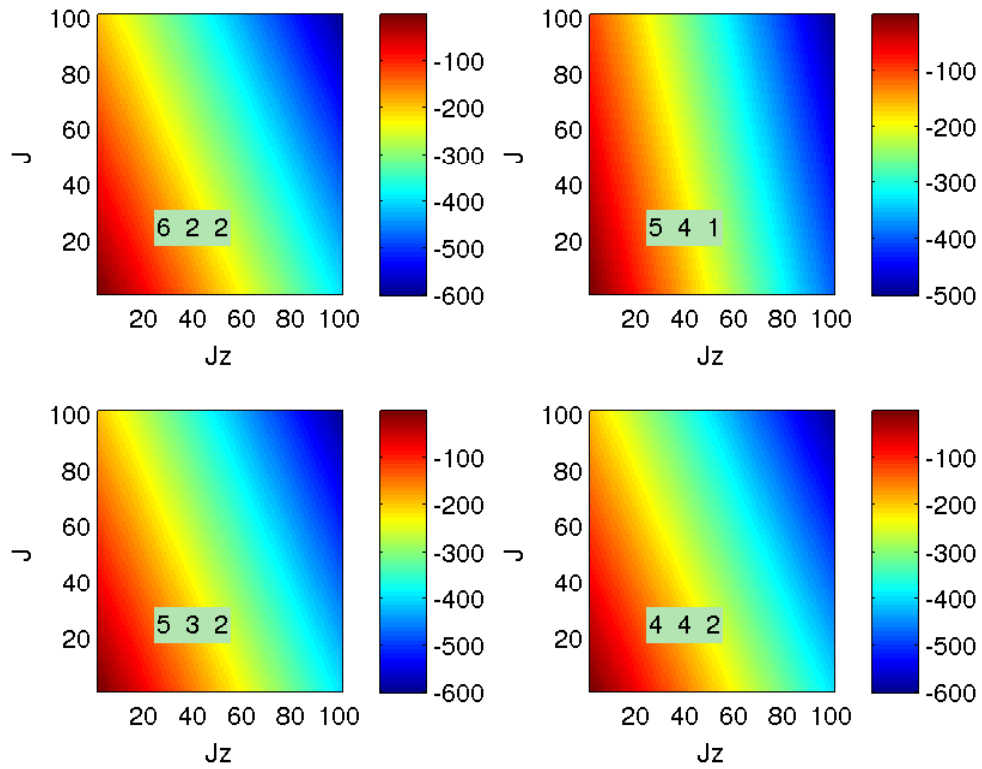


(a)

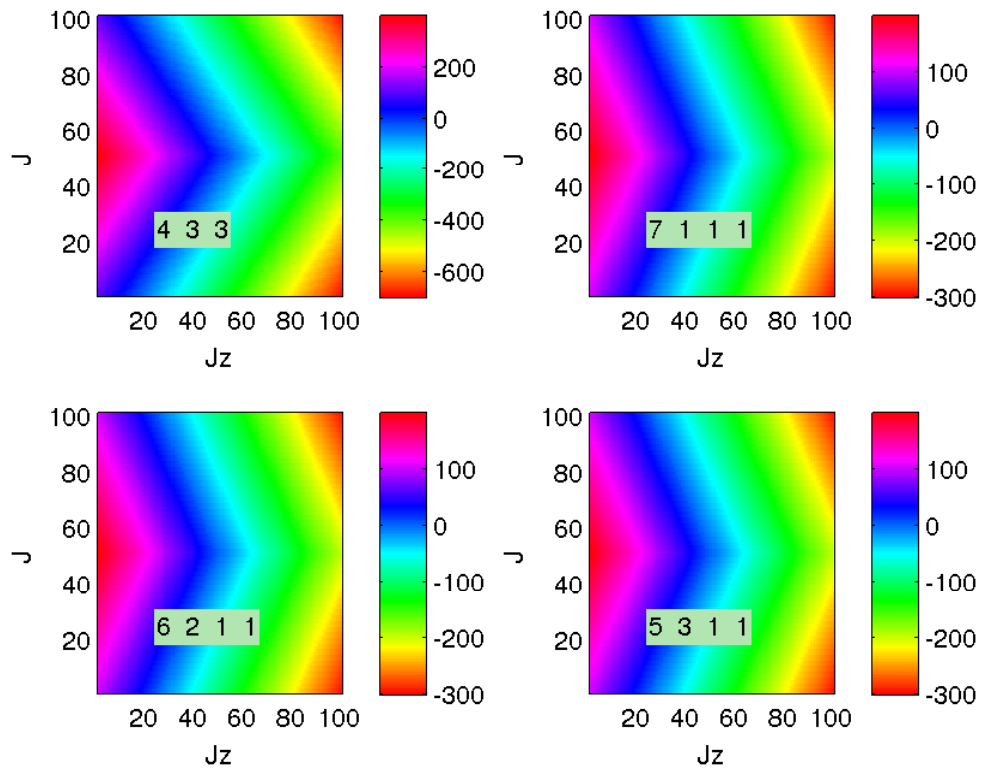


(b)

Figure 4.4: The ground state energy is plotted for various partitions of  $N=10$  shown in the light green patch (for example (9, 1), (8, 2) etc). The color variation of the graph shows the magnitude of ground state energy.

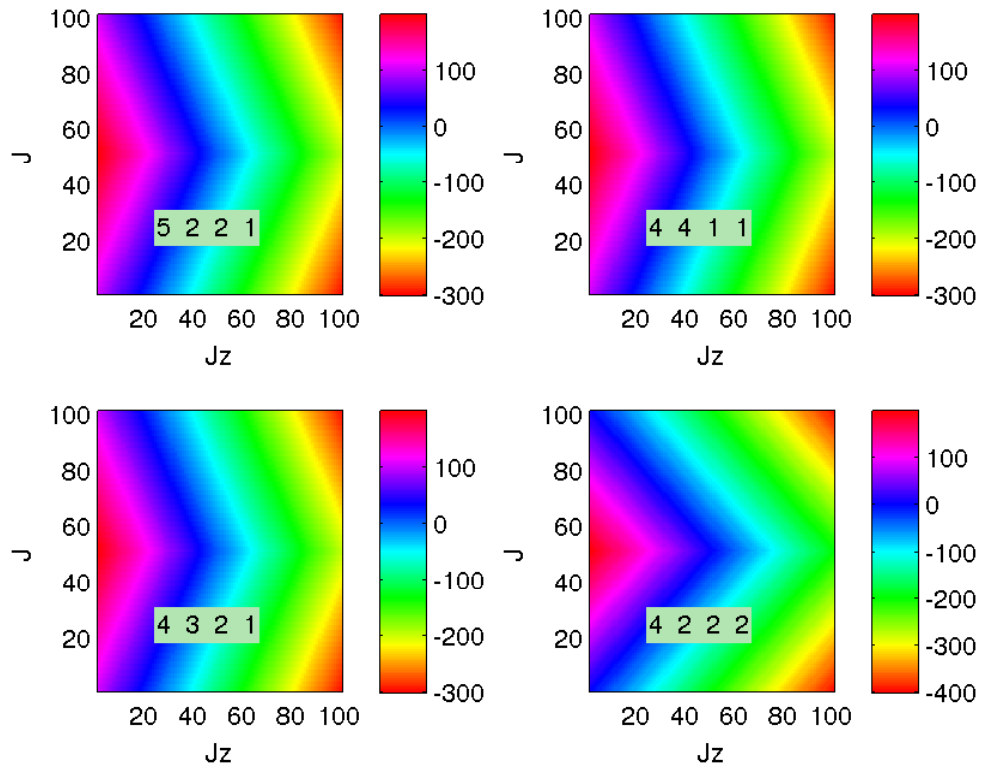


(a)

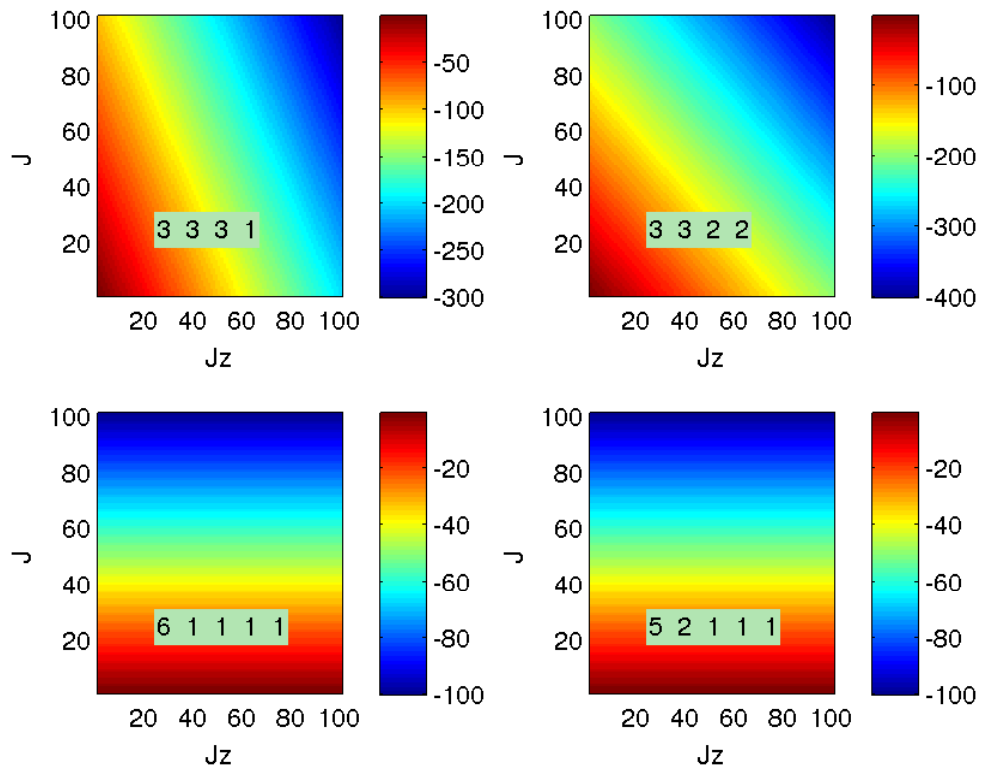


(b)

Figure 4.5: The ground state energy is plotted for various partitions of  $N=10$  shown in the light green patch. The color variation of the graph shows the magnitude of ground state energy.

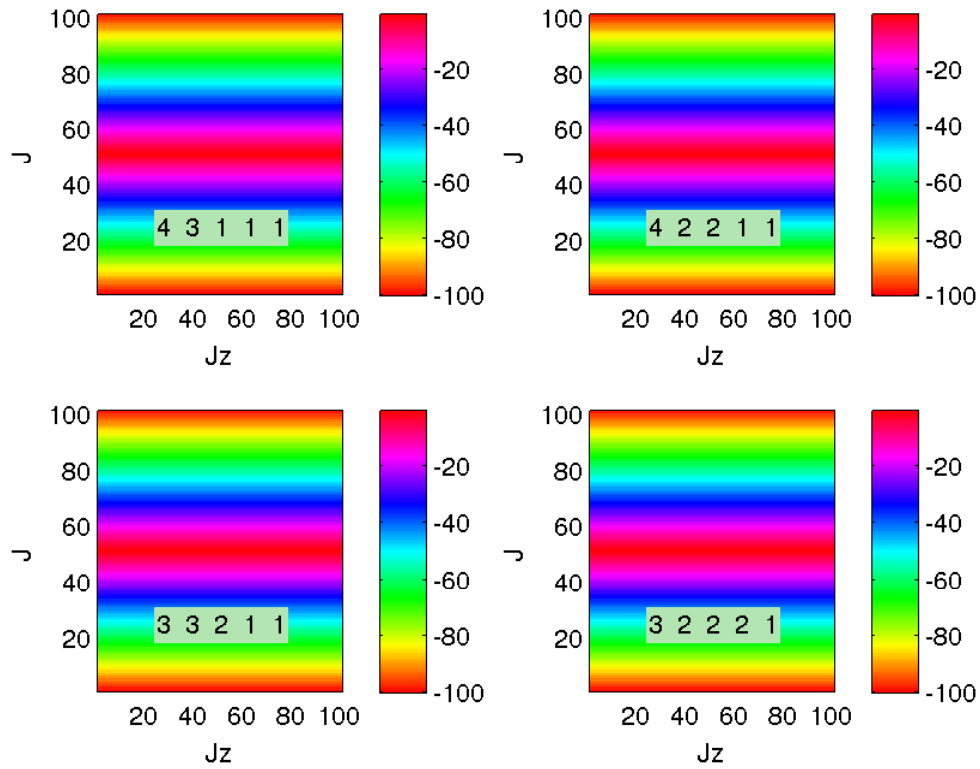


(a)

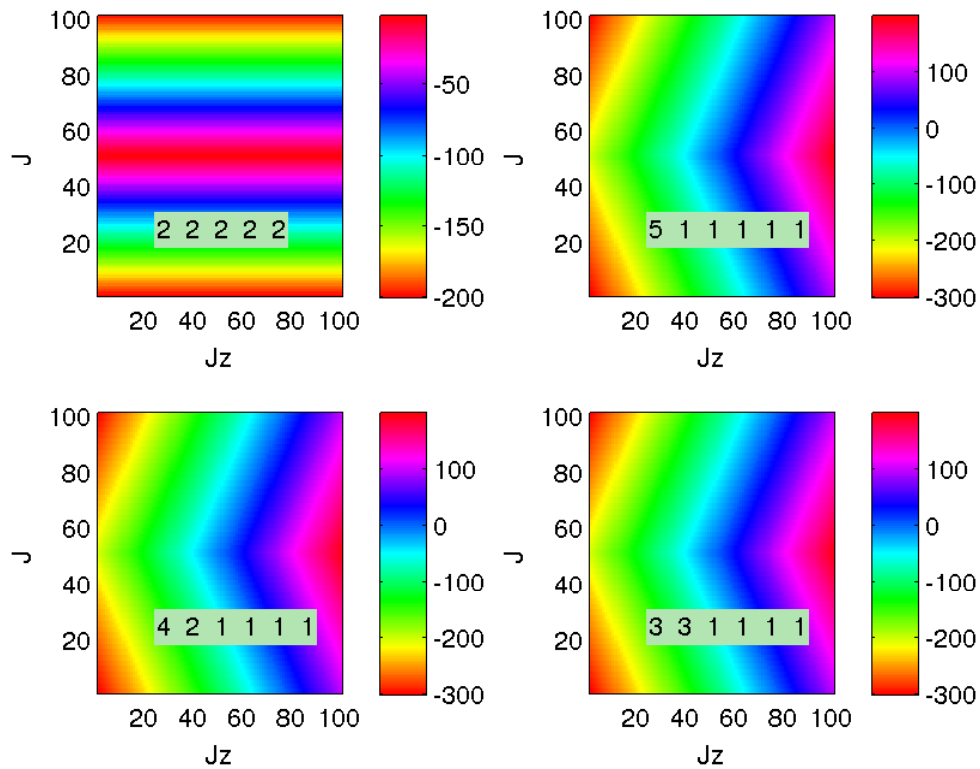


(b)

Figure 4.6: The ground state energy is plotted for various partitions of  $N=10$  shown in the light green patch. The color variation of the graph shows the magnitude of ground state energy.

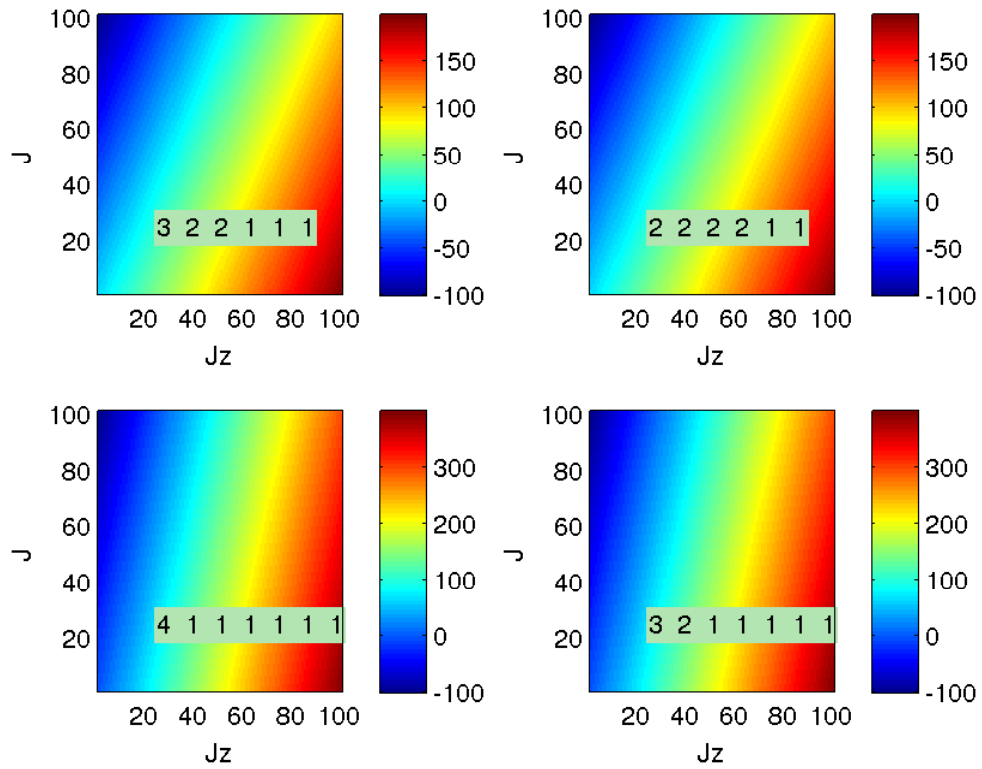


(a)

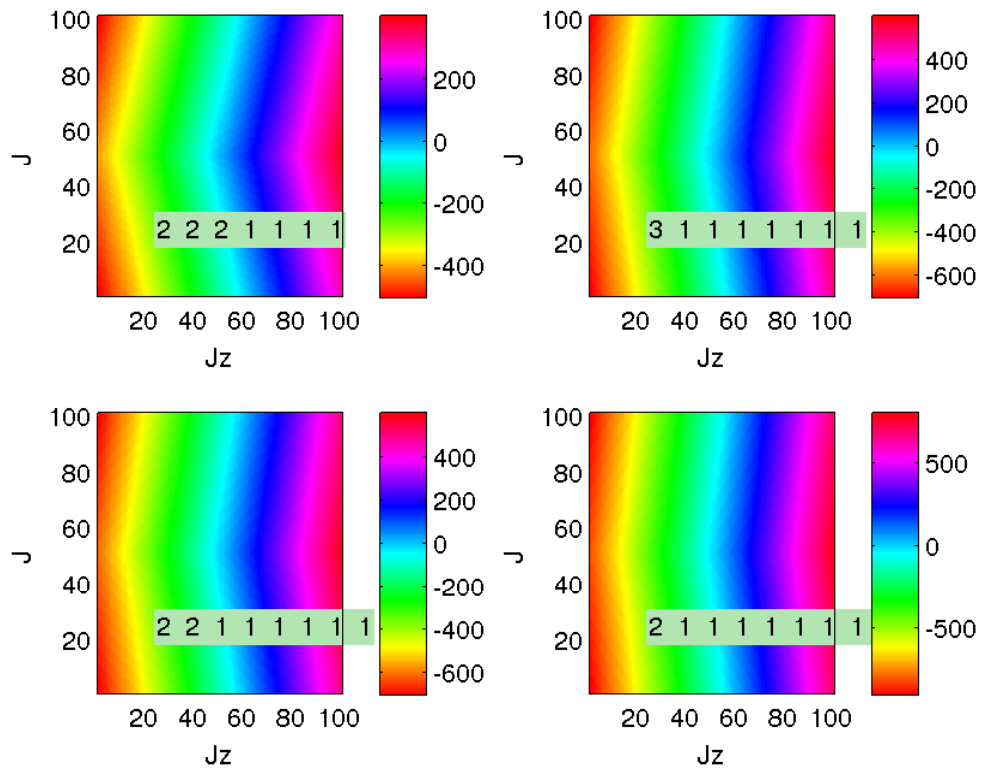


(b)

Figure 4.7: The ground state energy is plotted for various partitions of  $N=10$  shown in the light green patch. The color variation of the graph shows the magnitude of ground state energy.



(a)



(b)

Figure 4.8: The ground state energy is plotted for various partitions of  $N=10$  shown in the light green patch. The color variation of the graph shows the magnitude of ground state energy.

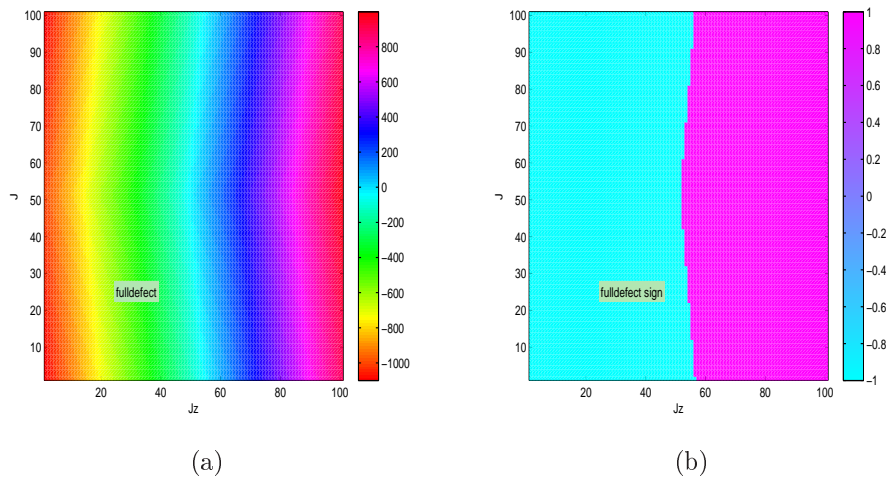


Figure 4.9: The ground state energy is plotted in full defect sector in  $J - J_z$  plane. The color variation of the graph in figure (a) shows the magnitude of the ground state energy and in figure (b) sign of the ground state energy.

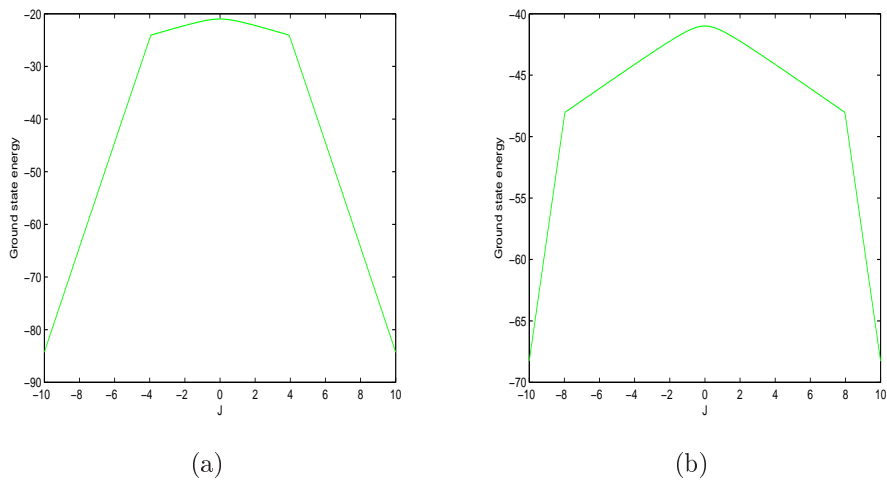


Figure 4.10: The ground state energy versus  $J$  is plotted for  $J_z = -2$  in figure (a) and for  $J_z = -4$  in figure (b). The kink in the ground state energy shows the first order transition.

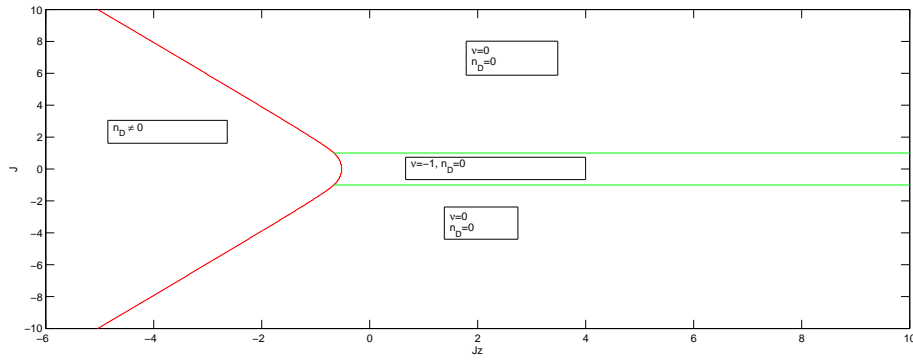


Figure 4.11: The red line in the phase diagram shows the first order transition and green line shows the topological phase transition at  $J = \pm 1$  described by the order parameter winding number.

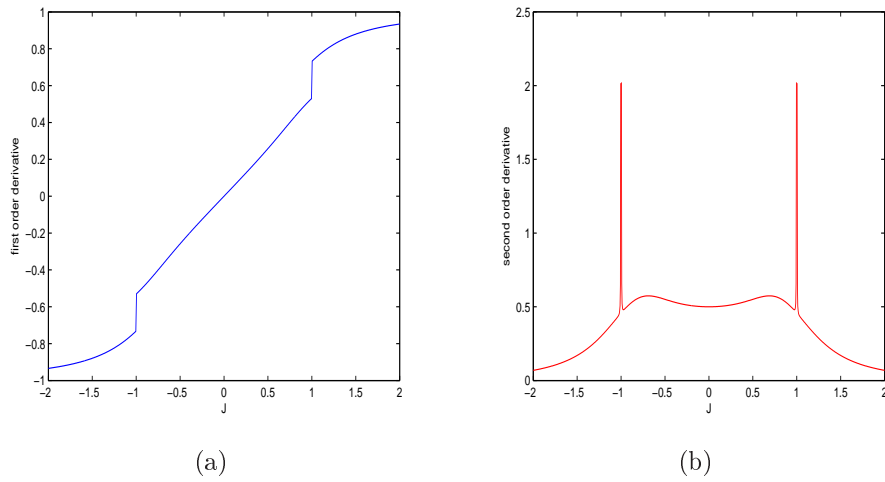


Figure 4.12: The first and second order derivative of the ground state energy is plotted in  $J - J_z$  plane for  $J_z > 0$  in figure (a) and figure (b).

# 5

## Topological Qubits in XY-Ising Model

The Tetrahedron model had localised unpaired Majorana modes which we can move around the lattice tuning the defects. We reproduce these results in the XY-Ising model. But this model has some advantage over Tetrahedron model. We have taken up this model because two spin operators are commuting with the model hamiltonian which can be constructed by Josephson junction quantum circuits. Further, we show that we can make a qubit with the two degenerate states, lying in the gap, of the model. This qubit is protected from decoherence by environmental perturbations for certain range of parameter of Hamiltonian. In the last section we show the possible physical realisation of the XY-Ising model. The environment can be created by electromagnetic influence of moving ion inside the quantum circuit or lattice imperfection in the physical realisation.

### 5.1 The Qubit

Whenever zero modes exist in the single particle eigenspectrum of any non-interacting Hamiltonian, the model will have two-fold degenerate multiparticle states. Further, if there is a gap in the single particle eigenspectrum of non-interacting Hamiltonian, the energy of the degenerate multiparticle ground states of the Hamiltonian are separated by a gap from the rest of the multiparticle eigenspectrum of Hamiltonian. As we have shown in chapter 3, the XY-Ising Hamiltonian is a non-interacting Hamiltonian of Majorana fermions, the model has two fold degenerate multiparticle states including the ground state. We have also shown that there is a gap in the single particle eigenspectrum of the model. Therefore, the model has a degenerate



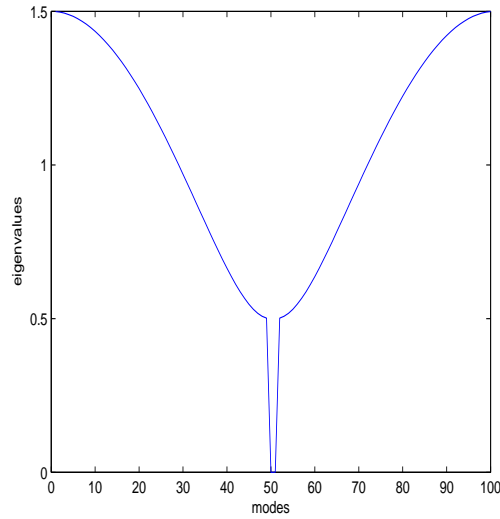


Figure 5.1: The absolute value of eigenvalues versus modes have been plotted.

multiparticle ground state separated by a gap from the rest of the eigenspectrum.

We have shown in chapter 3 that degenerate groundstates of the Hamiltonian are

$$\begin{aligned} &|0\rangle, \\ &\chi^{1\dagger}|0\rangle \text{ where } \chi^{i\dagger}|0\rangle = 0 \quad \forall i. \end{aligned} \quad (5.1)$$

The corresponding energy of these ground states are,

$$E_0 = - \sum_{n=2}^N \epsilon_n. \quad (5.2)$$

In one defect sector of the XY-Ising model, there are two zero energy modes in the single particle eigenspectrum lying in the gap, as shown in the figure (5.1).

The gap  $\Delta$  in the single particle eigenspectrum is defined as twice the value of the lowest single-particle energy eigenvalue. The lowest single particle eigenstate is in the ground state sector. As we have shown in the chapter 3,  $u_i = -1$  is the ground state sector. In the ground state sector energy eigenspectrum is given by

$$\epsilon_{1,2}(k) = \pm \frac{1}{2} \sqrt{(J^2 - 2J \cos(ka) + 1)}. \quad (5.3)$$

The lowest single particle state has the energy  $\frac{1}{2}|(1 - J)|$  and therefore the gap is given by,

$$\Delta = |(1 - J)|. \quad (5.4)$$

Thus, the energy of the degenerate multiparticle ground states of the Hamiltonian are separated by the gap  $\Delta$  from the rest of the multiparticle eigenspectrum of Hamiltonian. Let us call them  $|0\rangle$  and  $|1\rangle$  of the proposed qubit i.e,

$$\begin{aligned} |0\rangle &= |0\rangle, \\ |1\rangle &= \chi^{1\dagger}|0\rangle. \end{aligned} \quad (5.5)$$

### 5.1.1 Tuning the flux configuration

In order to make any flux configuration ground state sector, we can add the following “chemical potential” term in the Hamiltonian,

$$H_\mu = \sum_i (\mu_i W_i). \quad (5.6)$$

This term, being the commuting operator, will not change the eigenstates but will alter the energy eigenvalues. Therefore, tuning  $\mu_i$  any particular flux configurations can be made the ground state. Accessing any flux configuration as a ground state, we can make one of the degenerate zero modes move along the one dimensional chain. If we put the  $n$  defects from the left end of the chain, the wavefunction of one of the zero mode gets suppressed up to  $n - 1^{th}$  unit cell and peaks at  $n^{th}$  unit cell to decrease afterwards (for  $J > 1$ ) by the factor of  $\frac{1}{J}$  as shown in figure (5.2).

The chemical potential term being 2-spin operators can be realized experimentally in Josephson junction quantum circuits.

## 5.2 Protection from Decoherence

In general, the environment can couple with the qubit and can lift the degeneracy between the qubit states  $|0\rangle$  and  $|1\rangle$  and, therefore, qubit can decohere in short time.. Here, we show, taking single spin terms as environment, that they can lift the degeneracy, but this splitting can be made small for a certain range of parameters of the Hamiltonian and, therefore, decoherence time of qubit can be made larger.

Let us take the environment modelled by potential,

$$V = V_x + V_y + V_z \quad (5.7)$$

where

$$\begin{aligned} V_x &= \sum_i (B_x^{i,1} \sigma_{i,1}^x + B_x^{i,2} \sigma_{i,2}^x), \\ V_y &= \sum_i (B_y^{i,1} \sigma_{i,1}^y + B_y^{i,2} \sigma_{i,2}^y), \\ V_z &= \sum_i (B_z^{i,1} \sigma_{i,1}^z + B_z^{i,2} \sigma_{i,2}^z). \end{aligned} \quad (5.8)$$

We find the condition for  $V_z$  which does not lift the degeneracy between qubit states. We also prove that the the degeneracy between qubit states is robust for  $V_x$  and  $V_y$  part of the potential.

In the Jordan-Wigner basis,  $V$  becomes,

$$\begin{aligned} V_x &= \sum_i \{B_x^{i,1} (i\eta_{i,1} \xi_{i,1}) - B_x^{i,2} (i\eta_{i,2} \xi_{i,2})\}, \\ V_y &= \sum_i \{B_y^{i,1} \eta_{i,1} \prod_{j=1}^{i-1} (\hat{u}_j) \prod_{j=1}^{i-1} (i\xi_{j,1} \xi_{j,2}) + B_y^{i,2} \eta_{i,1} \prod_{j=1}^{i-1} (\hat{u}_j) \prod_{j=1}^i (i\xi_{j,1} \xi_{j,2})\}, \\ V_z &= \sum_i \{B_z^{i,1} \prod_{j=1}^{i-1} (\hat{u}_j) \xi_{i,1} \prod_{j=1}^{i-1} (i\xi_{j,1} \xi_{j,2}) + B_z^{i,2} \prod_{j=1}^i (\hat{u}_j) \xi_{i,1} \prod_{j=1}^{i-1} (i\xi_{j,1} \xi_{j,2})\}. \end{aligned} \quad (5.9)$$

As zero modes exist in the sector of Hamiltonian  $u_1 = +1, u_2 = -1, u_3 = -1$  etc.,

we relabel the degenerate states of the the proposed qubit as,

$$\begin{aligned} |0\rangle &\rightarrow |\{u_n\}\rangle|0\rangle, \\ \chi^{1\dagger}|0\rangle &\rightarrow |\{u_n\}\rangle\chi^{1\dagger}|0\rangle, \end{aligned} \quad (5.10)$$

and do first order perturbation theory in this degenerate subspace.

The effective Hamiltonian in the twofold degenerate subspace for the system is given by,

$$H_{eff} = \sum_{i,\alpha} \begin{bmatrix} \langle\{u_n\}|\langle 0|V|0\rangle|\{u_n\}\rangle & \langle\{u_n\}|\langle 0|V|1\rangle|\{u_n\}\rangle \\ \langle\{u_n\}|\langle 1|V|0\rangle|\{u_n\}\rangle & \langle\{u_n\}|\langle 1|V|1\rangle|\{u_n\}\rangle \end{bmatrix}. \quad (5.11)$$

If  $|\alpha\rangle$  and  $|\beta\rangle$  are the degenerate states of the qubit then we evaluate  $\langle\{u_n\}|\langle\alpha|V_x|\beta\rangle|\{u_n\}\rangle$

$$= \sum_i \{iB_x^{i,1}\langle\{u_n\}|\eta_{i,1}|\{u_n\}\rangle\langle\alpha|\xi_{i,1}|\beta\rangle - iB_x^{i,2}\langle\{u_n\}|\eta_{i,2}|\{u_n\}\rangle\langle\alpha|\xi_{i,2}|\beta\rangle\} = 0, \quad (5.12)$$

because  $|\{u_n\}\rangle$  is not eigenstate of  $\eta_{i,1}$ .

Similarly, we evaluate  $\langle\{u_n\}|\langle\alpha|V_y|\beta\rangle|\{u_n\}\rangle$

$$\begin{aligned} &= \sum_i \{B_y^{i,1}\langle\{u_n\}|\eta_{i,1} \prod_{j=1}^{i-1}(\hat{u}_j)|\{u_n\}\rangle\langle\alpha|\prod_{j=1}^{i-1}(i\xi_{j,1}\xi_{j,2})|\beta\rangle \\ &+ B_y^{i,2}\langle\{u_n\}|\eta_{i,1} \prod_{j=1}^{i-1}(\hat{u}_j)|\{u_n\}\rangle\langle\alpha|\prod_{j=1}^i(i\xi_{j,1}\xi_{j,2})|\beta\rangle\} = 0. \end{aligned} \quad (5.13)$$

Finally, we evaluate  $\langle\{u_n\}|\langle\alpha|V_z|\beta\rangle|\{u_n\}\rangle$

$$\begin{aligned} &= \sum_i \{B_z^{i,1}\langle\{u_n\}|\prod_{j=1}^{i-1}(\hat{u}_j)|\{u_n\}\rangle\langle\alpha|\xi_{i,1} \prod_{j=1}^{i-1}(i\xi_{j,1}\xi_{j,2})|\beta\rangle \\ &+ B_z^{i,2}\langle\{u_n\}|\prod_{j=1}^i(\hat{u}_j)|\{u_n\}\rangle\langle\alpha|\xi_{i,1} \prod_{j=1}^{i-1}(i\xi_{j,1}\xi_{j,2})|\beta\rangle\} \\ &= \sum_i B_z^{i,1}\{\langle\alpha|\xi_{i,1} \prod_{j=1}^{i-1}(i\xi_{j,1}\xi_{j,2})|\beta\rangle + B_z^{i,2}\langle\alpha|\xi_{i,1} \prod_{j=1}^{i-1}(i\xi_{j,1}\xi_{j,2})|\beta\rangle\}. \end{aligned} \quad (5.14)$$

Thus,

$$\begin{aligned}
 \langle \{u_i\} | \langle \alpha | V_x | \beta \rangle | \{u_i\} \rangle &= 0, \\
 \langle \{u_i\} | \langle \alpha | V_y | \beta \rangle | \{u_i\} \rangle &= 0, \\
 \langle \{u_i\} | \langle \alpha | V_z | \beta \rangle | \{u_i\} \rangle &= \sum_i B_z^{i,1} \langle \alpha | \xi_{i,1} \prod_{j=1}^{i-1} (i \xi_{j,1} \xi_{j,2}) | \beta \rangle \\
 &\quad + B_z^{i,2} \langle \alpha | \xi_{i,1} \prod_{j=1}^{i-1} (i \xi_{j,1} \xi_{j,2}) | \beta \rangle. \tag{5.15}
 \end{aligned}$$

To calculate the matrix element of  $V_z$  part, we have to express all  $\xi$  operators in terms of  $\chi$  operators using,

$$\xi_{i,\alpha} = \sum_n \phi_{i,\alpha}^{n*} \chi^n + \phi_{i,\alpha}^n \chi^{n\dagger}, \tag{5.16}$$

where  $n$  runs over the modes belonging to positive energy eigenvalue.

Then, we start getting sum of one  $\chi$  operator term, three  $\chi$  operators, five  $\chi$  operators and so on. To handle this, we solve the system for each spin separately defining J-W transformation for each spin individually and finally add them to get only one  $\chi$  operator term. Defining Jordan-Wigner transformation for each spin individually does not change the original Hamiltonian. We solve the system for each spin at  $i, \alpha$  separately defining J-W transformation for each spin individually.

Now, we calculate  $\langle \alpha | \xi_{i,\alpha} | \beta \rangle$  where  $|\alpha\rangle$  and  $|\beta\rangle$  are  $|0\rangle$  or  $|1\rangle = \chi^1 |0\rangle$ .

$$\begin{aligned}
 \langle 0 | \xi_{i,\alpha} | 0 \rangle &= \langle 0 | \chi^1 \phi_{i,\alpha}^{*1} + \chi^{1\dagger} \phi_{i,\alpha}^1 | 0 \rangle + \langle 0 | \sum_{n \neq 1} \chi^n \phi_{i,\alpha}^{*n} + \chi^{n\dagger} \phi_{i,\alpha}^n | 0 \rangle \\
 &= 0, \\
 \langle 0 | \xi_{i,\alpha} | 1 \rangle &= \langle 0 | \chi^1 \phi_{i,\alpha}^{*1} + \chi^{1\dagger} \phi_{i,\alpha}^1 | 1 \rangle + \langle 0 | \sum_{n \neq 1} \chi^n \phi_{i,\alpha}^{*n} + \chi^{n\dagger} \phi_{i,\alpha}^n | 1 \rangle \\
 &= \phi_{i,\alpha}^{*1}, \\
 \langle 1 | \xi_{i,\alpha} | 0 \rangle &= \langle 1 | \chi^1 \phi_{i,\alpha}^{*1} + \chi^{1\dagger} \phi_{i,\alpha}^1 | 0 \rangle + \langle 1 | \sum_{n \neq 1} \chi^n \phi_{i,\alpha}^{*n} + \chi^{n\dagger} \phi_{i,\alpha}^n | 0 \rangle, \\
 &= \phi_{i,\alpha}^1,
 \end{aligned}$$

and finally,

$$\begin{aligned}\langle 1|\xi_{i,\alpha}|1\rangle &= \langle 1|\chi^1\phi_{i,\alpha}^{*1} + \chi^{1\dagger}\phi_{i,\alpha}^1|1\rangle + \langle 1|\sum_{n\neq 1}\chi^n\phi_{i,\alpha}^{*n} + \chi^{n\dagger}\phi_{i,\alpha}^n|1\rangle \\ &= 0.\end{aligned}\tag{5.17}$$

Substituting all these values in eqn. (5.11) we get,

$$H_{eff} = \sum_{i,\alpha} B_z^{i,\alpha} \begin{pmatrix} 0 & \phi_{i,\alpha}^{*1} \\ \phi_{i,\alpha}^1 & 0 \end{pmatrix}.\tag{5.18}$$

Now, we substitute  $\phi_{i,\alpha}$  solving the recursion relation in chapter 3 in the sector  $u_1 = +1$  and all other  $u_i = -1$  using the normalisation condition,

$$\sum_i^N |\phi_{i,1}|^2 + |\phi_{i,2}|^2 = 1\tag{5.19}$$

and the boundary condition  $\phi_{N+1,1} = 0$ .

We found that all

$$\text{all } \phi_{i,1} = 0\tag{5.20}$$

and  $\phi_{i,2}$  can be found out from boundary condition  $\phi_{0,2} = 0$ . For  $J_x = J_y = \frac{J}{2}$  and in sector  $u_1 = +1, u_2 = -1, u_3 = -1\dots$  (the zero mode condition),  $\phi_{i,2}$  is given by

$$\phi_{i,2} = \aleph \left(\frac{1}{J}\right)^{i-1},\tag{5.21}$$

where  $\aleph$  is normalisation constant.

Now plugging in all these values from  $\phi_{i,1}$  and  $\phi_{i,2}$  in normalisation condition, we get,

$$\aleph^2 = \frac{\frac{1}{J^2} - 1}{\left(\frac{1}{J^2}\right)^N - 1}.\tag{5.22}$$

The wavefunctions  $\phi_{i,1}$  and  $\phi_{i,2}$  for  $1/J = a$  are given by,

$$\begin{aligned}\phi_{i,1} &= 0, \\ \phi_{i,2} &= \sqrt{\frac{a^2 - 1}{a^{2N} - 1}} a^{i-1}.\end{aligned}\quad (5.23)$$

If  $a > 1$  then, for large  $N$ , the eqn. (5.23) for  $\phi_{i,2}$  becomes,

$$\phi_{i,2} = \frac{\sqrt{a^2 - 1}}{a^N} a^{i-1}.\quad (5.24)$$

Thus, the largest term for  $a > 1$  is,

$$\phi_{N,2} = \frac{\sqrt{a^2 - 1}}{a}.\quad (5.25)$$

If  $a < 1$  then, for large  $N$ ,  $a^{2N} = 0$  in eqn. (5.23).  $\phi_{i,2}$  is then given by,

$$\phi_{i,2} = \sqrt{1 - a^2} a^{i-1}.\quad (5.26)$$

Thus, the largest term for  $a < 1$  is,

$$\phi_{1,2} = \sqrt{1 - a^2}.\quad (5.27)$$

For large  $N$ , in both cases ( $a > 1$  and  $a < 1$ ), wavefunctions and, therefore, matrix elements of eqn. (5.18) do not vanish which would mean degeneracy between the qubit states is lifted. The matrix elements vanish only when  $a = 1$  ( $\phi_{i,2} = \frac{1}{\sqrt{N}}$  becomes zero when  $N \rightarrow \infty$ ) but then, gap becomes smaller or zero and, therefore, second order correction in perturbation theory becomes dominant. From second order degenerate perturbation theory,

$$\langle m | H_{eff}^2 | m' \rangle = \sum_n \frac{\langle m | V | n \rangle \langle n | V | m' \rangle}{E_m - E_n},\quad (5.28)$$

where  $n$  runs over all excited states and  $m$  and  $m'$  belong to degenerate ground state space.

So, the second or higher order perturbation theory becomes dominant if the gap between the degenerate ground states and other states is small or zero. In

order to make second order correction term in perturbation theory ineffective, we have to maximize the gap while maintaining the zero mode condition  $J_x = J_y = \frac{J}{2}$ . So, we can vary only  $J$ .

The largest term of effective second order Hamiltonian is,

$$\langle m|H_{eff}^2|m'\rangle = \frac{\langle m|V|f.s\rangle\langle f.s|V|m'\rangle}{-J|1-a|}, \quad (5.29)$$

where  $|f.s\rangle$  is the first excited state separated by a gap  $|J-1| = J|1-a|$  from the ground state.

Substituting  $V = \sum_{i,\alpha,a} B_a^{i,\alpha} \sigma_{i,\alpha}^a$ , we get,

$$\langle m|H_{eff}^2|m'\rangle = \sum_{i,\alpha,a;j,\beta,b} B_a^{i,\alpha} B_b^{j,\beta} \frac{\langle m|\sigma_{i,\alpha}^a|f.s\rangle\langle f.s|\sigma_{j,\beta}^b|m'\rangle}{-J|1-a|}. \quad (5.30)$$

The second order correction is ineffective when we choose  $J$  such that

$$\frac{\min\{B_a^{i,\alpha} B_b^{j,\beta}\}}{|1-a|} < J. \quad (5.31)$$

Thus, we can make first order correction in Hamiltonian small by setting  $a \approx 1$  and can make second order correction in Hamiltonian small if we choose  $J$  according to eqn. (5.31). Therefore, the environment  $V$  lifts the degeneracy of the state of qubit which can be made small by tuning the parameter of Hamiltonian. This results in making decoherence time of qubit larger. Further, the protection from decoherence is robust for  $V_x$  and  $V_y$  part of potential.

In the next section, we discuss a physical realisation of qubit in the model by Josephson junction quantum circuits. The environment potential which we have taken here is actually created by external voltage applied by some nearby ion in the quantum circuit or error in tuning the gate capacitor. (It creates a  $\sigma_z$  term in the superconducting qubit box as shown in eqn. (1.98) of chapter 1). We know that protection from decoherence is perfect for  $V_x$  and  $V_y$ . So, if we rotate the spins at each site around  $x$  axis of XY-Ising model then  $z$ ,  $y$  and  $x$  bond becomes  $y$ ,  $z$  and  $x$  bonds respectively as shown in figure (5.3). Then, the protection from decoherence is perfect for  $V_x$  and  $V_z$  part of potential. Therefore, the qubit is protected perfectly by external voltage fluctuation in the superconducting qubit



box.

### 5.3 Physical Realisation

In the introduction of this thesis, we have shown how to design an artificial lattice using Josephson junction quantum circuits (superconducting quantum circuit) to engineer the model Hamiltonian. Here, we give a proposal to realise the XY-Ising Model. It consists of superconducting qubit boxes (labeled 1-4) as shown in figure 5.4. To design x bond, superconducting qubit box 1 and 2 are coupled via a mutual inductor  $M$ . To design y bond, superconducting qubit box 1 and 2 are coupled via a wire. To design z bond, superconducting circuit box 2 and 3 are coupled via a capacitor  $C_m$ , and so on. Here, each superconducting qubit box consists of a superconducting ring connected with two identical Josephson junctions each with coupling energy  $E_J$  and capacitance  $C_J$  (shown by a cross on the box). These Josephson junctions form a SQUID loop and are connected to LC oscillator. Each circuit box is controlled by both a voltage  $V_i$  (applied via the gate capacitor  $C_g$ ) and a magnetic flux  $\Phi_i$  passing through the SQUID loop. The parameters of the Hamiltonian  $J_x, J_y$  can be tuned by tuning the magnetic flux and  $J_z$  can be tuned by capacitor  $C_m$ . So, in order to get the ground state degeneracy in many particle spectrum, we can tune  $\Phi_i$ 's to make  $J_x$  and  $J_y$  equal to get a zero mode in single particle eigenspectrum. Any moving charge in the circuit creates magnetic flux passing through each superconducting qubit box randomly. Once we create the condition for zero mode by tuning  $J_x$  and  $J_y$ , the random fluxes created by moving ions can not destroy the zero mode because zero mode exists for inhomogenous chain (when strength parameters  $J_x$  and  $J_y$  is not uniform over the full chain). This would result in only the rescaling of  $J_x$  and  $J_y$  by a common factor inside each unit cell and  $J_z$  remains unaffected. Therefore, the degeneracy in the many particle state is well protected against random magnetic fluxes applied by ions. Further, in order to manipulate the zero mode, we can add the commuting operators  $\sigma_1^z \sigma_2^z$  in the Hamiltonian by connecting superconducting qubit box 1 with superconducting qubit box 2 via a capacitor  $C_m$ .

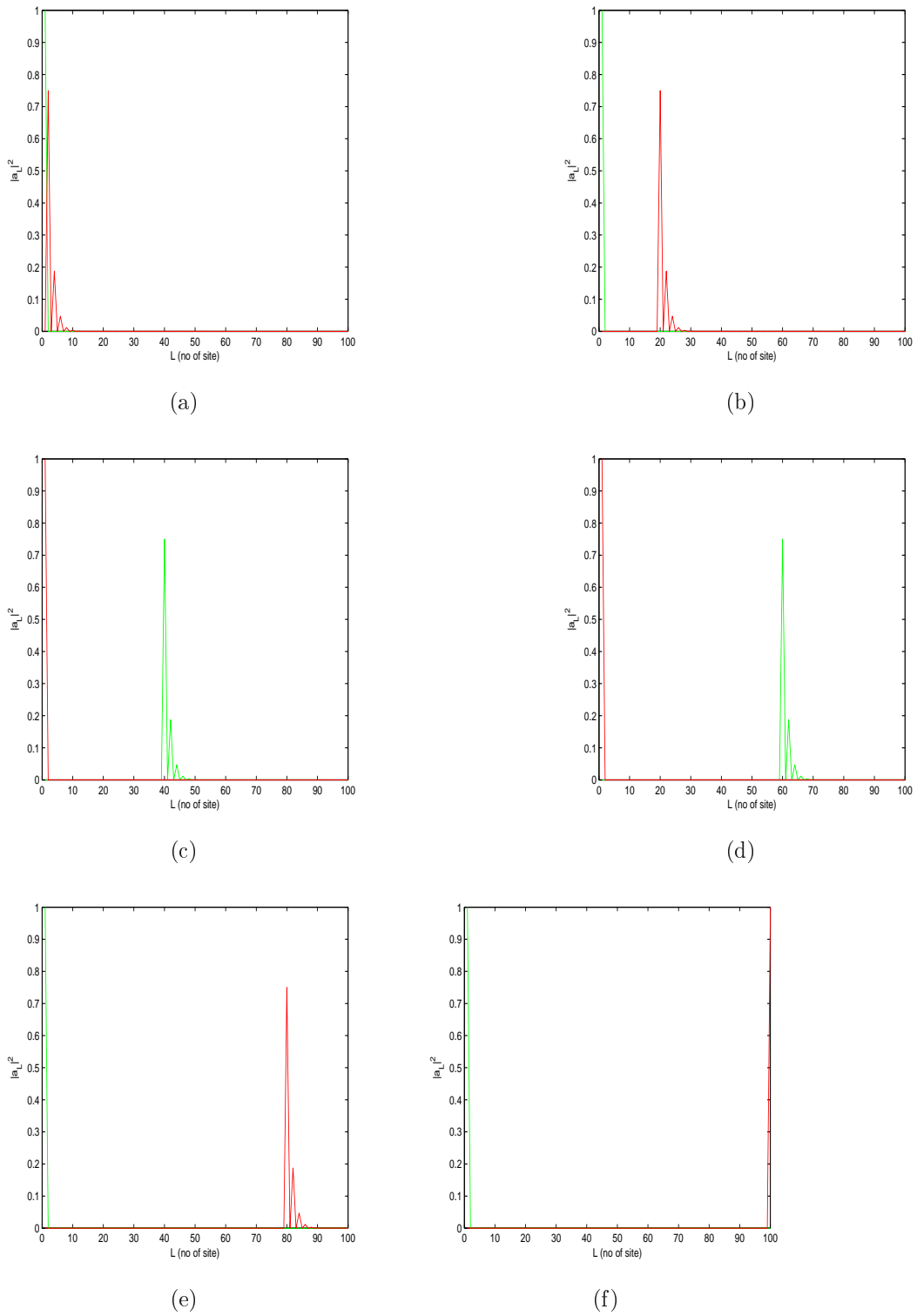


Figure 5.2: The unpaired zero mode is moving on the chain with 1, 10, 20, 30, 40 and 50 defects shown in fig.(a), (b), (c), (d), (e) and (f). The defects have been put from the left end of the chain.

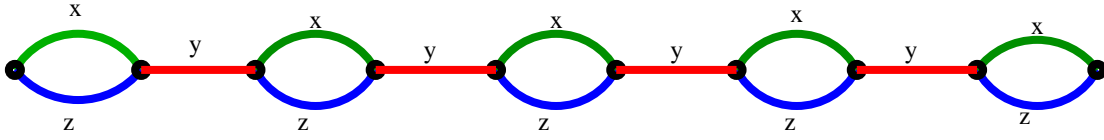


Figure 5.3: There are two sites per unit cell in the model. The  $x, y$  and  $z$  bonds are as indicated.

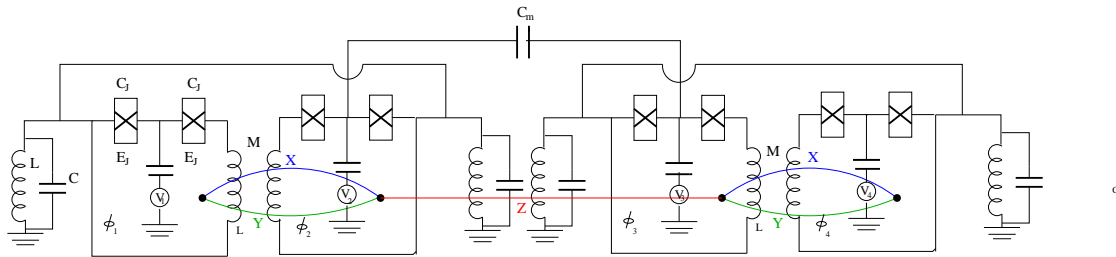


Figure 5.4: The circuit equivalent of XY-Ising Model. The  $x, y$  and  $z$  bonds are designed by coupling the superconducting qubit box through mutual inductance  $M$ , wire and capacitor  $C_m$  respectively. We have shown a unit cell of the XY-Ising model of the corresponding circuit diagram where  $x, y$  and  $z$  bonds are shown by blue, green and red colour lines.

# 6

## Conclusion

In the concluding chapter, we summarize our results which we have presented in the thesis and indicate possible future work arising out of the approach presented here.

### 6.1 Summary

In this thesis, we studied two one dimensional generalised versions of the Kitaev's model. Since they reduce to a non-interacting Hamiltonians, it became possible for us to give analytic solutions.

In the Tetrahedral model, we found out numerically that the translationally invariant fluxes through the unit cells, namely  $u_i^L = -1$  and  $u_i^R = -1$  is the ground state sector of the model. We gave a generic expression for fermionic gap. The closed form solution for the zero modes of the Majorana fermions has been derived. Unpairing and manipulation of zero Majorana modes tuning  $Z_2$  flux configurations has been shown. The regions in parameter space for homogenous chains has been shown where the zero modes occur. We further showed that there is a large parameter space for inhomogenous chains where the unpaired modes occur. Another important result we proved in the model using transfer matrix method that every state of the system has a  $2^{N/4}$  fold degeneracy, where  $N$  is the number of sites.

The XY-Ising model was studied under periodic boundary condition and we solved the model exactly for  $J_x = J_y$  for all flux configurations and proved that for  $J_x = J_y$  the ground state lies in translationally invariant flux sector  $u_i = -1$ . We

gave an expression for fermionic gap. The closed form solution for the zero modes of the Majorana fermions was derived and unpairing and manipulation of zero Majorana modes was shown. The topological nature of the zero mode has been found. Further, it was shown that qubit made up of degenerate Majorana modes of the model are protected from decoherence by environmental perturbations.

We also studied ground state properties of the XYZ-Ising model for all  $J_x, J_y$  and  $J_z$  numerically which agree with analytical results in extreme limits. The zero temperature phase diagram of the system was plotted by numerically calculating the ground state in various sectors. It was found that the model undergoes a first order phase transition for  $J_z < 0$  and for  $J_z > 0$  the phase transition is described by a topological order parameter called winding number.

Finally, physical realisation of XY-Ising model with its commuting operator has been achieved.

## 6.2 Outlook

There are some loose ends in our work which we would like to tie up in future.

We have studied zero temperature phase diagram of the XYZ-Ising model. In future, we would like to study finite temperature behaviour of the model.

In our scheme, the flux configuration sector we want to access, we make it a ground state sector. At low temperature the system will be in ground state, therefore, the system would access the required flux configuration sector. But in order to be at low temperature system would have to interact with the environment. Still it has to be shown that how the system will go from one flux configuration sector to another flux configuration sector interacting with environment.

Our aim, above all, was to design a logic gate which would perform quantum computation on a qubit. In future, we would like to embark upon this venture.

# Bibliography

- [1] J. Preskill. Preskill Lecture Notes.
- [2] A. Y. Kitaev. Anyons in an exactly solved model and beyond. **321**, 2 (2006).
- [3] Alicea, Jason and Oreg, Yuval and Refael, Gil and von Oppen, Felix and Fisher, Matthew P. A. Non-Abelian statistics and topological quantum information processing in 1D wire networks. *Nature Physics*, 7 (5), 412-417, (2011).
- [4] J. Q. You, X. F. Shi, X. Hu and F. Nori. Quantum emulation of a spin system with topologically protected ground states using superconducting quantum circuits. *Phys. Rev. B* **81**,014505 (2010).
- [5] R. P. Feynman. *Lectures on Computation*. (1985).
- [6] P. Benioff. Quantum mechanical Hamiltonian models of Turing machines. *J. Stat. Phys.* , **29:515** (1982).
- [7] R. P. Feynman. Quantum mechanical computers. *Opt. News* 11 11 (1985).
- [8] A. M. Turing. On Computable Numbers with an Application to the Entscheidungsproblem. *Proceedings of the London Mathematical Society*. 2 **42**: 230-65 (1937).
- [9] A. M. Turing. On Computable Numbers, with an Application to the Entscheidungsproblem: A correction, *Proceedings of the London Mathematical Society*. 2 **43** (6): 544-6 (1938).
- [10] M. Nielsen and Issac L. Chuang. *Quantum Computation and Quantum Information*. Cambridge: Cambridge University Press. ISBN 0-521-63503-9. OCLC 174527496 (2000).
- [11] D. Deutsch. Quantum theory, the Church-Turing principle and the universal quantum computer. *Proceedings of the Royal Society of London, Series A, Mathematical and Physical Sciences*, **400** (1818): 97-117 (1985).
- [12] R. Landauer. Irreversibility and heat generation in the computing process. *IBM Journal of Research and Development*. **5**, 183-191 (1961).

- [13] C. H. Bennett. IBM J. Res. Develop. **17**, 525-532 (1973).
- [14] T. Toffoli. Automata, Languages and Programming. (eds. J. W. de Bakker and J. van Leeuwen), 632, Springer: New York, (1980).
- [15] D. Deutsch. Quantum Theory, the Church-Turing Principle and the Universal Quantum Computer. Proc. R. Soc. London Ser. A, **400**, 97 (1985).
- [16] P. W. Shor. Polynomial-Time Algorithms for Prime Factorization and Discrete Logarithms on a Quantum Computer. SIAM Journal on Scientific and Statistical Computing **26**: 1484, arXiv:quant-ph/9508027, (1997).
- [17] L. K. Grover. A fast quantum mechanical algorithm for database search. arXiv:quant-ph/9605043, (1996).
- [18] D. Deutsch and R. Jozsa. Rapid solutions of problems by quantum computation. Proceedings of the Royal Society of London A **439**: 553 (1992).
- [19] P. Shor. Scheme for reducing decoherence in quantum memory. Phys. Rev. A **52**, 2493 (1995).
- [20] P. Shor. Fault-tolerant quantum computation. Proceedings of the Symposium on the Foundations of Computer Science, (Los Alamitos, CA: IEEE Press, arXiv:quant-ph/9605011, 1996).
- [21] A. M. Steane. Active stabilization, quantum computation and quantum state synthesis. Phys. Rev. Lett. **78**, 2252 (1997).
- [22] J. I. Cirac and P. Zoller. Quantum computation with cold trapped ions. Phys. Rev. Lett. **74**:4091 (1995).
- [23] D. P. DiVincenzo. Two qubit gate are universal for quantum computation. Phys. Rev. A **51**(2):1015-1022 (1995).
- [24] N. Gershenfeld and I. L. Chuang. Bulk spin resonance quantum computation. Science, 275:350 (1997).
- [25] D. G. Cory, A. F. Fahmy and T. F. Havel. Ensemble quantum computing by NMR spectroscopy, Proc. Nat. Acad. Sci. USA, **94**:1634 (1997)

- [26] T. Pellizzari, S. A. Gardiner, J. I. Cirac and P. Zoller. Decoherence, Continuous Observation, and Quantum Computing: A Cavity QED Model, *Phys. Rev. Lett.* **75**, 3788-3791 (1995).
- [27] C. Nayak, S. Simon, H. Ady Stern, M. Freedman and S. Das Sarma. Non-Abelian Anyons and Topological Quantum Computation. *Rev. Mod. Phys.* **80**, 1083, (2008).
- [28] J. M. Leinaas and J. Myrheim. On the theory of identical particles. *Il Nuovo Cimento B* **37** (1): 1-23 (1977).
- [29] S. Das Sarma, M. Freedman and C. Nayak. Topologically Protected Qubits from a Possible Non-Abelian Fractional Quantum Hall State. *Phys. Rev. Lett.* **94**, 166802 (2005).
- [30] G. Moore and N. Read. Nonabelions in the fractional quantum Hall effect. *Nucl. Phys. B* **360**, **362** (1991).
- [31] A. Y. Kitaev. Fault-tolerant quantum computation by anyons. *Ann. Phys. (N.Y.)* **303**, (2003).
- [32] Lara Faoro, Jens Siewert and Rosario Fazio. Non-Abelian Holonomies, Charge Pumping, and Quantum Computation with Josephson Junction. *Phys. Rev. Lett.* **90**, 028301 (2003).
- [33] Jeffrey C. Y. Teo and C. L. Kane. Majorana Fermions and Non-Abelian Statistics in Three Dimensions. *Phys. Rev. Lett.* **104**, 046401 (2010).
- [34] Michael Freedman, Matthew B. Hastings, Chetan Nayak and Xiao-Liang Qi. Weakly coupled non-Abelian anyons in three dimensions. *Phys. Rev. B* **84**, 245119 (2011).
- [35] H. Yao and S. A. Kivelson. Exact Chiral Spin Liquid with Non-Abelian Anyons. *Phys. Rev. Lett.* **99**, 247203 (2007).
- [36] S. Yang, D. L. Zhou and C. P. Sun. Mosaic spin models with topological order. *Phys. Rev. B* **76**, 180404(R)(2007).



- [37] S. Mandal and N. Surendran. Exactly solvable Kitaev model in three dimensions. *Phys. Rev. B* **79**, 024426 (2009).
- [38] Z. Nussinov and G. Ortiz. Bond algebras and exact solvability of Hamiltonians: Spin  $S=1/2$  multilayer systems *Phys. Rev. B* **79**, 214440 (2009).
- [39] G. Baskaran, S. Santhosh and R. Shankar. Exact quantum spin liquids with Fermi surfaces in spin-1/2 models arXiv:0908.1614 (unpublished).
- [40] L. M. Duan, E. Demler and M. D. Lukin. Controlling Spin Exchange Interactions of Ultracold Atoms in Optical Lattices. *Phys. Rev. Lett.* **91**, 090402 (2003).
- [41] S. Tewari, S. Das Sarma, C. Nayak, C. Zhang and P. Zoller. Quantum Computation using Vortices and Majorana Zero Modes of a  $px+ipy$  Superfluid of Fermionic Cold Atoms. *Phys. Rev. Lett.* **98**, 010506 (2007).
- [42] D. A. Ivanov. Non-Abelian Statistics of Half-Quantum Vortices in p-wave Superconductors. *Phys. Rev. Lett.* **86**, 268 (2001).
- [43] Y. Makhlin, G. Schon and A. Shirman. Quantum-state engineering with Josephson-junction devices. *Rev. Mod. Phys.* **73**, 357 (2001).
- [44] A. Kitaev. Unpaired Majorana fermions in quantum wires. *Usp. Fiz. Nauk (Suppl.)* **171**, 131 (2001).
- [45] Uma Divakaran and Amit Dutta. Reverse quenching in a one-dimensional Kitaev model. *Phys. Rev. B* **79**, 224408 (2009).
- [46] Dusuel, Schmidt, Vidal and Zaffino. Perturbative study of the Kitaev model with spontaneous time-reversal symmetry breaking. *Phys. Rev. B* **78**, 125102 (2008)
- [47] Nash and Connor. Zero Temperature Phase Diagram of the Kitaev Model. *Phys. Rev. Lett.* **102**, 147203 (2009)
- [48] Kamfor, Dusuel, Vidal and Schmidt. Kitaev model and dimer coverings on the honeycomb lattice. *J. Stat. Mech.* P08010 (2010)

- [49] E. Lieb, T. Schultz and D. Mattis. Two Soluble Models of an Antiferromagnetic Chain. *Annals of Physics*: **16**, 407-466 (1961).